50272-101

REPORT DOCUMENTATION PAGE	1. REPORT NO. NSF/RA-800247	2.	3. Recipient's Accession No. PB81 117178

4. Title and Subtitle	5. Report Date
Upper Bound Limit Analysis of the Stability of a Seismic-Infirmed Earthslope	September 1980
	6.
7. Author(s) S. W. Chan, S. L. Koh, W. F. Chen	8. Performing Organization Rept. No. CE-STR-80-16
9. Performing Organization Name and Address Purdue University School of Civil Engineering West Lafayette, IN 47907	10. Project/Task/Work Unit No. 11. Contract(C) or Grant(G) No. (C) (G) PFR7809326
12. Sponsoring Organization Name and Address Engineering and Applied Science (EAS) National Science Foundation 1800 G Street, N.W. Washington, D.C. 20550	13. Type of Report & Period Covered 14.

15. Supplementary Notes

16. Abstract (Limit: 200 words)

The upper bound limit analysis of perfect plasticity was applied to obtain a formulation for the critical height of a seismic-infirmed earthslope. Variation of the force magnitude and direction along the slope elevation was accounted for through two orthogonal seismic profiles. A rotational logarithmic spiral proved to be the most critical shape of sliding surface for any seismic profiles. Results for deadweight induced instability and data for constant and linear seismic profiles agree well with existing values. Appreciable reductions in critical heights for a more general horizontal seismic profile were observed. Reductions caused by a vertical seismic profile of similar shape but with relative magnitudes of 0.1 and 0.5 times that of the horizontal profile were shown to be rather insignificant. Determination of the location of the most critical slip-surface for a slope of specific geometry and height also has been demonstrated with this model. Adaptation of this model to future analyses related to seismic-infirmed earthquakes has been facilitated by computer coding.

17. Document Analysis a. Descriptors

Earthquakes	Orthogonality
Mathematical models	Seismology
Landslides	Stress analysis
Plastic properties	Computerized simulation

b. Identifiers/Open-Ended Terms

Earthslopes
Computer coding

Earthquake Hazards Mitigation

c. COSATI Field/Group

18. Availability Statement	19. Security Class (This Report)	21. No. of Pages
NTIS	20. Security Class (This Page)	22. Price

(See ANSI-Z39.18) See Instructions on Reverse OPTIONAL FORM 272 (4-77) (Formerly NTIS-35) Department of Commerce

CE-STR-80-16

UPPER BOUND LIMIT ANALYSIS OF THE STABILITY OF A SEISMIC-INFIRMED EARTHSLOPE

by

S. W. Chan, S. L. Koh and W. F. Chen

This material is based on Master Thesis of S. W. Chan. A computer coding of the model has been implemented, which includes a complete listing of the program and some sample outputs. This work is supported by the National Science Foundation under Grant No. PFR-7809326 to Purdue University.

School of Civil Engineering
Purdue University
West Lafayette, IN 47907

September, 1980

TABLE OF CONTENTS

Page

LIST OF TABLES

LIST OF FIGURES

Figure		Page

Appendix
Figure

ABSTRACT

The upper bound limit analysis of perfect plasticity is applied to obtain a formulation for the critical height of a seismic-infirmed earthslope. The variation of the force magnitude and direction along the slope elevation is accounted for through two orthogonal seismic profiles. Based on earlier work for the dead-weight case, a rotational logarithmic spiral surface is again shown to be the most critical shape of sliding surface for any seismic profiles. Results for dead-weight induced instability obtained from the present model agree well with existing values. Also in good agreement with published values are the data for the constant and linear seismic profiles. Appreciable reductions in critical heights for a more general horizontal seismic profile are observed. The reductions caused by a vertical seismic profile of similar shape but with relative magnitudes of 0.1 and 0.5 times that of the horizontal profile are shown to be rather insignificant. The determination of the location of the most critical slip-surface for a slope of specific geometry and height has also been demonstrated with this model.

CHAPTER I. INTRODUCTION

Earthquakes continue to be a subject of intensive studies. The damage to properties and the widespread deaths that may be traced back to earthquakes as the main cause are well-recorded. In many instances, the severest destructions and greatest number of casualties result from earthquake-induced landslides. Records show that landslides occur most frequently on sloping earthmasses. They are observed on the slopes of dams, embankments and other man-made cuts; on the banks of rivers, lakes, reservoirs, and along coasts as well as on mountain slopes. For simplicity, such sloping earthmasses will be referred to as 'earthslopes' throughout this report.

Because of the potential threats associated with these landslides, there is an urgent need to advance the state of the art to develop more effective methods for the assessment of such dangers. Common practice in such analyses involves the neglecting of the more complex soil behaviors and properties, as well as the simplification of the seismic forces as being constant. While at the present, attempts are underway by other investigators [Ref. 18 & 21] to more precisely formulate the critical soil behaviors, this study will be limited to the improvement of the analysis through the incorporation of non-constant seismic forces throughout the slope height. This study will not only allow for the refinement of results, but would also shed light on the possibility of incorporating the nonhomogeneity of some soil properties. To this end, more realistic estimation on the earthslope stability can be made with relative ease.

Historically, the study of an earthslope's potential for collapse under its own weight has been the main concern of the earth-structure engineers. Because of its geometrical configuration, density, and strength properties, a slope with a height above certain critical value may become too weak to support the weight of its own mass. This soil mass is then assumed to move downslope by the gravitational pull along a well-defined failure surface. Practices have been to approach the problem in a phenomalistic way, where the variety of post-elastic soil behavior is replaced by a model of perfect plasticity [Ref. 4 & 11-15]. The idealized homogeneous and isotropic soil is further assumed to yield under the well-known Coulomb criterion and its associated flow rule. Then methods were derived to predict the existence of a slip surface, which would yield without restrictions, carrying the soil mass above it downslope. Among the more famous methods are the slip-line method, the limit-equilibrium methods, and the limit analysis approach. Of these, the limit analysis approach is relatively easier and have applications to a larger range of slope geometries.

The extension of the limit analysis method for the static case to the case of seismic loadings is a logical step forward. The existing approach involves essentially adding to the dead-weight of the potential collapse mass a pseudo-static force simulating the seismic load. This force acting through the center of gravity of the soil mass is expressed as the product of the soil mass and a "seismic coefficient". As shown in Fig. 1, $m\Upsilon$ is the soil mass and K_x is the seismic coefficient. The choice of such a coefficient is to reflect the maximum force exerted on the slope for the time history of an earth-quake.

The criticism on this rather crude approach are: (i)The seismic coefficient of a slope is not a constant value during any instant of an earthquake. Owing to the non-rigidity of the soil layers, the reactive forces developed throughout the height of the slope as a result of the movement of the ground always vary. (ii)Because of the granular nature of the soil, it is reasonable to expect the density and strength properties to vary along the height as the consequence of different degrees of water saturation inside the inter-granular voids of the soil.

To get around the first problem, a more recent effort [Ref. 17] was made to incorporate zones of different seismic coefficients along the height to approximate the actual variation (Fig. 2). While such approach is a definite improvement over the earlier ones, there are also restrictions to its applications. A conceivable difficulty is the case where the variation of the seismic coefficient is so sharp that a large number of thin zones have to be used. In the presence of a secondary slope as shown in Fig. 2 with $\alpha > 0$, the analysis will necessitate the handling of two different slope geometries. In this case, rather than considering the original slope with one knee (section BEDB in Fig. 2a), one will have to consider a fictitious slope with two knees (FEDGF). With the need to prepare a map of coefficient zones for each profile of seismic forces at each instant, it would be quite time-consuming when investigating the hazard of the slope at intervals within the duration of the earthquake.

The next logical step towards a better analysis of the earthslope is to develop formulations to account for a more accurate seismic profile. The seismic coefficient as a function of the elevation above the ground level must be recognized. The vertical component of the seismic force, neglected in earlier works, must be included. Through appropriate interpretation, the vertical seismic profile can also be used to represent the variation of density along the height as well. With more rigorous and general formulations, further implications of the possibility of incorporating the profiles of strength parameters into the model can be made. All these are undertaken in this study.

Since every mathematical model has its limitations, it is the wise application of a model to different situations that determines its usefulness and efficiency. The slight changes of the model for the analysis of the location of the most critical slip surface in a given slope are demonstrated. Further directions for the applications of the model, as well as improvements for the future, are also discussed.

CHAPTER II. THE UPPER BOUND THEOREM OF THE PERFECT PLASTICITY LIMIT ANALYSIS

One of the most effective method of analysis of slope stability is that of limit analysis. The theorems of limit analysis were developed during the fifties. These theorems are based on the generalized perfect plasticity model of material behavior. With such a model, a material deforms indefinitely or yield flows under a constant collapse load. The stress-strain response curve beyond the elastic range is represented by a horizontal line. Generally speaking, the post-elastic strain behavior of soil can be approximated by this model (Fig. 3). By such an idealization, work-hardening or work-softening, which are usually not too prominent at the onset of yielding, are neglected.

Another important assumption is that the changes in the geometry of the yielding material are insignificant. The direct consequence of this assumption is the result that "when the limit (collapse) load is reached and the deformation proceeds under constant loading, all stresses remain constant; only plastic (non-elastic) increments of strain occur."

Subsequently, a number of theorems were established through the consideration of virtual work and energy. These theorems, when applied appropriately to analyze the limiting state of the passing from the elastic to the plastic range, have been used by several investigators [Ref. 4 & 11-15] to determine the lower and upper bounds on the actual critical load. The determination of the lower bound involves the assumption of a stress state for the material body studied. The stress field in a slope is usually complicated. This presents a problem in calculating the lower bound. On the other hand, it is with relative ease that one may apply the upper bound limit analysis.

The upper bound limit analysis is based essentially on two of the limit theorems, namely:

i) Initial stresses or deformations have no effect on the plastic limit or collapse load, provided that the geometry is essentially unaltered; and

ii) The Upper Bound Theorem --- If a compatible and kinematically admissible mechanism of plastic deformation ($\dot{\varepsilon}^{p*}_{ij}$, $\dot{u}^{p*}_{ij}$) is assumed, which satisfies the condition $\dot{u}^{p*}_{i}=0$ on the displacement boundary; then the loads T_i & F_i, determined by equating the rate of external work to the rate of internal energy dissipation, will be either higher than or equal to the actual limit load.

In other words, the Upper Bound Theorem states that collapse must impend or have taken place if a path of failure exists. The external work rate is given as

$$\dot{W}_E = \int_A T_i \dot{u}^{p*}_i \, dA + \int_V F_i \dot{u}^{p*}_i \, dV \tag{1}$$

and the rate of internal energy dissipation is

$$\dot{W}_I = \int_V \sigma_{ij}^{p*} \cdot \dot{\varepsilon}_{ij}^{p*} \, dV \tag{2}$$

In the Upper Bound Theorem, a reference is made to a kinematically admissible mechanism of plastic deformation. It is often useful to consider discontinuous velocity fields as such mechanisms. By discontinuous velocity field, it is meant not an actual fracture type of discontinuity across a fixed surface. Rather, this discontinuity is simply an idealization of a continuous distribution in which the velocity changes very rapidly across a thin transition layer (Fig. 4). Such idealization is permissible provided that the stresses on the assumed discontinuity surface are chosen as the limiting values of the stresses on the surfaces bounding the transition layer as the thickness of this layer approaches zero. It should be noted that the rate of internal energy dissipation in this transition layer will approach a finite value in the limit as the thickness of the layer approaches zero.

In the application of the limit analysis to soil by approximating the stress-strain curve as an inclined and a horizontal line (Fig. 3), the yield stress level used should be chosen to represent the average stress in an appropriate range of strain. As in all stability problems, the maximum average stress mobilized over the whole of the failure surface in a real soil will be less than the peak value and more than the residual value. Its relative position between these two limits is being determined both by the properties of the soil and by the geometry and boundary stresses in the problem to be analyzed.

Like metals, soil as an engineering material can be described by a yield criterion of its transition from an elastic state to the state of plastic flow. It is generally assumed that plastic flow occurs in soil when, on any plane at any point in a mass of soil, the shear stress τ reaches an amount that depends linearly upon the cohesion stress c, and the compressive stress σ (Fig. 5):

$$\tau = c + \sigma \cdot \tan\phi \tag{3}$$

This is the Coulomb's criterion, in which ϕ is the angle of internal friction of the soil. The two constants c and ϕ can be looked upon as the parameters that characterize the total shear resistance of the soil media. It should be noted that for a purely cohesive soil (ϕ=0), Coulomb's criterion is identical to Tresca's criterion for metal.

In dealing with plastic strain rates of an ideally plastic and isotropic material, the principal axes of strain rate and stress are assumed to be coincident. The direct consequence of this assumption for a granular material like soil, whose shear strength depends directly on the normal stress, is the associated flow rule. The associated flow rule asserts that any plastic deformation of a Coulomb material must be accompanied by an increase in volume, or dilatancy, provided that $\phi \neq 0$. The result of this dilatancy is the inclination of the strain or displacement vector at an angle of ϕ to the shearing surface (Fig.6).

Since real soils are quite complex and theories proposed to characterize them do not exactly describe their physical behavior, discrepancies between theoretical and empirical results should be expected. An example is the excessive dilatancy predicted by the perfect plasticity theory. Clearly, to account for the complexity of the problem with more elaborate models will mean a trade-off of the convenience for the physical reality. However, in certain circumstances, such as the stability problems in soil mechanics, the deformation conditions are often insufficiently restrictive for the soil deformation properties to affect the collapse load to a great extent. The adoption of the limit analysis based upon Coulomb's criterion and its associated flow rule is justified. It is, therefore, used in the present study.

CHAPTER III. FAILURE SURFACE

III.A. The Neccessity for a Failure Mechanism

In the analysis of slope stability, the determination of the critical height of the slope, the height at which the slope is at the verge of collapse, yields an important criterion. According to the Upper Bound Theorem, failure can occur if a compatible failure mechanism exists in the body. A convenient way to approach the problem is to assume that a single, well-defined slip surface exists for the slope. If a virtual displacement is induced along the surface, the rate of the input of work energy due to the applied forces would be equal to or in excess of the rate of internal dissipation of energy. This results in an indefinite or unrestrained shear deformation along the length of the slip surface. The soil mass resting immediately upon the slip surface is carried along and can be treated as a rigid block undergoing rigid-body motion. The soil mass beneath the failure surface is viewed as being stationary (Fig. 7).

The velocity field in the sliding block is significantly different from that of the stationary block, with an extremely thin shear flow soil layer separating the two. Thus, the earthslope is considered to have a discontinuous velocity field with the shear flow layer treated as a surface of discontinuity.

With a Coulomb material like soil, the associated flow rule requires a separation or overlap of the material on the two sides of the layer to accompany a tangential velocity discontinuity. The actual transition layer must have appreciable thickness, but the idealization to a discontinuity surface may still be useful. This is the case as long as the very small thickness of the layer remains uniform throughout its entire length.

III.B. The Kinematically Admissible Mechanisms

Since the motion of the sliding block above the failure surface is caused by the shear flow of the surface along its entire length, the type of motion acquired by the sliding soil mass then reflects the shape of the sliding mechanism that carries it. Thus, for a translational failure mode, the slip surface is neccessarily an inclined straight layer. For the rotational failure without dilatation, the mechanism would be circular in shape. However, this is only true in the case of a purely cohesive soil (ϕ=0).

For most soils, where internal friction is significant, a dilatation equal to tanϕ is observed according to the associated flow rule (Fig. 6). With this, then the only admissible failure mechanisms are the straight (plane) layer surface for translation, and the ϕ-logspiral surface for rotation (Fig. 8). The qualification for these two kinds of surface is that they are the only ones that insure the uniformity of the thickness throughout the surface length during yielding.

That the plane surface of translational displacement is admissible is rather obvious. The shear strain rate vector, inclined at an angle ϕ to the surface as a result of dilatation, is constant along the length of the surface. This insures that every point on one side will displace the same amount at a small time interval, thereby preserving the uniformity of the thickness.

For the case of the rotational mechanism, an examination of the geometry at the onset of yielding and at a small interval later is neccessary (Fig. 9). Suppose the angular displacement is $d\theta$; then the radius $\overline{OA}$ of an arbitrary point A on the surface is moved to the new position $\overline{OA'}$. However, this new position of the radius $\overline{OA'}$ will coincide with the old position of the radius $\overline{OB}$ of the point B before the displacement. From the geometry, $\overline{AA'}$ ($=rd\theta$) is neccessarily perpendicular to $\overline{OA'}$. Now, since $\overline{AA'}$ coincides with the velocity vector, which forms an angle ϕ with the surface according to the associated flow rule, then radius $\overline{OB}$ must be greater than $\overline{OA}$ by an amount of $rd\theta(\tan\phi)$. In other words,

$$\overline{OB} - \overline{OA} = rd\theta(\tan\phi) , \tag{4}$$

or

$$r(\theta+d\theta) - r(\theta) = dr = r \cdot \tan\phi \cdot d\theta. \qquad (5)$$

By integration, and noting that θ_o and r_o stand for the initial angle and radius, the equation for the only admissible rotational failure mechanism is

$$\int_{r_o}^{r} \frac{dr}{r} = \int_{\theta_o}^{\theta} \tan\phi d\theta \qquad (6)$$

or

$$\ell n(r/r_o) = (\theta-\theta_o)\tan\phi. \qquad (7)$$

Thus,

$$r = r_o \exp[(\theta-\theta_o)\tan\phi]. \qquad (8)$$

III.C. The Most Critical Type of Mechanisms

In the discussion of Section III.B. above of the straight and ϕ-logspiral surfaces as the translational and rotational mechanisms, the arguments were essentially based on the geometric compatibilities. The question that remains is that of these two types of mechanisms, which one would be more critical? That is, which one would be developed with the least input of external work? For the earthslope under the static loads, the ϕ-logspiral has been shown to be the most critical [Ref. 15]. However, it is still neccessary to find out, for more complicated loading situations, whether this type of failure mechanism is still the most likely to occur.

Since different shapes of failure surface will result in earthslopes of different soil masses, the stress state along the slip surface is mechanism-dependent. The process of determining the most critical surface is thus controlled by the consideration of the shape function and the stress-distribution function. The problem is then reduced to one in which both the shape of the mechanism and the resulting stresses along the failure surface must be chosen in such a way that the external loads from the soil mass above this surface will be just balanced by the stresses developed at the surface. At the incipience of any collapse, when the stress state satisfies Coulomb's criterion, the flow of the velocity discontinuity will then carry the block it supports along. Of all the possible shapes that satisfy the above requirement, the one that needs the minimum of applied load would be the most critical. This then is the criterion of optimization.

Using the techniques of variational calculus, the applied load on a potential slip surface can be defined by a functional (Fig. 10):

$$W = \int_H [(dF_x)^2+(dF_y)^2]^{\frac{1}{2}}, \tag{9}$$

where dF_x and dF_y are the orthogonal force components of an infinitesimal soil layer at an arbitrary elevation. They are defined as

$$dF_x = \gamma K_x \xi dh, \text{ and} \tag{10}$$

$$dF_y = \gamma K_y \xi dh. \tag{11}$$

Here, γ is the specific weight, K_x and K_y are the loading coefficients, ξ is the length of the infinitesimal soil layer, and dh is its thickness. For the static case involving the gravitational force only, $K_x=0$ and $K_y=1$. For seismic loading, both K_x and K_y are non-zero. The present formulation permits the consideration of cases where the seismic load has a vertical component; for this case, $K_y \neq 1$.

To account for the variations of loadings along the vertical and horizontal distances from the toe of the slope, K_x and K_y are allowed to be any functions of r and θ, the reference polar coordinates, as

$$K_x = K_x(r,\theta), \text{ and} \tag{12}$$

$$K_y = K_y(r,\theta). \tag{13}$$

The function ξ depends on the shape of the slip surface, the geometry of the slope, as well as their relative positions with respect to each other. (See Appendix B.) Thus,

$$\xi = \xi(r,\theta,\alpha,\beta). \tag{14}$$

From the consideration of the geometry along the slip line,

$$dh = ds \cdot \cos(\theta - \zeta), \tag{15}$$

where ζ is the angle between the perpendicular to the radius and the surface element ds, which is

$$ds = r \cdot d\theta / \cos\zeta. \tag{16}$$

Therefore,

$$dh = f(r, \theta, \zeta) d\theta. \tag{17}$$

With respect to the polar coordinates, and with θ_o and θ_h being the initial and final angles of the slip surface, the functional W may be expressed as

$$W = \int_{\theta_o}^{\theta_h} \gamma \xi(r, \theta, \alpha, \beta) [K_x^2(r, \theta) + K_y^2(r, \theta)]^{\frac{1}{2}} f(r, \theta, \zeta) d\theta. \tag{18}$$

The additional equations are the equations of equilibrium:

$$\sum F_x = 0 \Rightarrow \int [\tau \cos\delta - \sigma \sin\delta] ds - \int \gamma K_x \xi dh = 0; \tag{19}$$

$$\sum F_y = 0 \Rightarrow \int [\tau \sin\delta + \sigma \cos\delta] ds + \int \gamma K_y \xi dh = 0; \text{ and} \tag{20}$$

$$\sum M_o = 0 \Rightarrow \int [r\sigma \sin\zeta - r\tau \cos\zeta] ds + \int \gamma [K_x r \xi \sin\theta + K_y \xi (r\cos\theta - \tfrac{1}{2}\xi)] dh = 0. \tag{21}$$

These three equations can be simplified from the geometry, in addition to the requirement that Coulomb's criterion of $\tau = c + \sigma \tan\phi$ be satisfied everywhere along the slip surface to assure the onset of yielding. Thus, they become

$$\Sigma F_x = \int_{\theta_o}^{\theta_h} (R_1 - B_1)d\theta = 0; \tag{22}$$

$$\Sigma F_y = \int_{\theta_o}^{\theta_h} (R_2 + B_2)d\theta = 0; \text{ and} \tag{23}$$

$$\Sigma M_o = \int_{\theta_o}^{\theta_h} (R_3 + B_3)d\theta = 0, \tag{24}$$

with

$$R_1 = -\sigma[(r\cos\theta)'\tan\phi + (r\sin\theta)'] - c(r\cos\theta)' = R_1(\theta, r, r', \phi, c, \sigma); \tag{25}$$

$$R_2 = \sigma[(r\cos\theta)' - (r\sin\theta)'\tan\phi] - c(r\sin\theta)' = R_2(\theta, r, r', \phi, c, \sigma); \tag{26}$$

$$R_3 = \sigma(rr' - r^2\tan\phi) - cr^2 = R_3(r, r', \phi, \sigma); \tag{27}$$

$$B_1 = \gamma\xi(\theta, r, \alpha, \beta)K_x(\theta, r)f(\theta, r, \zeta) = B_1(\theta, r, \zeta, \alpha, \beta, \gamma); \tag{28}$$

$$B_2 = \gamma\xi(\theta, r, \alpha, \beta)K_y(\theta, r)f(\theta, r, \zeta) = B_2(\theta, r, \zeta, \alpha, \beta, \gamma); \tag{29}$$

$$B_3 = \gamma\xi(\theta, r, \alpha, \beta)\{(r\sin\theta)K_x(\theta, r) + [r\cos\theta - \tfrac{1}{2}\xi(\theta, r, \alpha, \beta)]K_y(\theta, r)\}$$
$$= B_3(\theta, r, \alpha, \beta, \gamma); \tag{30}$$

where the R's are the reaction forces from the stress state of the slip surface, and the B's are the applied forces contributed by the soil block supported by the surface.

In minimizing the functional

$$W = \int_{\theta_o}^{\theta_h} P(\theta, r, \alpha, \beta, \zeta)d\theta, \tag{31}$$

subjected to the three constraints, it is neccessary to make use of the Lagrangian multipliers:

$$I = P+\lambda_1(R_1-B_1)+\lambda_2(R_2+B_2)+\lambda_3(R_3+B_3). \tag{32}$$

By the Euler-Lagrange differential equation for multi-variable variational calculus, we get

$$\frac{\partial I}{\partial r} - \frac{\partial^2 I}{\partial r'\partial\theta} - r'\frac{\partial^2 I}{\partial r'\partial r} - r''\frac{\partial^2 I}{\partial r'\partial r'} = 0; \text{ and} \tag{33}$$

$$\frac{\partial I}{\partial \sigma} - \frac{\partial^2 I}{\partial \sigma'\partial\theta} - \sigma'\frac{\partial^2 I}{\partial \sigma'\partial \sigma} - \sigma''\frac{\partial^2 I}{\partial \sigma'\partial \sigma'} = 0. \tag{34}$$

From the fact that P, B_1, B_2, and B_3 are independent of σ, it is obvious that

$$\frac{\partial B_1}{\partial\sigma} = \frac{\partial B_2}{\partial\sigma} = \frac{\partial B_3}{\partial\sigma} = \frac{\partial P}{\partial\sigma} = 0. \tag{35}$$

With these, and the condition that

$$\frac{\partial I}{\partial \sigma'} = 0, \tag{36}$$

Equation (34) becomes

$$\lambda_1\frac{\partial R_1}{\partial\sigma} + \lambda_2\frac{\partial R_2}{\partial\sigma} + \lambda_3\frac{\partial R_3}{\partial\sigma} = 0. \tag{37}$$

Substituting into Equation (37) the expressions for R_1, R_2, and R_3 from Eqs.(25)-(27), we obtain

$$\lambda_1\{-[(r'\cos\theta-r\sin\theta)\tan\phi+(r'\sin\theta+r\cos\theta)]\}+\lambda_2\{[(r'\cos\theta-r\sin\theta) -\tan\phi(r'\sin\theta+r\cos\theta)]\}+\lambda_3\{(rr'-r^2\tan\phi)\} = 0. \quad (38)$$

To convert the coordinates to the cartesian system, the following transformation indentities are used:

$$x = r\cos\theta; \quad (39)$$

$$y = r\sin\theta; \quad (40)$$

$$\frac{dx}{d\theta} = r'\cos\theta-r\sin\theta; \quad (41)$$

$$\frac{dy}{d\theta} = r'\sin\theta+r\cos\theta; \quad (42)$$

$$x\frac{dy}{d\theta}-y\frac{dx}{d\theta} = r^2; \text{ and} \quad (43)$$

$$x\frac{dx}{d\theta}+y\frac{dy}{d\theta} = rr'. \quad (44)$$

Equation (38) is then reduced to

$$\lambda_1[-\tan\phi\frac{dx}{d\theta}-\frac{dy}{d\theta}]+\lambda_2[\frac{dx}{d\theta}-\tan\phi\frac{dy}{d\theta}]+\lambda_3[x\frac{dx}{d\theta}+y\frac{dy}{d\theta}-\tan\phi(x\frac{dy}{d\theta}-y\frac{dx}{d\theta})] = 0. \quad (45)$$

Knowing that

$$\frac{dy}{dx} = (\frac{dy}{d\theta})/(\frac{dx}{d\theta}), \quad (46)$$

we get

$$\lambda_1[-\tan\phi-\frac{dy}{dx}]+\lambda_2[1-\tan\phi\frac{dy}{dx}]+\lambda_3[x+y\frac{dy}{dx}-\tan\phi(x\frac{dy}{dx}-y)] = 0. \qquad (47)$$

By collecting terms, it becomes

$$(y-\frac{\lambda_1}{\lambda_3})\frac{dy}{dx}+(x+\frac{\lambda_2}{\lambda_3})+\tan\phi[(y-\frac{\lambda_1}{\lambda_3})-(x+\frac{\lambda_2}{\lambda_3})\frac{dy}{dx}] = 0. \qquad (48)$$

Translating the origin (0,0) of the x-y system to $(-\frac{\lambda_2}{\lambda_3},\frac{\lambda_1}{\lambda_3})$ of the new X-Y system (Fig. 11), the differential equation evolves into:

$$Y\frac{dY}{dX}+X+\tan\phi(Y-X\frac{dY}{dX}) = 0 \qquad (49)$$

or

$$(Y-X\tan\phi)dY+(Y\tan\phi+X)dX = 0. \qquad (50)$$

Substituting

$$Y = vX \quad \text{and} \qquad (51)$$

$$dY = vdX+Xdv \qquad (52)$$

into Eq.(49), we obtain the following

$$(v^2X+X)dX+(vX^2-X^2\tan\phi)dv = 0. \qquad (53)$$

Integrating Eq.(53), we get

$$\int\frac{dX}{X} = \tan\phi\int\frac{dv}{1+v^2}-\int\frac{vdv}{1+v^2}+c_o \ , \qquad (54)$$

or

$$\ell nX = \tan\phi[\arctan(v)] - \tfrac{1}{2}\ell n(1+v^2) + c_o \ . \tag{55}$$

Since v=Y/X, then obviously

$$\bar{\theta} = \arctan(v) \tag{56}$$

and

$$(\bar{r}/X)^2 = 1+v^2. \tag{57}$$

Therefore,

$$\ell nX = \bar{\theta}\tan\phi - \tfrac{1}{2}\ell n(\bar{r}/X)^2 + c_o \tag{58}$$

or $$\ell n\bar{r} = \bar{\theta}\tan\phi + c_o \tag{59}$$

From the boundary condition, where $\bar{r}_o$ corresponds to $\bar{\theta}_o$ for the initiation of the slip surface curve,

$$\ell n\bar{r}_o = \bar{\theta}_o\tan\phi + c_o \tag{60}$$

or $$c_o = \ell n\bar{r}_o - \bar{\theta}_o\tan\phi. \tag{61}$$

Substituting Eq.(61) back into Eq.(59), we finally get

$$\bar{r} = \bar{r}_o\exp[(\bar{\theta}-\bar{\theta}_o)\tan\phi]. \tag{62}$$

This is the equation for a ϕ-logspiral. The ϕ-logspiral is then the most critical slip surface.

From the solution of Eq.(34), it is obvious that the process of solving the Eq.(33) will be even more tedious. The solution will be very complicated, and will only result in the profile of the normal stress distribution along the slip surface. Since the normal stresses along the entire surface are directed toward the center of rotation, they have no contribution in the internal dissipation of energy for our rotational mechanism. It is therefore sufficient to know from the examination of Eq.(33) that the normal stress distribution along the slip surface varies with different loadings.

Note that by means of similar derivations, the following statement can be obtained: For the case where body forces as well as soil non-homogeneity and anisotropy in cohesion are considered only, the most critical failure surface is still the ϕ-logspiral.

CHAPTER IV. DETERMINATION OF THE CRITICAL HEIGHT FOR SEISMIC STABILITY

IV.A. General Formulation of the Seismic Force Profile

As shown in Chapter III, the ϕ-logspiral surface may be used as the failure mechanism in the stability analysis of an earthslope under seismic loading situations. Following traditional approach in slope stability analysis, we predict the critical height of the slope rather than the critical load itself. Such a prediction is an upper bound on the actual value. It is quite useful in providing insight to the evaluation of the slope stability as well as guidelines for the design of earth-projects.

Pertinent to the analysis of the stability of an earthslope under seismic loads is the development of a suitable representation for the loads. In earlier works (e.g. Ref. [20]), the seismic load is considered constant and in the horizontal direction only. More recent studies (Ref. [7] to [10]) considered the seismic load to increase with height. In addition, studies have taken into consideration the vertical component of seismic loads.

More realistically, the seismic profile is non-linear. A convenient representation is to treat profiles of the vertical and horizontal components as polynomials of the elevation, as follows:

$$K_x(h) = a_o+a_1h+a_2h^2+ \ldots a_mh^m = \sum_{j=0}^{m}[a_jh^j]; \text{ and} \tag{63}$$

$$K_y(h) = b_o+b_1h+b_2h^2+ \ldots b_nh^n = \sum_{j=0}^{n}[b_jh^j]. \tag{64}$$

However, to conform to the polar coordinates used to describe the failure spiral surface, these must be expressed in terms of θ and r. If the spiral is to pass through the toe of the slope, then the height of any horizontal layer of soil is (Fig. 12):

$$h = \eta-y, \tag{65}$$

where

$$\eta = r_h\sin\theta_h = r_o\exp[(\theta_h-\theta_o)\tan\phi]\sin\theta_h, \text{ and} \tag{66}$$

$$y = r\sin\theta = r\cdot\exp[(\theta-\theta_o)\tan\phi]\sin\theta, \tag{67}$$

$$\text{with} \quad \theta_o \leq \theta \leq \theta_h. \tag{68}$$

Substituting Eq.(65) into Eq.(63) for $K_x(h)$, we obtain:

$$K_x(y) = a_o+a_1(\eta-y)+a_2(\eta-y)^2+ \ldots a_m(\eta-y)^m, \tag{69}$$

which expands to

$$K_x(y) = a_o+a_1\eta-a_1y+a_2\eta^2-2a_2\eta y+a_2y^2+a_3\eta^3-3a_3\eta^2y+$$

$$3a_3\eta y^2-a_3y^3+ \ldots +a_m\eta^m+a_m\sum_{k=1}^{m}\left[{m \atop k}\right]\eta^{(m-k)}y^k. \tag{70}$$

Eq.(70) may be rewritten as

$$K_x(y) = (a_o+a_1\eta+a_2\eta^2+a_3\eta^3+\ldots a_m\eta^m)-(a_1+2a_2\eta+3a_3\eta^2+4a_4\eta^3+ \ldots a_m[{}^m_1]\eta^{m-1})y+(a_2+3a_3\eta+6a_4\eta^2+\ldots a_m[{}^m_2]\eta^{m-2})y^2- (a_3+4a_4\eta+\ldots a_m[{}^m_3]\eta^{m-3})y^3+\ldots(a_m[{}^m_m]\eta^{m-m})y^m. \quad (71)$$

If we set

$$\nu_j = \sum_{j=0}^{m}[{}^i_j]a_i\eta^{i-j}\cdot(-1)^j, \quad (72)$$

Eq.(71) can be expressed as

$$K_x(y) = \sum_{j=0}^{m}\nu_j y^j = \sum_{j=0}^{m}\nu_j(r\sin\theta)^j = K_x(r,\theta). \quad (74)$$

Similarly, for $K_y(y)$ with

$$\mu_j = \sum_{j=0}^{n}[{}^i_j]b_i\eta^{i-j}\cdot(-1)^j, \quad (75)$$

we have

$$K_y(y) = \sum_{j=0}^{n}\mu_j y^j = \sum_{j=0}^{n}\mu_j(r\sin\theta)^j = K_y(r,\theta). \quad (76)$$

IV.B. The Critical Height of a Toe-Spiral

A spiral that begins somewhere in the α-portion and terminates at the base of the β-portion of the slope shall be referred to as a toe-spiral. With the toe-spiral prescribed as the failure surface, together with the seismic profiles specified along the slope, the critical height of the slope may be derived.

The critical height of a toe-spiral is the height of the slope at which such a failure mechanism can be developed so that the soil mass resting upon the failure surface will be carried down in the fashion of pure rotation. Yielding impends when the loads from the rotating mass perform external work at a rate equal to the internal rate of energy dissipation in the mechanism. It is then only neccessary to impose a virtually small rotational velocity to the rotational block, and require that the energy rate equilibrium be observed. Equating of the external work rate to the internal dissipation rate will provide the basis for the calculation of the critical height.

By means of superposition, the rate of external work done contributed by the rotating soil mass DBED (Figs.12,13 & 14) can be found as the rate of work done by ABEFA (the gross work rate), minus the work rate by ABDCA and CDEFC (the fictitious work rate). Considering the region of ABEFA first, we have (Fig.14):

$$\dot{W}_1 = \int d\dot{W}_{1x} + \int d\dot{W}_{1y} = \int \Omega y dF_x + \int \tfrac{1}{2}\Omega x dF_y \, , \tag{77}$$

with
$$dF_x = \gamma K_x(y) dA, \tag{78}$$

$$dF_y = \gamma K_y(y) dA, \tag{79}$$

$$x = r\cos\theta, \text{ and} \tag{80}$$

$$y = r\sin\theta\,. \tag{81}$$

Noting that

$$\begin{aligned} dy &= (dr/d\theta)\sin\theta + r\cos\theta d\theta \\ &= \sin\theta d[r_o \exp\{(\theta-\theta_o)\tan\phi\}]/d\theta + r\cos\theta d\theta \\ &= (\sin\theta\tan\phi + \cos\theta) r d\theta, \end{aligned} \tag{82}$$

and

$$dA = xdy = (\sin\theta\cos\theta\tan\phi + \cos^2\theta) r^2 d\theta, \tag{83}$$

we have

$$\int d\dot{W}_{1x} = \int_{\theta_o}^{\theta_h} \gamma\Omega K_x(y) r^3 [\sin^2\theta\cos\theta\tan\phi + \sin\theta\cos^2\theta] d\theta, \text{ and} \tag{84}$$

$$\int d\dot{W}_{1y} = \tfrac{1}{2}\gamma\Omega \int_{\theta_o}^{\theta_h} K_y(y) r^3 [\sin\theta\cos^2\theta\tan\phi + \cos^3\theta] d\theta. \tag{85}$$

For region ABDCA, we have:

$$\dot{W}_2 = \int d\dot{W}_{2x} + \int d\dot{W}_{2y} = \int_{y_B}^{y_D} \gamma\Omega K_x(y)\,[y(x_2 dy)] + \int_{y_B}^{y_D} \tfrac{1}{2}\gamma\Omega K_y(y)\,[x_2^2 dy]. \tag{86}$$

From the geometry, the expression of x_2 can be derived from

$$\tan\alpha = (y - y_B)/(x_B - x_2)\ , \tag{87}$$

so that

$$x_2 = (x_B + y_B/\tan\alpha) - y/\tan\alpha = \xi_2 - y/\tan\alpha \tag{88}$$

for

$$y_D \geqq y \geqq y_B\ . \tag{89}$$

Thus,

$$\int d\dot{W}_{2x} = \int_{y_B}^{y_D} \gamma\Omega K_x(y)[(\xi_2 - y/\tan\alpha)y]dy, \text{ and} \tag{90}$$

$$\int d\dot{W}_{2y} = \int_{y_B}^{y_D} \tfrac{1}{2}\gamma\Omega K_y(y)[(\xi_2 - y/\tan\alpha)^2]dy. \tag{91}$$

Similarly, for region CDEFC:

$$\dot{W}_3 = \int d\dot{W}_{3x} + \int d\dot{W}_{3y} = \int_{y_D}^{y_E} \gamma\Omega K_x(y)\,[y(x_3 dy)] + \int_{y_D}^{y_E} \tfrac{1}{2}\gamma\Omega K_y(y)\,[x_3^2 dy], \tag{92}$$

where from

$$\tan\beta = (y_E - y)/(x_3 - x_E) \tag{93}$$

x_3 is derived:

$$x_3 = (x_E + y_E/\tan\beta) - y/\tan\beta = \xi_3 - y/\tan\beta, \tag{94}$$

for

$$y_E \geqq y \geqq y_D \ . \tag{95}$$

Thus,

$$\int d\dot{W}_{3x} = \int_{y_D}^{y_E} \gamma\Omega K_x(y)[(\xi_3 - y/\tan\beta)y]dy, \text{ and} \tag{96}$$

$$\int d\dot{W}_{3y} = \int_{y_D}^{y_E} \tfrac{1}{2}\gamma\Omega K_y(y)[(\xi_3 - y/\tan\beta)^2]dy. \tag{97}$$

The above six equations, Eqs.(84,85,90,91,96,97), can be expanded by substituting the expressions for $K_x(y)$ and $K_y(y)$ into them:

$$\int d\dot{W}_{1x} = \int_{\theta o}^{\theta h} \gamma\Omega \sum_{j=0}^{m} [\nu_j r^{j+3}(\sin^{j+1}\theta\cos^2\theta+\sin^{j+2}\theta\cos\theta\tan\phi)]d\theta; \quad (98)$$

$$\int d\dot{W}_{1y} = \tfrac{1}{2}\int_{\theta o}^{\theta h} \gamma\Omega \sum_{j=0}^{n} [\mu_j r^{j+3}(\sin^{j}\theta\cos^3\theta+\sin^{j+1}\theta\cos^2\theta\tan\phi)]d\theta; \quad (99)$$

$$\int d\dot{W}_{2x} = \int_{y_B}^{y_D} \gamma\Omega \sum_{j=0}^{m} [\nu_j(\xi_2 y^{j+1}-y^{j+2}/\tan\alpha)]dy; \quad (100)$$

$$\int d\dot{W}_{2y} = \tfrac{1}{2}\int_{y_B}^{y_D} \gamma\Omega \sum_{j=0}^{n} [\mu_j(\xi_2^2 y^j-2\xi_2 y^{j+1}/\tan\alpha+y^{j+2}/\tan^2\alpha)]dy; \quad (101)$$

$$\int d\dot{W}_{3x} = \int_{y_D}^{y_E} \gamma\Omega \sum_{j=0}^{m} [\nu_j(\xi_3 y^{j+1}-y^{j+2}/\tan\beta)]dy; \text{ and} \quad (102)$$

$$\int d\dot{W}_{3y} = \tfrac{1}{2}\int_{y_D}^{y_E} \gamma\Omega \sum_{j=0}^{n} [\mu_j(\xi_3^2 y^j-2\xi_3 y^{j+1}/\tan\beta+y^{j+2}/\tan^2\beta)]dy. \quad (103)$$

Eqns.(98) & (99) are expressed into more consistent forms with the application of the following identities:

$$\cos^2\theta = 1-\sin^2\theta, \quad (104)$$

and

$$r = \rho[\exp(\theta\tan\phi)], \quad (105)$$

where

$$\rho = r_o\exp(-\theta_o\tan\phi). \quad (106)$$

Thus, we have

$$\int d\dot{W}_{1x} = \gamma\Omega \sum_{j=0}^{m} [\nu_j \rho^{j+3} \int_{\theta_o}^{\theta_h} e^{\theta(j+3)\tan\phi}(\sin^{j+1}\theta - \sin^{j+3}\theta + \cos\theta\sin^{j+2}\theta\tan\phi)d\theta], \qquad (107)$$

and

$$\int d\dot{W}_{1y} = \tfrac{1}{2}\gamma\Omega \sum_{j=0}^{n} [\mu_j \rho^{j+3} \int_{\theta_o}^{\theta_h} e^{\theta(j+3)\tan\phi}(\cos\theta\sin^{j}\theta - \cos\theta\sin^{j+2}\theta + \sin^{j+1}\theta\tan\phi - \sin^{j+3}\theta\tan\phi)d\theta]. \qquad (108)$$

Each of these two equations involves two integral forms, namely:

$\int e^{A\theta}\sin^B\theta\cos\theta d\theta$, and $\int e^{A\theta}\sin^B\theta d\theta$.

Their solutions are:

$$\int e^{A\theta}\sin^B\theta\cos\theta d\theta = \frac{e^{A\theta}\sin^B\theta[A\cos\theta+(B+1)\sin\theta]}{A^2+(B+1)^2} - \frac{AB}{A^2+(B+1)^2}\int e^{A\theta}\sin^{B-1}\theta d\theta, \text{ and} \qquad (109)$$

$$\int e^{A\theta}\sin^B\theta d\theta = \frac{e^{A\theta}\sin^{B-1}\theta(A\sin\theta - B\cos\theta)}{A^2+B^2} + \frac{B(B-1)}{A^2+B^2}\int e^{A\theta}\sin^{B-2}\theta d\theta. \qquad (110)$$

After some manipulation, the iterative formulas can be shown (App.C) as:

$$\int e^{A\theta}\sin^B\theta d\theta = e^{A\theta}\cdot\sum_{s=0}^{\mathrm{int}(\frac{1}{2}B)} \left[{B \atop 2s}\right](2s)!\,\frac{[A\sin\theta-(B-2s)\cos\theta]\sin^{B-2s-1}\theta}{\prod_{t=0}^{s}[A^2+(B-2t)^2]} = I[A,B]; \text{ and} \qquad (111)$$

$$\int e^{A\theta}\sin^{B}\theta\cos\theta d\theta = \frac{e^{A\theta}\sin^{B}\theta[A\cos\theta+(B+1)\sin\theta]}{A^2+(B+1)^2} - \frac{AB}{A^2+(B+1)^2}I[A,B-1]$$

$$= J[A,B]. \qquad (112)$$

Ultimately, Eqs.(107) and (108) can be reduced to the final forms:

$$\int d\dot{W}_{1x} = \gamma\Omega r_o^3 f_{1x}(r_o,\theta_o,\theta_h), \text{ and} \qquad (113)$$

$$\int d\dot{W}_{1y} = \gamma\Omega\tfrac{1}{2} r_o^3 f_{1y}(r_o,\theta_o,\theta_h), \qquad (114)$$

where

$$f_{1x}(r_o,\theta_o,\theta_h) = r_o^{-3}\cdot\sum_{j=0}^{m}\nu_j\rho^{j+3}\{I[(j+3)\tan\phi,j+1]_{\theta_o}^{\theta_h} - I[(j+3)\tan\phi,$$
$$j+3]_{\theta_o}^{\theta_h} + \tan\phi J[(j+3)\tan\phi,j+2]_{\theta_o}^{\theta_h}\}, \qquad (115)$$

and

$$f_{1y}(r_o,\theta_o,\theta_h) = r_o^{-3}\cdot\sum_{j=0}^{n}\mu_j\rho^{j+3}\{J[(j+3)\tan\phi,j]_{\theta_o}^{\theta_h} - J[(j+3)\tan\phi,j+2]_{\theta_o}^{\theta_h}$$
$$+\tan\phi I[(j+3)\tan\phi,j+1]_{\theta_o}^{\theta_h} - \tan\phi I[(j+3)\tan\phi,j+3]_{\theta_o}^{\theta_h}\}. \qquad (116)$$

Next, the coordinates of the points B, D, and E of the soil mass DBED are seen to be

$$y_B = r_o\sin\theta_o\ , \qquad (117)$$

$$y_D = r_o\sin\theta_o + L\sin\alpha, \text{ and} \qquad (118)$$

$$y_E = r_h\sin\theta_h = r_o\exp[(\theta_h-\theta_o)\tan\phi]\sin\theta_h. \qquad (119)$$

Therefore, from Eqs. (88) and (94):

$$\xi_2 = x_B+y_B/\tan\alpha = r_o(\cos\theta_o+\sin\theta_o/\tan\alpha) \quad \text{, and} \tag{120}$$

$$\xi_3 = x_E+y_E/\tan\beta = r_o\exp[(\theta_h-\theta_o)\tan\phi](\cos\theta_h+\sin\theta_h/\tan\beta). \tag{121}$$

The variable L, like H, is the geometric parameter describing the rotating soil mass DBED. From the geometrical configuration of the slope, we have the following relations:

$$r_o\cos\theta_o-r_h\cos\theta_h-H/\tan\beta-L\cos\alpha = 0; \text{ and} \tag{122}$$

$$r_h\sin\theta_h-r_o\sin\theta_o-H-L\sin\alpha= 0. \tag{123}$$

The solution of these two simultaneous equations gives explicit expressions for both L and H:

$$L = [r_o\sin(\theta_o+\beta)-r_h\sin(\theta_h+\beta)]/\sin(\beta-\alpha); \text{ and} \tag{124}$$

$$H = [r_h\sin(\theta_h+\alpha)-r_o\sin(\theta_o+\alpha)]\sin\beta/\sin(\beta-\alpha). \tag{125}$$

Then, Eqs.(100) to (103) are all in integrable forms, and can be expressed formally as

$$\int d\dot{W}_{2x} = \gamma\Omega r_o^3 f_{2x}(r_o,\theta_o,\theta_h); \tag{126}$$

$$\int d\dot{W}_{2y} = \tfrac{1}{2}\gamma\Omega r_o^3 f_{2y}(r_o,\theta_o,\theta_h); \tag{127}$$

$$\int d\dot{W}_{3x} = \gamma\Omega r_o^3 f_{3x}(r_o,\theta_o,\theta_h); \text{ and} \tag{128}$$

$$\int d\dot{W}_{3y} = \tfrac{1}{2}\gamma\Omega r_o^3 f_{3y}(r_o,\theta_o,\theta_h), \tag{129}$$

where

$$f_{2x}(r_o,\theta_o,\theta_h) = r_o^{-3} \sum_{j=0}^{m} \nu_j \left[\frac{\xi_2 y^{j+2}}{j+2} - \frac{y^{j+3}}{(j+3)\tan\alpha}\right]\Bigg|_{y_B}^{y_D} ; \tag{130}$$

$$f_{2y}(r_o,\theta_o,\theta_h) = r_o^{-3} \sum_{j=0}^{n} \mu_j \left[\frac{\xi_2^2 y^{j+1}}{j+1} - \frac{2\xi_2 y^{j+2}}{(j+2)\tan\alpha} + \frac{y^{j+3}}{(j+3)\tan^2\alpha}\right]\Bigg|_{y_B}^{y_D} ; \tag{131}$$

$$f_{3x}(r_o,\theta_o,\theta_h) = r_o^{-3} \sum_{j=0}^{m} \nu_j \left[\frac{\xi_3 y^{j+2}}{j+2} - \frac{y^{j+3}}{(j+3)\tan\beta}\right]\Bigg|_{y_D}^{y_E} ; \tag{132}$$

$$f_{3y}(r_o,\theta_o,\theta_h) = r_o^{-3} \sum_{j=0}^{n} \mu_j \left[\frac{\xi_3^2 y^{j+1}}{j+1} - \frac{2\xi_2 y^{j+2}}{(j+2)\tan\beta} + \frac{y^{j+3}}{(j+3)\tan^2\beta}\right]\Bigg|_{y_D}^{y_E} . \tag{133}$$

The total rate of external work done is now expressed as

$$\dot{W}_E = \dot{W}_1 - \dot{W}_2 - \dot{W}_3 = \int d\dot{W}_{1x} + \int d\dot{W}_{1y} - \int d\dot{W}_{2x} - \int d\dot{W}_{2y} - \int d\dot{W}_{3x} - \int d\dot{W}_{3y}, \text{ or} \tag{134}$$

$$\dot{W}_E = \gamma\Omega r_o^3 [f_{1x} + \tfrac{1}{2} f_{1y} - f_{2x} - \tfrac{1}{2} f_{2y} - f_{3x} - \tfrac{1}{2} f_{3y}]. \tag{135}$$

The next step is to calculate the rate of internal energy dissipation along the velocity discontinuity surface BE, where yielding occurs. From Eq.(2), this dissipation rate for an infinitesimal surface element is:

$$d\dot{W}_I = (\tau\dot{T} - \sigma\dot{T}\tan\phi)\, d\Delta ds, \tag{136}$$

where

$$\dot{T} = r\Omega\cos\phi/t, \tag{137}$$

with t being the extremely small thickness of the velocity transition zone resulting from the dilatation (Fig. 6). The negative sign for the second term is neccessary because σ represents the compressive normal stress while $\dot{T}\tan\phi$ stands for the outward dilatation. Since the Coulomb's criterion must be satisfied, from Eq.(3), we have

$$-\sigma\tan\phi = c - \tau. \tag{138}$$

Substituting this into Eq.(136) and integrating over the entire region of the mechanism results in

$$\int_V d\dot{W}_I = \int_S\int_0^t (cr\Omega\cos\phi/t)\,d\Delta ds = \frac{c\Omega\cos\phi}{t}\int_S r\int_0^t d\Delta ds. \tag{139}$$

Here, $d\Delta$ is the differential thickness of an element. The extremely small thickness of the transition zone is constant throughout. Noting that

$$ds = rd\theta/\cos\phi, \tag{140}$$

we have for the total internal energy dissipation rate the expression:

$$\begin{aligned}\dot{W}_I &= \frac{c\Omega}{t}\int_{\theta_o}^{\theta_h} r^2 t d\theta = c\Omega\int_{\theta_o}^{\theta_h}\{r_o\exp[(\theta-\theta_o)\tan\phi]\}^2 d\theta \\ &= \tfrac{1}{2}c\Omega r_o^2\cdot\{\exp[2(\theta_h-\theta_o)\tan\phi]-1\}/(2\tan\phi).\end{aligned} \tag{141}$$

Equating the external work rate to the internal rate of dissipation:

$$\dot{W}_E = \dot{W}_I, \tag{142}$$

we have

$$r_o = \frac{c}{\gamma}\cdot\frac{\exp[2(\theta_h-\theta_o)\tan\phi]-1}{2\tan\phi[(f_{1x}-f_{2x}-f_{3x})+\frac{1}{2}(f_{1y}-f_{2y}-f_{3y})]} \quad . \tag{143}$$

By the Upper Bound Theorem, this means that any toe-spiral satisfying the above equation will be a surface along which yielding impends. Substitution of Eq.(143) into Eq.(135) gives an expanded expression for H, the vertical distance of the knee D above the ground, or the height of the slope:

$$H = \frac{c}{\gamma}\cdot F(r_o,\theta_o,\theta_h), \tag{144}$$

where

$$F(r_o,\theta_o,\theta_h) = \frac{\sin\beta[e^{(\theta_h-\theta_o)\tan\phi}\sin(\theta_h+\alpha)-\sin(\theta_o+\alpha)][e^{2(\theta_h-\theta_o)\tan\phi}-1]}{2\tan\phi\sin(\beta-\alpha)[f_{1x}-f_{2x}-f_{3x}+\frac{1}{2}(f_{1y}-f_{2y}-f_{3y})]} \quad . \tag{145}$$

The critical height of instability is then the minimum value of H attainable for a combination of ϕ, α, and β, as well as $K_x(y)$ and $K_y(y)$. It may be written as

$$H^* \leqq \frac{c}{\gamma}\cdot N^* \quad , \tag{146}$$

with

$$N^* = \min[F(r_o,\theta_o,\theta_h)] = F(r_o^*,\theta_o^*,\theta_h^*) \quad , \tag{147}$$

such that r_o^*, θ_o^* & θ_h^* satisfy the conditions of

$$\frac{\partial F}{\partial r_o} = 0 \quad ; \quad \frac{\partial F}{\partial \theta_o} = 0 \quad ; \quad \frac{\partial F}{\partial \theta_h} = 0 \ . \tag{148}$$

The dimensionless number N^* is the seismic stability factor of the earthslope. The value of N^* is a pure number, and is dependent on ϕ, α, β, $K_x(y)$ and $K_y(y)$.

Note that when the loading force is a constant (i.e. zeroth degree polynomial in y), the function F becomes dependent on θ_o and θ_h only, and

$$F(K_x = K_y = \text{constant}) = F(\theta_o, \theta_h). \tag{149}$$

IV.C. Earthslope of Purely Cohesive Soil

A purely cohesive soil is one in which there is no internal friction (ϕ=0). It is also called the Tresca Material.

It is observed from Eq.(145) that

$$F = \frac{g(\phi)}{q(\phi)}, \tag{150}$$

where

$$g(\phi) = \sin\beta[e^{(\theta_h - \theta_o)\tan\phi}\sin(\theta_h+\alpha) - \sin(\theta_o+\alpha)][e^{2(\theta_h-\theta_o)\tan\phi} - 1], \tag{151}$$

and

$$q(\phi) = 2\tan\phi\sin(\beta-\alpha)[f_{1x}-f_{2x}-f_{3x}+\tfrac{1}{2}(f_{1y}-f_{2y}-f_{3y})]. \tag{152}$$

For $\phi=0$, function F becomes

$$F(\phi=0) = \frac{g(\phi=0)}{q(\phi=0)} = \frac{0}{0}\ . \tag{153}$$

By the l'Hôpital rule, we have

$$F(\phi=0) = \lim_{\phi\to 0}\frac{g(\phi)}{q(\phi)} = \frac{g'(0)}{q'(0)}\ . \tag{154}$$

Differentiating functions $g(\phi)$ and $q(\phi)$ from Eqs.(151) and (152) with respect to ϕ, collecting terms, and evaluating at $\phi=0$, we have

$$g'(0) = 2(\theta_h-\theta_o)[\sin(\theta_h+\alpha)-\sin(\theta_o+\alpha)]\sin\beta, \tag{155}$$

$$q'(0) = 2\sin(\beta-\alpha)[(f_{1x}-f_{2x}-f_{3x})+\tfrac{1}{2}(f_{1y}-f_{2y}-f_{3y})]\Big|_{\phi=0}. \tag{156}$$

Accordingly,

$$F(r_o,\theta_o,\theta_h)\Big|_{\phi=0} = \frac{(\theta_h-\theta_o)[\sin(\theta_h+\alpha)-\sin(\theta_o+\alpha)]\sin\beta}{\sin(\beta-\alpha)[f_{1x}-f_{2x}-f_{3x}+\tfrac{1}{2}(f_{1y}-f_{2y}-f_{3y})]\Big|_{\phi=0}}. \tag{157}$$

IV.D. Physical Ranges and Constraints

Since the problem concerned has been associated with certain geometries, it is neccessary to identify the physical constraints corresponding to the geometrical restrictions. Applicability of the analysis to physical situations are discussed in this section.

A total of eleven constraints, stemming from physical considerations, can be identified. These are:

CONSTRAINT
NO.

i) $$r_o - \frac{c}{\gamma} \cdot \frac{\exp[2(\theta_h - \theta_o)\tan\phi] - 1}{2\tan\phi[(f_{1x} - f_{2x} - f_{3x}) + \frac{1}{2}(f_{1y} - f_{2y} - f_{3y})]} = 0 \qquad (158)$$

ii) $$r_h \sin\theta_h - r_o \sin\theta_o - L\sin\alpha > 0 \qquad (159)$$

iii) $$L > 0 \qquad (160)$$

iv) $$f_{1x} - f_{2x} - f_{3x} + \frac{1}{2}(f_{1y} - f_{2y} - f_{3y}) > 0 \qquad (161)$$

v) $$L/H > 0.1 \qquad (162)$$

vi) $$H/L > 0.1 \qquad (163)$$

vii) $$\{\exp[(\theta_h - \theta_o)\tan\phi]\sin(\theta_h + \alpha) - \sin(\theta_o + \alpha)\}\sin\beta/\sin(\beta - \alpha) > 0$$

viii) $$\theta_o > \pi - 2\beta - \theta_h \qquad (165)$$

ix) $\theta_o < \pi - 2\alpha - \theta_h$; for purely cohesive soil only (166)

x) $$\theta_h > \theta_o \qquad (167)$$

xi) $H_s > H$; for the determination of the location of the most critical spiral for a slope of given height only (168)

The first constraint is the only equality constraint. It is the same as Eq.(143), which must be satisfied for spiral failure mechanisms.

The second constraint is similar to the second of the two simultaneous equations for the slope geometry, Eq.(123). Its inclusion in this list imposes the restriction that the spiral must terminate in the β-portion of the slope.

The third constraint requires that the spiral be started out in the α-zone of the slope. Thus, the second and third constraints assure the condition that the spiral traverses both zones of the slope under investigation.

A close examination of the equation for the critical height as formally stated in Eq.(146) reveals that the value for the critical height can still be illusively positive yet physically unrealistic. This is the case when both the numerator and the denominator expressions are negative-valued. In order to rule out such a possibility, the constraints number 4 & 7 are introduced. As it may seem quite redundant to use both expressions as constraints instead of just either one of these, it must be pointed out that using both can safeguard the function from assuming negative values. This is extremely important as long as the optimization process is concerned.

The fifth constraint essentially requires that the spiral not be skewed towards and along the height of the slope (that most part of it lies in the β-zone; Fig.15), whereas the sixth constraint specifies that a spiral skewing out of proportions towards and along the top of the slope (with most part inside the α-zone;Fig.15) is not acceptable. Such skewing tendencies are observable when the slope angle α is equal or close to the internal friction angle ϕ, in addition to a small β angle. The presence of these skewness usually results in critical height values that are very low. Two reasons are given to dispell such skewing spirals. The first being that for such spirals, the geometry is quite different from the ideal picture on which the derivations are based. So, results obtained may be questionable. Secondly, even if these skewed spirals are perfectly alright, the degree of hazard associated with them may not be as great as the less-skewed ones. Based on these considerations, the ratios are set as shown. Of course, they are subject to relaxations or further restrictions, according to the judgements of the investigators.

Constraint number 10 assures that the spiral does not go backward.

The eleventh constraint is only applicable when the problem is to locate the most critical failure surface in a slope of given height (Refer to Chapter VI). It assures the spiral height is not higher than the allowable height, that of the slope.

Constraints 8 & 9 are related to the physical ranges of the spiral angles θ_o & θ_h. The first of these two is more general. It is derived from a consideration of the expression for the length L, Eq.(124). For the length to be greater than zero, the following must be true:

$$\sin(\theta_o+\beta)-\exp[(\theta_h-\theta_o)\tan\phi]\sin(\theta_h+\beta) > 0. \tag{169}$$

Since $\exp[(\theta_h-\theta_o)\tan\phi] > 1,$ (170)

then $\sin(\theta_o+\beta)-\sin(\theta_h+\beta) > 0.$ (171)

This can only be satisfied if

$\theta_h > \frac{1}{2}\pi-\beta,$ (172)

and

$\theta_o+\beta > \frac{1}{2}\pi \quad ; \quad \text{or} \quad \theta_o+\beta < \frac{1}{2}\pi \ .$ (173)

The result is then for the first case:

$\theta_h > \theta_o \ ,$ (174)

which is reflected in the tenth constraint. For the second case, it is

$\theta_o+\beta > \pi-(\theta_h+\beta),$ (175)

which is Constraint number 8. As for the ninth constraint, the expression for the slope height H, Eq.(125), is used. In order that it is positive, the following must be true:

$\exp[(\theta_h-\theta_o)\tan\phi]\sin(\theta_h+\alpha)-\sin(\theta_o+\alpha) > 0.$ (176)

If the slope under investigation is composed of purely cohesive soil, then Eq.(176) becomes

$\sin(\theta_h+\alpha) > \sin(\theta_o+\alpha),$ (177)

or $$|\theta_h+\alpha-\tfrac{1}{2}\pi| < \tfrac{1}{2}\pi-(\theta_o+\alpha). \qquad (178)$$

This gives

$$\theta_o < \pi-2\alpha-\theta_h \qquad (179)$$

and $$\theta_o < \theta_h , \qquad (180)$$

which are Constraints number 9 and 10.

While much have been said of the constraints, the importance of the ranges of the independent variables r_o, θ_o, and θ_h must not be overlooked. Although no specific statement has been made in the derivations, the validity of these formulations can be easily seen to rest on the following implied variable ranges:

$$0 < r_o < \infty, \qquad (181)$$

$$\theta_o > 0, \text{ and} \qquad (182)$$

$$\theta_h < \pi. \qquad (183)$$

However , to provide greater insight into the applicability of these formulations as well as to expedite the optimization process, better refining of these ranges is neccessary. These narrowing down of the ranges can be achieved by geometric and algebraic considerations. The geometry of the model requires that the spiral be confined within the slope by the perimeter of the slope. This results in the upper and lower limit for θ_o and θ_h, respectively (Fig.16):

$$\theta_o < \tfrac{1}{2}\pi+\phi-\alpha, \tag{184}$$

$$\theta_h > \tfrac{1}{2}\pi+\phi-\beta. \tag{185}$$

The upper limit for θ_h can be further refined by next considering the expression for the slope height again, Eq.(125). To satisfy the fact that H is positive, the expression is reduced to

$$\sin(\theta_h+\alpha) > \frac{r_o}{r_h}\sin(\theta_o+\alpha), \tag{186}$$

with $\quad 0 < r_o/r_h < 1, \quad$ (187)

and the implied and established limits for θ_o. It is obvious that

$$\sin(\theta_h+\alpha) > 0, \text{ or} \tag{188}$$

$$0 < \theta_h+\alpha < \pi, \text{ or} \tag{189}$$

$$-\alpha < \theta_h < \pi-\alpha. \tag{190}$$

Accounting for the above refinements, the ranges now becomes:

$$0 < r_o < \infty, \tag{191}$$

$$0 < \theta_o < \tfrac{1}{2}\pi+\phi-\alpha, \text{ and} \tag{192}$$

$$\tfrac{1}{2}\pi+\phi-\beta < \theta_h < \pi-\alpha. \tag{193}$$

These restrictions should further reduce the efforts needed in the optimization.

CHAPTER V. SPECIAL SPIRAL-SLOPE CONFIGURATIONS

The discussions presented in Chapter IV pertain essentially to failure mechanisms with the ending at the toe of the slope. However, for special cases, it is possible that the spiral may terminate at some distance vertically above the toe, or even stretched horizontally away from the toe.

V.A. Sagging Spiral

Before discussing the special cases mentioned above, it is worth noting yet another possibility, the case of a sagging spiral (Fig.17). A spiral will be termed "sagging" if its point vertically farthest away from the origin (M in Fig.17) is not its endpoint E. This point of the largest vertical distance is a stationary point in the spiral:

$$y = r\sin\theta = r_o\exp[(\theta-\theta_o)\tan\phi]\sin\theta. \qquad (194)$$

This point which corresponds to the maximum of y, is determined by solving the equation:

$$dy/d\theta = 0 = r_o\exp[(\theta-\theta_o)\tan\phi](\tan\phi\sin\theta+\cos\theta). \qquad (195)$$

The solution is

$$\theta_m = \tfrac{1}{2}\pi+\phi. \qquad (196)$$

From this, a criterion can be set to determine whether a given spiral is sagging or not. Clearly, we have

ordinary spiral : $\theta_h \leqq \theta_m$

sagging spiral : $\theta_h > \theta_m$

In view of the possibility of having a sagging spiral failure surface, it is important that the analytical procedure developed for ordinary spiral failure surfaces be re-examined to determine its applicability to the case of sagging spirals. That the procedure is equally applicable to both cases is easily demonstrated. We note that the evaluation of the external work rate contributed by the soil block BMEDB (Fig.17), defined by the spiral and part of the perimeter of the slope, is equivalent to the evaluation of the area inside two curves $\Psi_1(y)$ and $\Psi_2(y)$. See Appendix B. In the case of the ordinary spiral, the external work rate is calculated formally:

$$\dot{W}_1 = \int d\dot{W}_{1x} + \int d\dot{W}_{1y} \; ; \text{ for } y_B \leqq y \leqq y_E \text{ , with boundary } \Psi_1(y). \tag{197}$$

$$\left.\begin{array}{l} \dot{W}_2 = \int d\dot{W}_{2x} + \int d\dot{W}_{2y} \; ; \text{ for } y_B \leqq y \leqq y_D \\ \dot{W}_3 = \int d\dot{W}_{3x} + \int d\dot{W}_{3y} \; ; \text{ for } y_D \leqq y \leqq y_E \end{array}\right\} \text{ with boundary } \Psi_2(y). \tag{198}$$

For the case of a sagging spiral (Fig.17), it is convenient to truncate the portion of $\Psi_1(y)$ at point M, and add the remaining portion of the curve to $\Psi_2(y)$, such that

$$(\dot{W}_1)_1 = \int d\dot{W}_1 \ ; \text{ for } y_B \leqq y \leqq y_m \text{ , with boundary } \Psi_1(y);$$

$$(\dot{W}_1)_2 = \int d\dot{W}_1 \ ; \text{ for } y_E \leqq y \leqq y_m \text{ , with boundary } \Psi_2(y);$$

with $$\dot{W}_1 = (\dot{W}_1)_1+(\dot{W}_1)_2 \ . \tag{199}$$

$$\left.\begin{aligned} \dot{W}_2 &= \int d\dot{W}_2 \ ; \text{ for } y_B \leqq y \leqq y_D \text{ , with boundary } \Psi_2(y) \\ \dot{W}_3 &= \int d\dot{W}_3 \ ; \text{ for } y_D \leqq y \leqq y_E \text{ , with boundary } \Psi_2(y) \end{aligned}\right\} \tag{200}$$

Therefore,

$$\begin{aligned} \dot{W}_E &= \int_{\theta_o}^{\theta_m} d\dot{W}_1 - \int_{\theta_h}^{\theta_m} d\dot{W}_1 - \int_{y_B}^{y_D} d\dot{W}_2 - \int_{y_D}^{y_E} d\dot{W}_3 \\ &= \int_{\theta_o}^{\theta_m} d\dot{W}_1 + \int_{\theta_m}^{\theta_h} d\dot{W}_1 - \int_{y_B}^{y_D} d\dot{W}_2 - \int_{y_D}^{y_E} d\dot{W}_3 \\ &= \int_{\theta_o}^{\theta_h} d\dot{W}_1 - \int_{y_B}^{y_D} d\dot{W}_2 - \int_{y_D}^{y_E} d\dot{W}_3 \end{aligned} \tag{201}$$

Formally, this is the same as Eq.(134). Thus, the same formula may be treated for both the case of the sagging spiral and the ordinary spiral. In these cases, the formula is applicable only when the entire length of the spiral is above the ground level.

The exception taken in the last statement is justified by the constant seismic force beneath the ground level; in contrary to the variation of the seismic coefficient above the ground, with the elevation. This essentially divides the seismic coefficients into two regions (Fig.17):

$$K_x(h) = \begin{cases} a_o & ; \text{ for } h \leqq 0 \\ a_o + \sum_{j=1}^{m} a_j h^j & ; \text{ for } h > 0 \end{cases} \tag{202}$$

$$K_y(h) = \begin{cases} b_o & ; \text{ for } h \leqq 0 \\ b_o + \sum_{j=1}^{n} b_j h^j & ; \text{ for } h > 0 \end{cases} \tag{203}$$

or

$$K_x(y) = \begin{cases} a_o & ; \text{ for } y \geqq \eta \\ \sum_{j=0}^{m} \nu_j y^j & ; \text{ for } y < \eta \end{cases} \tag{204}$$

$$K_y(y) = \begin{cases} b_o & ; \text{ for } y \geqq \eta \\ \sum_{j=0}^{n} \mu_j y^j & ; \text{ for } y < \eta \end{cases} \tag{205}$$

A close examination of the geometry of the earthslope and the possible combinations of relative position between the slope and the spiral failure surface reveals that there are basically four major categories of spiral failure mechanisms. These are illustrated in Fig.18 and are categorized as follows:

i) normal --- (a) the spiral terminates at the toe and there is no sagging ($\theta_h \leqq \theta_m, \eta = r_h \sin\theta_h$).

(b) the spiral ends some elevations above the ground and there is no sagging ($\theta_h \leqq \theta_m$, $\eta > r_h \sin\theta_h$).

(c) the spiral is sagging, but its end is raised and it has no point below the ground ($\theta_h > \theta_m$, $\eta > r_m \sin\theta_m$).

ii) partially sunken --- the spiral is sagging; despite the elevation of its end above the ground, part of its length is below the ground ($\theta_h > \theta_m$, $r_h \sin\theta_h < \eta < r_m \sin\theta_m$).

iii) sunken --- the spiral is sagging, ends at the toe, and the portion between the end and a certain point is completely below the ground ($\theta_h > \theta_m$, $r_h \sin\theta_h = \eta < r_m \sin\theta_m$, $d=0$).

iv) stretched --- the spiral is sagging, ends some horizontal distance d from the toe, and the portion between the end and a certain point is completely grounded ($\theta_h > \theta_m$, $d > 0$, $r_h \sin\theta_h = \eta < r_m \sin\theta_m$).

V.B. Raised Spiral

A spiral which has its end at an elevation above the toe of the slope is hereby referred to as a raised spiral. Typical slopes are shown in Fig.18,i.b,i.c and ii. For such a spiral, the two simultaneous equations, Eqs.(122) and (123), governing the dimensions of the rotating block are unchanged. In fact, only minor modification of the formulations need be made.

The modified expression for η is

$$\eta = r_o \exp[(\theta_h-\theta_o)\tan\phi]\sin\theta_h + H_T \ , \tag{206}$$

where H_T is the height of the raised spiral terminal. Corresponding changes in the expression for H^* are:

$$H = \frac{c}{\gamma}\cdot F(r_o,\theta_o,\theta_h,H_T), \tag{207}$$

with

$$F(r_o,\theta_o,\theta_h,H_T) = H_T +$$

$$\frac{\sin\beta[e^{(\theta_h-\theta_o)\tan\phi}\sin(\theta_h+\alpha)-\sin(\theta_o+\alpha)][e^{2(\theta_h-\theta_o)\tan\phi}-1]}{2\tan\phi\sin(\beta-\alpha)[f_{1x}-f_{2x}-f_{3x}+\frac{1}{2}(f_{1y}-f_{2y}-f_{3y})]}, \tag{208}$$

such that $\quad H^* \leq \frac{c}{\gamma}\cdot N^* \ ,$ (209)

where $\quad N^* = \min[F(r_o,\theta_o,\theta_h,H_T)] = F(r_o^*,\theta_o^*,\theta_h^*,H_T^*).$ (210)

In addition, r_o^*, θ_o^*, θ_h^*, H_T^* must satisfy the conditions:

$$\frac{\partial F}{\partial r_o} = 0 \; ; \quad \frac{\partial F}{\partial \theta_o} = 0 \; ; \quad \frac{\partial F}{\partial \theta_h} = 0 \; ; \quad \frac{\partial F}{\partial H_T} = 0 \; . \tag{211}$$

These modifications are sufficiently general and would include the toe spiral as a special case (H_T=0). When the raised spiral qualifies for the first category as a normal spiral, no modification is needed.

For the spiral of the third category, (Fig.18.iii), the sunken spiral, the raised height is zero, but the spiral cuts through the ground level once. Referring to the angle corresponding to the ground level point G (Fig.17) of the spiral as θ_g, the external work rate (gross) can be modified as

$$\int_{\theta_o}^{\theta_h} d\dot{W}_1 = \int_{\theta_o}^{\theta_g} d\dot{W}_{1A} + \int_{\theta_g}^{\theta_h} d\dot{W}_{1B} \; , \tag{212}$$

where

$$\int_{\theta_o}^{\theta_g} d\dot{W}_{1A} = \gamma\Omega r_o^3 [f_{1x}(r_o,\theta_o,\theta_h)\Big|_{\theta_o}^{\theta_g} + \tfrac{1}{2} f_{1y}(r_o,\theta_o,\theta_h)\Big|_{\theta_o}^{\theta_g}], \tag{213}$$

$$\int_{\theta_g}^{\theta_h} d\dot{W}_{1B} = \int_{\theta_g}^{\theta_h} \gamma\Omega a_o r^3 [\sin^2\theta\cos\theta\tan\phi + \sin\theta\cos^2\theta] d\theta \; + \tfrac{1}{2}\int_{\theta_g}^{\theta_h} \gamma\Omega b_o r^3 [\sin\theta\cos^2\theta\tan\phi + \cos^3\theta] d\theta \tag{214}$$

$$= \gamma\Omega r_o^3 [f_{1x}^B(r_o,\theta_o,\theta_h)\Big|_{\theta_g}^{\theta_h} + \tfrac{1}{2} f_{1y}^B(r_o,\theta_o,\theta_h)\Big|_{\theta_g}^{\theta_h}], \tag{215}$$

with

$$f^B_{1x}(r_o,\theta_o,\theta_h)\Big|_{\theta_g}^{\theta_h} = r_o^{-3}a_o\rho^3\{I[3\tan\phi,1]\Big|_{\theta_g}^{\theta_h}-I[3\tan\phi,3]\Big|_{\theta_g}^{\theta_h}+$$

$$\tan\phi J[3\tan\phi,2]\Big|_{\theta_g}^{\theta_h}\}, \tag{216}$$

$$f^B_{1y}(r_o,\theta_o,\theta_h)\Big|_{\theta}^{\theta_h} = r_o^{-3}b_o\rho^3\{J[3\tan\phi,0]\Big|_{\theta_g}^{\theta_h}-J[3\tan\phi,2]\Big|_{\theta_g}^{\theta_h}+$$

$$\tan\phi I[3\tan\phi,1]\Big|_{\theta_g}^{\theta_h}-\tan\phi I[3\tan\phi,3]\Big|_{\theta_g}^{\theta_h}, \tag{217}$$

Thus, the earlier equations for $\dot{W}_1$, Eqs.(113) and (114), can still be used, as long as the Eqs.(115) and (116) are modified as

$$f_{1x}(r_o,\theta_o,\theta_h)\Big|_{\theta_o}^{\theta_h} = f_{1x}(r_o,\theta_o,\theta_h)\Big|_{\theta_o}^{\theta_g}+f^B_{1x}(r_o,\theta_o,\theta_h)\Big|_{\theta_g}^{\theta_h}, \tag{218}$$

$$f_{1y}(r_o,\theta_o,\theta_h)\Big|_{\theta_o}^{\theta_h} = f_{1y}(r_o,\theta_o,\theta_h)\Big|_{\theta_o}^{\theta_g}+f^B_{1y}(r_o,\theta_o,\theta_h)\Big|_{\theta_g}^{\theta_h}, \tag{219}$$

The ground point angle θ_g can be found from the following equation derived from the geometry:

$$G_1 = r_o e^{(\theta_h-\theta_o)\tan\phi}\sin\theta_h - r_o e^{(\theta_g-\theta_o)\tan\phi}\sin\theta_g = 0 \tag{220}$$

The elevation is to be carried out with Newton's iterative root finding method:

$$\theta_g^{(n+1)} = \theta_g^{(n)} - G_1/G_1' , \tag{221}$$

$$G_1' = dG_1/d\theta_g = r_o e^{(\theta_g-\theta_o)\tan\phi}(\tan\phi\sin\theta_g+\cos\theta_g). \tag{222}$$

The superscripts stand for the iteration number. For the initiation of the iteration process, or at the zeroth iteration, $\theta_g^{(0)}$ can be estimated by assuming that

$$\theta_h - \theta_m \simeq \theta_m - \theta_g . \tag{223}$$

So $$\theta_g^{(0)} = 2\theta_m - \theta_h = \pi+2\phi-\theta_h. \tag{224}$$

Since the possibility of divergency exists in Newton's method, the following bounds will assure that such possibility will be eliminated:

$$\theta_o < \theta_g < \theta_m. \tag{225}$$

For the spiral of the second category, the partially sunken spiral (Fig.18.ii), the raised height is non-zero and the spiral cuts through the ground level twice. Referring to the angles corresponding to the ground level points G_1 and G_2 as θ_{g1} and θ_{g2}, respectively, we have the following expressions for the functions f_{1x} and f_{1y} associated with the gross external work rate:

$$f_{1x}(r_o,\theta_o,\theta_h)\Big|_{\theta_o}^{\theta_h} = f_{1x}(r_o,\theta_o,\theta_h)\Big|_{\theta_o}^{\theta_{g1}} + f_{1x}^B(r_o,\theta_o,\theta_h)\Big|_{\theta_{g1}}^{\theta_{g2}} + f_{1x}(r_o,\theta_o,\theta_h)\Big|_{\theta_{g2}}^{\theta_h}, \tag{226}$$

$$f_{1y}(r_o,\theta_o,\theta_h)\Big|_{\theta_o}^{\theta_h} = f_{1y}(r_o,\theta_o,\theta_h)\Big|_{\theta_o}^{\theta_{g1}} + f_{1y}^B(r_o,\theta_o,\theta_h)\Big|_{\theta_{g1}}^{\theta_{g2}} + f_{1y}(r_o,\theta_o,\theta_h)\Big|_{\theta_{g2}}^{\theta_h}, \tag{227}$$

The angles θ_{g1} and θ_{g2} can be found from the following equation of geometric consideration:

$$G_2 = r_o e^{(\theta_h-\theta_o)\tan\phi} \sin\theta_h + H_T - r_o e^{(\theta_g-\theta_o)\tan\phi} \sin\theta_g = 0. \qquad (228)$$

As before, the evaluation formula is Newton's iterative formula:

$$\theta_{g1,2}^{(n+1)} = \theta_{g1,2}^{(n)} - G_2/G_2' , \qquad (229)$$

where $\quad G_2' = G_1' . \qquad (230)$

The initial estimation for θ_{g1} and θ_{g2} are made in a similar procedure as before:

$$\theta_{g1}^{(0)} = 2\theta_m - \theta_h , \text{ and} \qquad (231)$$

$$\theta_{g2}^{(0)} = 2\theta_m - \theta_{g1} . \qquad (232)$$

Their safety range for convergency are

$$\theta_o < \theta_{g1} < \theta_m , \text{ and} \qquad (233)$$

$$\theta_m < \theta_{g2} < \theta_h . \qquad (234)$$

V.C. Stretched Spiral

When the end of a spiral is stretched a horizontal distance d away from the toe, the two simultaneous equations for geometry are changed to

$$r_o\cos\theta_o - r_h\cos\theta_h - H/\tan\beta - d - L\cos\alpha = 0, \tag{235}$$

$$r_h\sin\theta_h - r_o\sin\theta_o - H - L\sin\alpha = 0. \tag{236}$$

Solving these equations simultaneously, we obtain

$$L = [r_o\sin(\theta_o+\beta) - r_h\sin(\theta_h+\beta) - d\cdot\sin\beta]/\sin(\beta-\alpha), \tag{237}$$

and

$$H = [r_h\sin(\theta_h+\alpha) - r_o\sin(\theta_o+\alpha) + d\cdot\sin\alpha\sin\beta]\sin\beta/\sin(\beta-\alpha), \tag{238}$$

$$\text{with} \quad 0 \leqq d < \infty; \quad \theta_m < \theta_h < \pi-\alpha. \tag{239}$$

Accordingly, for the formulation of x_E, used in Eq.(121), modification is neccessary:

$$x_E = r_h\cos\theta_h + d, \tag{240}$$

where it is noted that $r_h\cos\theta_h$ is negative because θ_h is larger than $\frac{1}{2}\pi$.

Also, since the spiral is sagging, the formulation for $\dot{W}_1$ must be modified as in Eqs.(212) to (219) for the sunken spiral. Eq.(144) now becomes

$$H = \frac{c}{\gamma}\cdot F(r_o,\theta_o,\theta_h,d), \text{ with} \tag{241}$$

$$F(r_o,\theta_o,\theta_h,d) = \frac{d\cdot\sin\alpha\sin\beta}{\sin(\beta-\alpha)} + \frac{\sin\beta[e^{(\theta_h-\theta_o)\tan\phi}\sin(\theta_h+\alpha)-\sin(\theta_o+\alpha)][e^{2(\theta_h-\theta_o)\tan\phi}-1]}{2\tan\phi\sin(\beta-\alpha)[f_{1x}-f_{2x}-f_{3x}+\frac{1}{2}(f_{1y}-f_{2y}-f_{3y})]} \tag{242}$$

The critical height H^* of the stretched slope is

$$H^* \leqq \frac{c}{\gamma} \cdot N^*, \text{ where} \tag{243}$$

$$N^* = \min[F(r_o, \theta_o, \theta_h, d)] = F(r_o^*, \theta_o^*, \theta_h^*, d^*), \tag{244}$$

such that r_o^*, θ_o^*, θ_h^*, d^* satisfy the conditions:

$$\frac{\partial F}{\partial r_o} = 0 \ ; \quad \frac{\partial F}{\partial \theta_o} = 0 \ ; \quad \frac{\partial F}{\partial \theta_h} = 0 \ ; \quad \frac{\partial F}{\partial d} = 0. \tag{246}$$

In addition, since a stretched spiral is neccessarily a sagging spiral, the range for θ_h must be restricted as

$$\theta_m < \theta_h < \pi - \alpha. \tag{247}$$

The other ranges and constraints for the simple toe spiral still apply.

CHAPTER VI. THE MOST CRITICAL SLIP SURFACE FOR A GIVEN EARTHSLOPE

The determination of the critical height for a slope of given geometry and soil properties is useful in that it provides valuable criteria for the safety design of earthslope structures. However, for an existing earthslope, it would be more vital to be able to predict the most critical failure surface under a given seismic load. Investigations of the cumulative soil mass displacement of a slope during an earthquake, similar to those suggested in Ref.[7] and [10], may be carried out.

To accommodate the analysis of the critical slip surface, in particular to determine the location of the probable failure of the existing slope, only a few modifications have to be made to the analysis presented in the preceding chapters. Foremost, we have to set:

$$\eta = r_o \sin\theta_o + L\sin\alpha + H_s \, , \qquad (248)$$

where H_s is the height of the given slope and L is as defined in Eq.(124). In addition, H_T, the elevation of the end point of the spiral above the ground, is now no longer an independent variable, but is given as

$$H_T = H_s - r_h \sin\theta_h . \qquad (249)$$

With these changes introduced, the rest of the formulations for the critical height of a toe-spiral can be used as discussed in Chapter V.

As for H^*, it is now defined as the vertical distance between the knee of the slope and the end of the most critical spiral. It can thus be used to specify the dimension of the most critical rotating block of soil mass.

In addition to the modifications to the formulations, an additional physical constraint must be recognized, namely:

$$H_s \geqq H^* \tag{250}$$

Adding this extra constraint to the original constraints assures that the height of the potential failure surface is not higher than the physical height of the slope.

CHAPTER VII. CALCULATED RESULTS AND DISCUSSIONS

In order that the formulations developed in this study can be readily applicable to related investigations, computer coding has been implemented. A listing of the computer program and some selected sample outputs are included in the appendices for easy references. An in-house optimization subroutine BIASLIB, developed by the Purdue University School of Mechanical Engineering, Ref.[23], has been used in the program. The program itself has been subjected to testings and debuggings, and should contain a minimum of residual errors.

A total of nine cases were investigated. Their results are tabulated in this thesis.

The first two of these cases deal with a static situation, with gravity as the sole influencing force. The stability factors associated with dead-weight induced collapse were calculated. For the static case, the loading profiles for the vertical and horizontal components are

$$K_y(h) = 1.0 \tag{251}$$

$$K_x(h) = 0.0 \tag{252}$$

Data for this simple loading are in abundance. The purpose here is to provide an indication on how good results from the new model agree with the existing ones. Such a comparison is possible because the present model is quite general and that the dead-weight collapse is but one special case. As shown in Tables 1 and 2, the stability factors are in good agreement with the published values (Ref.[15]), both for the non-stretched and the stretched spirals.

Also listed in these two tables are the coordinates and dimensional parameters of the spirals. These parameters are useful because they provide valuable insight into the estimation of the coordinates of the most critical spiral for a slope of similar geometry and properties. The estimation corresponds to the choice of a feasible starting point for the optimization process. This optimization process can be quite sensitive to the choice taken.

Tables 3 and 4 present the results for the cases of constant and linear pseudo-seismic profiles. The constant seismic profile is taken so that

$$K_y(h) = 1.0 \tag{253}$$

$$K_x(h) = 0.325 \tag{254}$$

Again, the stability factors obtained from our analysis are in good agreement with the published values (Ref.[17]).

It should be noted that for the linear profile, the profile itself is not the same for each slope. Instead, shorter slopes have steeper profiles as tall slopes have more gentle ones. This is due to the fact that the first published data (Ref.[17]) for a linear profile were obtained by imposing on the slopes a maximum of four zones of equal thickness. These zones are of different seismic coefficient values (K_{x1}=0.25, K_{x2}=0.30, K_{x3}=0.35, K_{x4}=0.40) to approximate the original profile of linear variation (Fig.2). Such a zone-restricting technique, which distributes the seismic load linearly through the slope height, tends to subject shorter slopes to heavier seismic loadings.

While it is neccessary to ascertain the validity of the philosophy underlying this technique, we dispense with the philosophical arguments and still use the published data to check the results of our study. For this comparative study, we first identify the equation of the seismic profile for the slope configuration for a published critical height. Thus, if the seismic coefficients for the slope are of the form

$$K_y(h) = 1.0, \text{ and} \tag{255}$$

$$k_x(h) = b_o+b_1h, \tag{256}$$

we may use equivalent data from the published data by arbitrarily fixing as conditions the following:

$$\text{at } H^*/8 : \quad K_x(H^*/8) = b_o + b_1(H^*/8) = 0.25 \tag{257}$$

$$\text{at } 7H^*/8 : \quad K_x(7H^*/8) = b_o + b_1(7H^*/8) = 0.40 \tag{258}$$

Solving these equations simultaneously, the coefficients b_o and b_1 are determined:

$$b_o = 0.225, \text{ and} \qquad b_1 = 0.20/H^* \tag{259}$$

This, of course, reflects the inverse relationship between the height of the slope and the seismic loading intensity. With the loading profile for each slope calculated as indicated above, the critical height can be analyzed using the new model formulated. Calculated results compare well with the previous published data as shown in Table 4.

The data in Table 5 reflect the reductions in critical heights resulting from a more realistic seismic profile (Fig.19). This profile was given in Ref.[8] and [10] for earthdams up to 300 feet tall. The equation of the profile can be approximated, between 0 and 50 feet of height, as

$$K_y(h) = 1.0 \tag{260}$$

$$K_x(h) = 0.0057+0.0084h-0.000076h^2+0.00000032h^3, \tag{261}$$

which is sufficiently accurate for the slope configurations studied. The data obtained are shown to be larger (from 1.5 to 2.5 times) than those for the constant profile of 0.325

in Table 3. On the other hand, they are less than those for the static case, as expected.

Tables 6 and 7 exhibit data corresponding, respectively, to the following loading profiles:

$$K_y(h) = 1.0+0.1K_x(h) \tag{262}$$

$$K_x(h) = 0.0057+0.0084h-0.000076h^2+0.00000032h^3 \tag{263}$$

and

$$K_y(h) = 1.0+0.5K_x(h) \tag{264}$$

$$K_x(h) = 0.0057+0.0084h-0.000076h^2+0.00000032h^3 \tag{265}$$

These calculations were made to understand the effect of a weak vertical seismic component on the critical height. The results indicate that while there are decreases in the values for an increase of the vertical component, these decreases are generally not too significant. This insignificant effect can be observed for a vertical component as strong as half the magnitude of the horizontal one. There are also relatively no significant change in the spiral coordinates. These small changes may be due to the fact that the two component profiles were assumed to be similar. Therefore any statements extracted from these two tables may not be general enough to warrant the omission of the vertical component profile in future works, as they might be quite different in real life. More detailed investigations concerning the vertical loadings should be made in the future when such profiles are available.

Tables 8 and 9 are the tabulations of the locations of the most critical slip surface in slopes of different configurations. The height of the slope was given as 30 feet in Table 8 and 50 feet in Table 9. Under loadings specified by Eqs.(260) and (261), the soil near the top of the slope experience the worst conditions and is the most likely place for a spiral to develop. The two tables reflect this fact and also the reductions in spiral heights as a result of the more intense loadings of a taller slope.

In all these tables, some more or less common features can be observed. They are:

i) stretched spirals are present only in slopes with low angle of internal friction, ϕ, and small slope angle β;

ii) sagging spirals are also found only when ϕ and β are small, but their ranges are usually larger than those of the stretched ones;

iii) partially sunken spirals have not been studied completely so far.

A close examination reveals a relatively general pattern for the variations of the spiral coordinates for similar configurations and loading conditions. This may be helpful in choosing the feasible starting points for future analyses with the computer coding.

Table 1. Stability Factor $N^* = H^*(\gamma/c)$ for Dead-Weight Induced Failure, Through Non-stretched Spirals.

Loading Profiles: $K_x = 0.$
$K_y = 1.$

ϕ	α	β	N^*	N^* (publ.)†	$\frac{\gamma}{c}L^*$	$\frac{\gamma}{c}r_o^*$	θ_o^*	θ_h^*	θ_g^*
(degrees)							(	radians	)
0	0	30	6.43	(6.51)	6.54	11.70	0.288	2.156	0.986
		60	5.25	(5.25)	4.37	7.73	0.327	1.581	1.561
		90	3.83	(3.83)	3.50	10.02	0.479	1.003	-----
5	0	30	9.14	(9.13)	5.75	14.98	0.427	2.048	1.259
		60	6.16	(6.16)	4.17	8.41	0.386	1.563	-----
		90	4.19	(4.19)	3.47	10.77	0.529	1.026	-----
10	0	30	13.50	(13.50)	5.58	21.31	0.571	1.986	1.497
		60	7.26	(7.26)	4.04	9.25	0.447	1.561	-----
		90	4.58	(4.58)	3.44	11.56	0.579	1.062	-----
	10	30	12.99	(12.89)	11.89	27.67	0.671	1.942	1.544
		60	6.99	(6.99)	5.17	9.96	0.445	1.562	-----
		90	4.47	(4.47)	3.92	10.45	0.521	1.105	-----
15	0	30	21.67	(21.69)	5.77	34.93	0.732	1.939	1.725
		60	8.63	(8.63)	3.96	10.31	0.512	1.568	-----
		90	5.02	(5.02)	3.42	12.35	0.630	1.081	-----
	10	30	21.16	(21.14)	9.26	36.60	0.730	1.945	1.718
		60	8.38	(8.38)	4.87	10.86	0.506	1.580	-----
		90	4.91	(4.91)	3.82	11.19	0.577	1.122	-----
20	0	30	41.22	(41.22)	6.46	73.65	0.917	1.891	-----
		60	10.39	(10.39)	3.91	11.68	0.581	1.580	-----
		90	5.51	(5.50)	3.40	13.30	0.684	1.110	-----
	10	30	40.69	(40.69)	8.93	73.61	0.904	1.896	-----
		60	10.16	(10.16)	4.68	12.13	0.573	1.587	-----
		90	5.40	(5.40)	3.75	12.01	0.634	1.144	-----
	20	30	38.81	(38.64)	18.63	76.15	0.887	1.909	-----
		60	9.79	(9.74)	7.31	16.01	0.669	1.570	-----
		90	5.24	(5.24)	4.38	11.18	0.586	1.188	-----
25	0	30	120.64	(119.9)	11.74	300.15	1.160	1.820	-----
		60	12.74	(12.74)	3.89	13.55	0.655	1.595	-----
		90	6.06	(6.06)	3.39	14.30	0.739	1.141	-----
	10	30	119.33	(119.4)	12.02	286.17	1.139	1.824	-----
		60	12.52	(12.52)	4.57	13.92	0.647	1.599	-----
		90	5.95	(5.95)	3.68	12.91	0.692	1.169	-----
	20	30	117.28	(117.4)	22.88	294.68	1.138	1.823	-----
		60	12.14	(12.14)	5.91	14.74	0.646	1.605	-----
		90	5.80	(5.80)	4.22	11.95	0.647	1.203	-----

Table 1. (cont'd)

ϕ	α	β	N^*	N^* (publ.)†	$\frac{\gamma}{c}L^*$	$\frac{\gamma}{c}r_o^*$	θ_o^*	θ_h^*	θ_g^*
(degrees)							(	radians	)
30	0	60	16.04	(16.04)	3.90	16.24	0.735	1.612	-----
		90	6.69	(6.69)	3.37	15.42	0.794	1.173	-----
	10	60	15.82	(15.82)	4.50	16.54	0.727	1.614	-----
		90	6.59	(6.59)	3.63	13.99	0.754	1.195	-----
	20	60	15.47	(15.47)	5.64	17.20	0.724	1.617	-----
		90	6.44	(6.44)	4.09	12.86	0.711	1.222	-----
	30	60	14.78	(14.78)	8.41	19.09	0.737	1.623	-----
		90	6.22	(6.22)	4.95	12.20	0.672	1.258	-----
35	0	60	20.94	(20.94)	3.94	20.43	0.822	1.630	-----
		90	7.42	(7.42)	3.36	16.70	0.851	1.205	-----
	10	60	20.73	(20.73)	4.49	20.69	0.815	1.631	-----
		90	7.32	(7.32)	3.58	15.26	0.816	1.222	-----
	20	60	20.40	(20.40)	5.51	21.22	0.811	1.633	-----
		90	7.19	(7.19)	4.04	15.27	0.800	1.234	-----
	30	60	19.78	(19.78)	7.67	22.57	0.814	1.635	-----
		90	6.98	(6.[illegible]9)	4.70	13.08	0.739	1.272	-----
40	0	60	28.92	(28.91)	4.03	27.69	0.918	1.647	-----
		90	8.29	(8.29)	3.33	17.84	0.906	1.239	-----
	10	60	28.71	(28.71)	4.56	27.91	0.913	1.648	-----
		90	8.19	(8.19)	3.54	16.58	0.878	1.252	-----
	20	60	28.39	(28.39)	5.50	28.37	0.908	1.649	-----
		90	8.06	(8.06)	3.90	15.41	0.847	1.268	-----
	30	60	27.82	(27.82)	7.35	29.40	0.907	1.650	-----
		90	7.87	(7.87)	4.55	15.42	0.830	1.279	-----
	40	60	26.46	(26.45)	12.05	31.82	0.908	1.654	-----
		90	7.56	(7.56)	5.73	13.69	0.779	1.320	-----

† Data published by Chen et al., [14] and [15].

Table 2. Stability Factor $N^*=(\gamma/c)H^*$ for Dead-Weight Induced Failure, Through Stretched Spirals.

Loading profiles: $K_x = 0.$ $K_y = 1.$

ϕ	α	β	N^*	N^*	$\frac{\gamma}{c}L^*$	$\frac{\gamma}{c}r_o^*$	θ_o^*	θ_h^*	θ_g^*	$\frac{\gamma}{c}d^*$
(degrees)				(publ.)†			(-	radians	)	
0	0	15	5.60	(5.53)	42.85	56.64	0.349	2.688	0.456	40.34
		30	5.56	(5.53)	32.81	39.77	0.332	2.657	0.484	30.36
		45	5.53	(5.53)	51.48	57.75	0.352	2.685	0.456	49.05
5	0	15	14.38	(14.38)	10.15	45.67	0.627	2.242	1.053	5.90
		30	9.13	(9.13)	6.09	15.21	0.402	2.119	1.184	1.30
		45	7.35	(7.35)	4.69	9.97	0.372	1.817	1.498	0.00
	5	15	13.71	(13.71)	18.49	50.97	0.646	2.239	1.056	7.42
		30	8.83	(8.83)	8.76	16.93	0.407	2.174	1.126	2.80
		45	7.18	(7.18)	5.62	10.52	0.379	1.825	1.490	0.00

† Data from Chen, [15].

Table 3. Stability Factor $N^* = (\gamma/c)H^*$ for Constant Seismic Horizontal Component.

Loading profiles: $K_x = 0.325$
$K_y = 1.$

ϕ	α	β	N^*	N^*	$\frac{\gamma}{c}L^*$	$\frac{\gamma}{c}r_o^*$	θ_o^*	θ_h^*	θ_g^*
(degrees)				(publ.)†			(	radians	)
10	0	30	4.98	(4.98)	12.80	16.86	0.882	2.107	1.367
		60	4.32	(4.32)	5.26	9.40	0.781	1.669	-----
		90	3.22	(3.22)	3.56	13.57	0.839	1.178	-----
20	0	30	8.83	(8.83)	6.94	17.32	0.949	2.058	1.776
		60	5.63	(5.63)	4.53	10.26	0.885	1.665	-----
		90	3.65	(3.65)	3.35	17.53	0.962	1.217	-----
30	0	60	7.44	(7.44)	4.20	11.78	1.008	1.697	-----
		90	4.13	(4.13)	3.14	18.65	1.058	1.284	-----
40	0	60	10.25	(10.25)	4.01	14.19	1.142	1.743	-----
		90	4.66	(4.65)	2.93	21.31	1.166	1.349	-----

† Data from Chen et al., [17].

Table 4. Stability Factor $N^* = (\gamma/c)H^*$ for Linear Seismic Horizontal Profile.

Loading profiles: $K_x = 0.225 + b_1 h$

$K_y = 1.$

ϕ	α	β	b_1 †	N^*	N^*	$\frac{\gamma}{c}L^*$	$\frac{\gamma}{c}r_o^*$	θ_o^*	θ_h^*	θ_g^*	$\frac{\gamma}{c}d^*$
(degrees)					(pub.)‡			(	radians	)	
10	0	30	.0388	5.24	(5.16)	10.96	18.26	0.941	2.005	1.478	0.0
		60	.0468	4.25	(4.27)	5.50	10.91	0.856	1.635	-----	
		90	.0635	3.13	(3.15)	3.59	16.39	0.888	1.168	-----	
20	0	30	.0221	9.09	(9.06)	8.25	22.49	1.064	1.998	1.840	0.0
		60	.0362	5.50	(5.53)	4.83	12.29	0.970	1.638	-----	
		90	.0562	3.54	(3.56)	3.35	18.95	0.990	1.222	-----	
30	0	60	.0275	7.22	(7.28)	4.55	14.67	1.101	1.673	-----	
		90	.0500	3.98	(4.00)	3.12	19.47	1.080	1.292	-----	
40	0	60	.0201	9.87	(9.97)	4.44	18.65	1.243	1.720	-----	
		90	.0447	4.47	(4.47)	2.88	18.42	1.166	1.369	-----	

† Imposing four equi-thickness zones of different coefficients (0.25, 0.30, 0.35, 0.40) indiscriminate of slope heights in effect results in the variation of seismic profile with the size of the slope.

‡ Data from Chen et al., [17].

Table 5. Stability Factor $N^*=(\gamma/c)H^*$ for the General Average Horizontal Profile.

Loading profiles:

$$K_x=0.0057+0.0084h-0.000076h^2+0.00000032h^3$$

$$K_y=1.$$

ϕ	α	β	N^*	$\frac{\gamma}{c}L^*$	$\frac{\gamma}{c}r_o^*$	θ_o^*	θ_h^*	θ_g^*	comment
(degrees)						(	radians	)	
0	0	30	6.12	7.00	12.02	0.349	2.123	1.019	
			5.15	36.97	44.02	0.365	2.648	0.494	$(\gamma/c)d^*=34.0$
		60	5.07	4.55	8.03	0.377	1.523	-----	
			5.07	46.96	53.53	0.380	2.658	0.484	$(\gamma/c)d^*=47.2$
		90	3.75	3.53	10.33	0.504	1.008	-----	
			5.06	50.05	53.54	0.380	2.660	0.481	$(\gamma/c)d^*=47.2$
10	0	30	11.63	6.29	20.65	0.647	1.963	1.522	
		60	6.87	4.24	9.61	0.509	1.555	-----	
		90	4.45	3.48	12.29	0.616	1.055	-----	
20	0	30	23.67	8.04	48.55	0.985	1.904	-----	
		60	9.48	4.16	12.08	0.658	1.575	-----	
		90	5.28	3.44	14.69	0.733	1.111	-----	
	20	30	9.55	98.29	122.15	1.124	1.922	1.919	see note #1
			10.59	100.0	144.37	1.174	1.921	1.919	$(\gamma/c)d^*=8.46$
		60	8.72	7.60	14.70	0.681	1.608	-----	
		90	5.00	4.54	11.74	0.631	1.202	-----	
30	0	60	13.58	4.25	16.39	0.831	1.611	-----	
		90	6.31	3.40	17.55	0.851	1.174	-----	
	20	60	12.88	6.70	18.21	0.835	1.623	-----	
		90	6.06	4.22	13.87	0.766	1.232	-----	
40	0	60	20.58	4.57	25.15	1.035	1.656	-----	
		90	7.63	3.37	22.26	0.981	1.239	-----	
	20	60	19.84	6.82	27.05	1.037	1.661	-----	
		90	7.39	4.02	17.24	0.913	1.278	-----	
	40	60	7.64	76.23	80.73	1.197	1.819	-----	see note #2
		90	6.84	6.42	15.16	0.855	1.350	-----	

notes: #1 --- $(\gamma/c)H_T^*=0.00022$

#2 --- $(\gamma/c)H_T^*=0.00001$

Table 6. Stability Factor $N^*=(\gamma/c)H^*$ for the General Profile Oriented at a Direction of Arctan(0.1) with the Horizon.

Loading profiles: $K_x=0.0057+0.0084h-0.000076h^2+0.00000032h^3$

$K_y=1.+0.1K_x$

ϕ	α	β	N^*	$\frac{\gamma}{c}L^*$	$\frac{\gamma}{c}r_o^*$	θ_o^*	θ_h^*	θ_g^*	$\bar{d}=\frac{\gamma}{c}d^*$ or $\bar{h}=\frac{\gamma}{c}H_T^*$
(degrees)						(	radians	)	(comments)
0	0	30	6.10	6.97	11.98	0.349	2.123	1.019	
			5.15	35.20	42.34	0.362	2.646	0.495	$\bar{d}$=32.73
		90	3.74	3.53	10.33	0.505	1.008	-----	
20	0	30	23.51	7.93	47.94	0.982	1.905	-----	
		90	5.27	3.43	14.57	0.732	1.112	-----	
	20	30	9.27	100.8	136.42	1.168	1.891	-----	$\bar{h}$=0.773
		90	4.99	4.54	11.74	0.632	1.202	-----	
40	0	60	20.45	4.51	24.84	1.032	1.656	-----	
		90	7.60	3.36	22.34	0.982	1.238	-----	
	40	60	7.61	76.08	79.81	1.195	1.821	-----	$\bar{h}$=0.0021
		90	6.81	6.41	15.15	0.856	1.350	-----	

Table 7. Stability Factor $N^*=(\gamma/c)H^*$ for the General Profile Oriented at a Direction of Arctan(0.5) from the Horizon.

Loading profiles:

$K_x=0.0057+0.0084h-0.000076h^2+0.00000032h^3$

$K_y=1.+0.5K_x$

ϕ	α	β	N^*	$\frac{\gamma}{c}L^*$	$\frac{\gamma}{c}r_o^*$	θ_o^*	θ_h^*	θ_g^*	$\bar{d}=\frac{\gamma}{c}{}^*$ or $\bar{h}=\frac{\gamma}{c}H_T^*$
(degrees)						(	radians	)	(comments)
0	0	30	6.02	6.89	11.82	0.349	2.124	1.018	
			5.14	31.13	37.74	0.352	2.639	0.502	$\bar{d}=28.47$
		90	3.70	3.50	10.33	0.508	1.006	-----	
20	0	30	22.91	7.49	45.53	0.970	1.911	-----	
		90	5.20	3.38	14.40	0.731	1.111	-----	
	20	30	9.02	98.15	122.05	1.129	1.920	-----	$\bar{h}=0.011$
		90	4.92	4.48	11.61	0.633	1.202	-----	
40	0	60	19.97	4.32	23.73	1.024	1.658	-----	
		90	7.48	3.31	21.91	0.981	1.238	-----	
	40	60	7.53	75.46	78.23	1.192	1.823	-----	
		90	6.69	6.33	14.96	0.858	1.351	-----	

Table 8. Location of the Most Critical Slip Surface for a Slope of 30 Feet in Height.

Loading profiles:

K_x=0.0057+0.0084h-0.000076h^2+0.00000032h^3

K_y=1.

Height of the slope: H_s=30 ft.

ϕ	α	β	$\frac{\gamma}{c}H^*$	$\frac{\gamma}{c}H_T^*$	$\frac{\gamma}{c}L^*$	$\frac{\gamma}{c}r_o^*$	θ_o^*	θ_h^*	θ_g^*
(degrees)							(	radians	)
0	0	30	3.10	26.90	27.87	21.74	0.602	2.353	------
		90	3.20	26.80	3.73	11.30	0.643	1.081	------
20	0	30	17.17	12.83	7.05	32.34	0.943	1.960	------
		90	4.32	25.68	3.41	16.99	0.872	1.162	------
	20	30	4.89	25.11	49.09	43.78	0.966	2.046	------
		90	4.03	25.97	4.99	11.20	0.741	1.308	------
40	0	60	16.22	13.78	4.30	19.85	1.055	1.686	------
		90	5.86	24.14	3.19	24.79	1.097	1.288	------
	40	60	4.65	25.35	46.24	34.82	1.084	1.894	------
		90	5.05	24.95	8.10	13.97	0.959	1.487	------

* values calculated for a (c/γ) ratio of 1.

Table 9. Location of the Most Critical Slip Surface for a Slope of 50 Feet in Height.

Loading profiles:

$K_x = 0.0057 + 0.0084h - 0.000076h^2 + 0.00000032h^3$

$K_y = 1.$

Height of the slope: $H_s = 50$ ft.

ϕ	α	β	$\frac{\gamma}{c}H^*$	$\frac{\gamma}{c}H_T^*$	$\frac{\gamma}{c}L^*$	$\frac{\gamma}{c}r_o^*$	θ_o^*	θ_h^*	θ_g^*
(degrees)							(	radians	)
0	0	30	2.03	47.97	21.49	14.92	0.491	2.489	------
		90	2.96	47.04	3.82	11.13	0.693	1.131	------
20	0	30	11.18	38.82	6.78	21.06	0.936	2.023	------
		90	3.90	46.10	3.39	17.70	0.931	1.193	------
	20	30	3.44	46.56	34.03	26.29	0.878	2.111	------
		90	3.60	46.40	5.42	10.74	0.793	1.386	------
40	0	60	12.22	37.78	4.12	16.09	1.107	1.719	------
		90	5.09	44.91	3.06	26.95	1.159	1.317	------
	40	60	3.49	46.51	34.77	22.26	1.020	1.933	------
		90	2.95	47.05	29.46	26.06	1.118	1.812	------

* values calculated for a (c/γ) ratio of 1.

CHAPTER VIII. SUMMARY, CONCLUSIONS AND RECOMMENDATIONS

VIII.A. Summary and Conclusions

The main purpose of this study has been to develop a more general and consistent mathematical model for the analysis of the instability of earthslopes under seismic loads. By recognizing the disadvantages of existing models and with a better understanding of the nature of an earthquake's influences, such a more involved model has been successfully formulated. The treatment of several possibilities has been categorized such that a better insight into the influence of the slope geometry on the spiral failure mechanism can be gained. By looking into the possible changes seismic loads may have on the shape of the most critical slip surface, far-reaching conclusions may be drawn. For instance, in the derivation of the slip surface equation, it could be observed that the inhomogeneity and anisotropy in the cohesion of the soil has no effect on the critical shape. In fact, the only controlling factor on the shape of the slip surface is the internal friction angle ϕ.

Most important of all is the flexibility inherent in the present formulation to account for the variations of the seismic forces along the height. In considering both vertical and horizontal components for the seismic loads, not only is the variation of magnitude of the seismic force with height, but also the variation of the direction of the seismic force accountable. Such loading profiles, if interpreted wisely and with care, can also be used to allow for the variation of the specific weight of the soil along the height.

To facilitate the adaptation of this present model to future analyses related to seismic-infirmed earthslopes, computer coding of the tedious formulations has been implemented, and results of fairly simple cases have been studied. These data constitute two main functions: to provide indicators of agreement between results of the present model and previous established models, and to provide further information relating to the seismic loadings that were not available previously. Of importance are the tables of the spiral coordinates for the different cases studied. They not only show the general patterns of the variation of the coordinates, but also provide good indications for estimating the initial coordinates for the spiral optimization process. Thus, the iterative algorithm of the optimization subroutine (used in the computer program) can be initiated in the right direction, resulting in the expedited analysis, cutting down on run time and cost, as well as preventing convergence onto local minimum.

The ability to predict and estimate the relative location of the most critical failure surface in an earthslope of given property, geometry, and height is even more significant It allows for the cumulative displacement analysis proposed in Ref.[7] and [10] to be carried out in the future.

All in all, the present model is a step forward in recent efforts to understand better the seismic effects on the stability of earthslopes. It is, nevertheless, quite idealized with respect to the actual time variation feature of the seismic forces, and the changes in soil properties. The changes in properties are results of compaction, pore water pressure variation, liquefaction, seepage forces, non-linear post-elastic responses, hysteretic strain behaviors, etc., caused by the loadings.

VIII.B. Recommendations for Future Work

In view of the limitations of the model developed in the present study, directions for future improvements and further studies can be identified. Three of the more important and yet reasonably attainable suggestions are listed below:

i) The present formulation may be extended to account for the inhomogeneity and anisotropy of the soil cohesion. It is obvious from this study that the varying cohesion has no effect on the spiral equation, and it does not enter in the equations of external work rate. Thus, all is needed is a modification of the internal energy dissipation rate equation to account for two cohesion profiles, one with respect to the elevation, the other with respect to the orientation. Such modification would be similar to that in Ref.[15], and should not induce too much changes in the formulation or the computer coding.

ii) An extensive computer program to incorporate the hazards of a slope at different time intervals during the occurrence of an earthquake should be attempted. Such coding should include the examination of the seismic profiles at different intervals, to see if displacements along a well defined slip surface are inflicted or not. The displacements at the end of each interval should be integrated to determine the total displacement after the quake. This is essentially the new approach to the assessment of seismic slope hazards proposed in Ref.[7] and [10]. However, no specific method of identifying the slip surface was mentioned in these earlier articles. The present study has provided part of the answer. The method developed for identifying the most critical slip surface for a slope of given height (such as those in Tables 8 and 9) can be used to determine the progressive development and movement of the failure surface in the course of the quake.

iii) In the case of dead-weight induced slope failure, the slope can be treated as an infinite prism with the cross-section of a slope. Such that the accompanying slip surface can be assumed with reasonable accuracy as an incomplete logspiral prism. However, in the case of seismic-infirmed slopes, the direction of the seismic load may not be on the plane of the slope cross-section. Nor do the seismic loads have to be distributed uniformly throughout the entire stretch of the slope. Thus, a three-dimensional failure surface will naturally result. A study of the family of 3-D slip surface can therefore be quite rewarding.

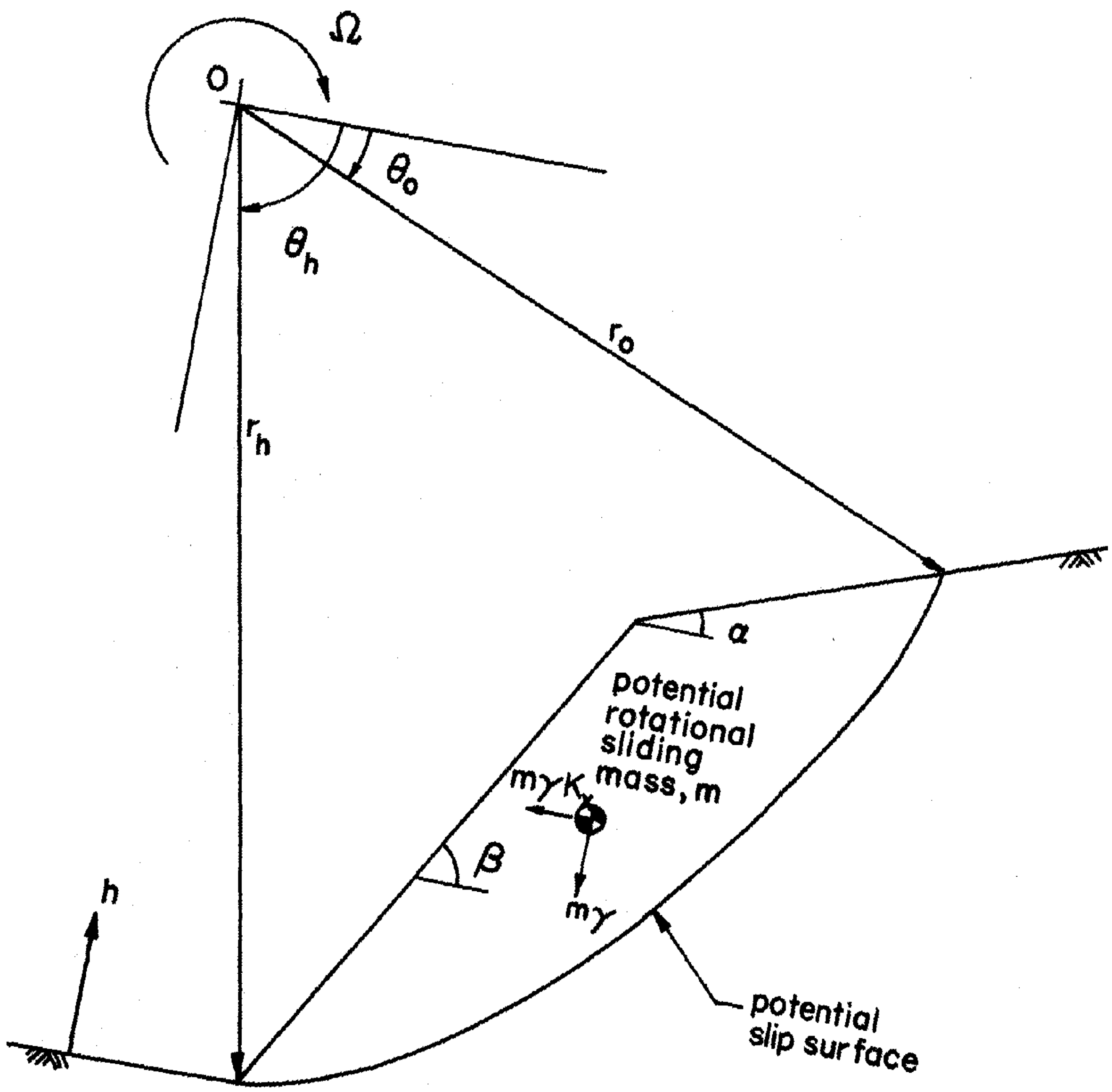

Fig. 1 Schematic of a Pseudo-Static Constant Seismic Profile Approach.

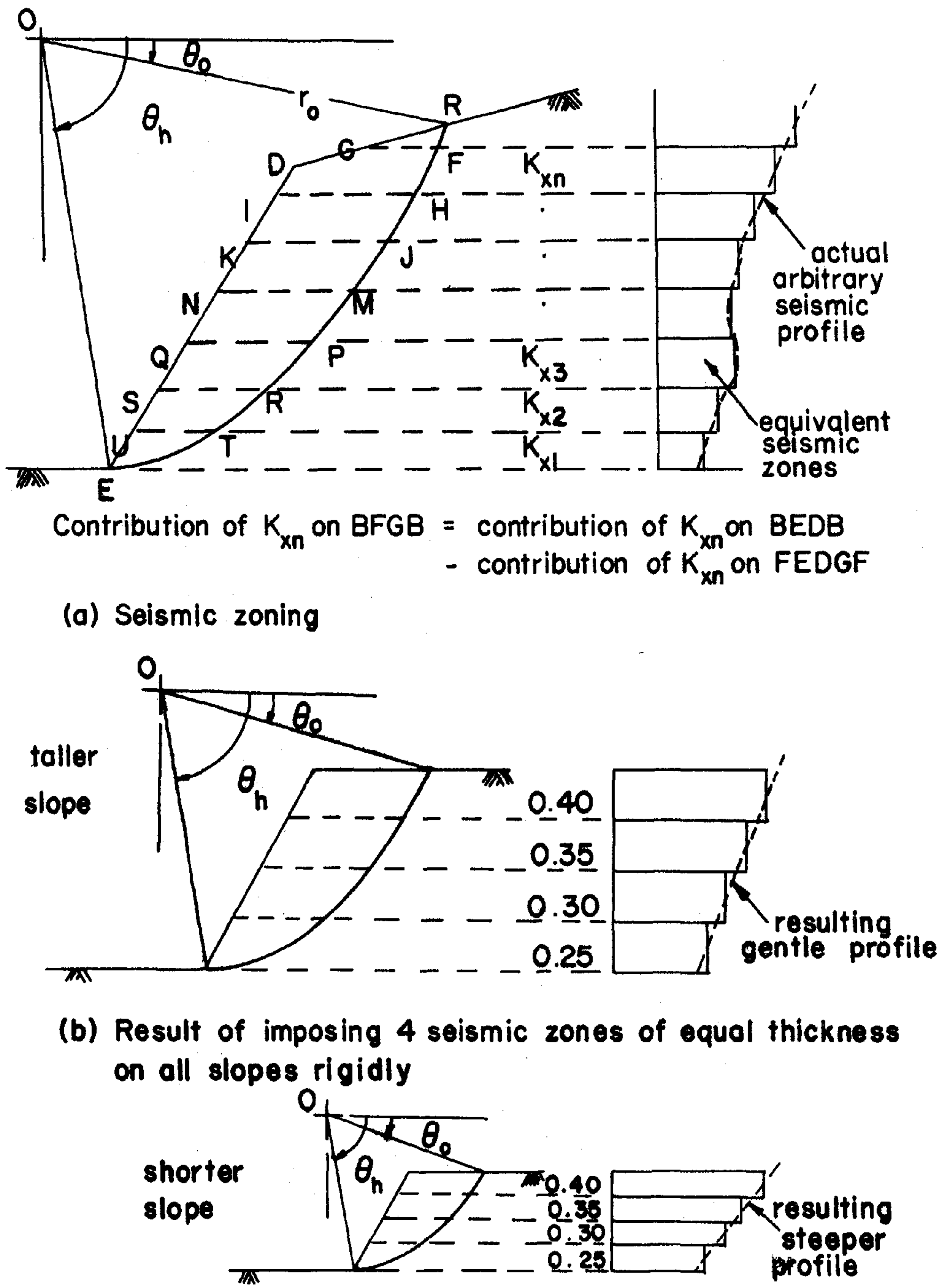

Fig. 2 Schematic of the Seismic Coefficient Zoning Approach.

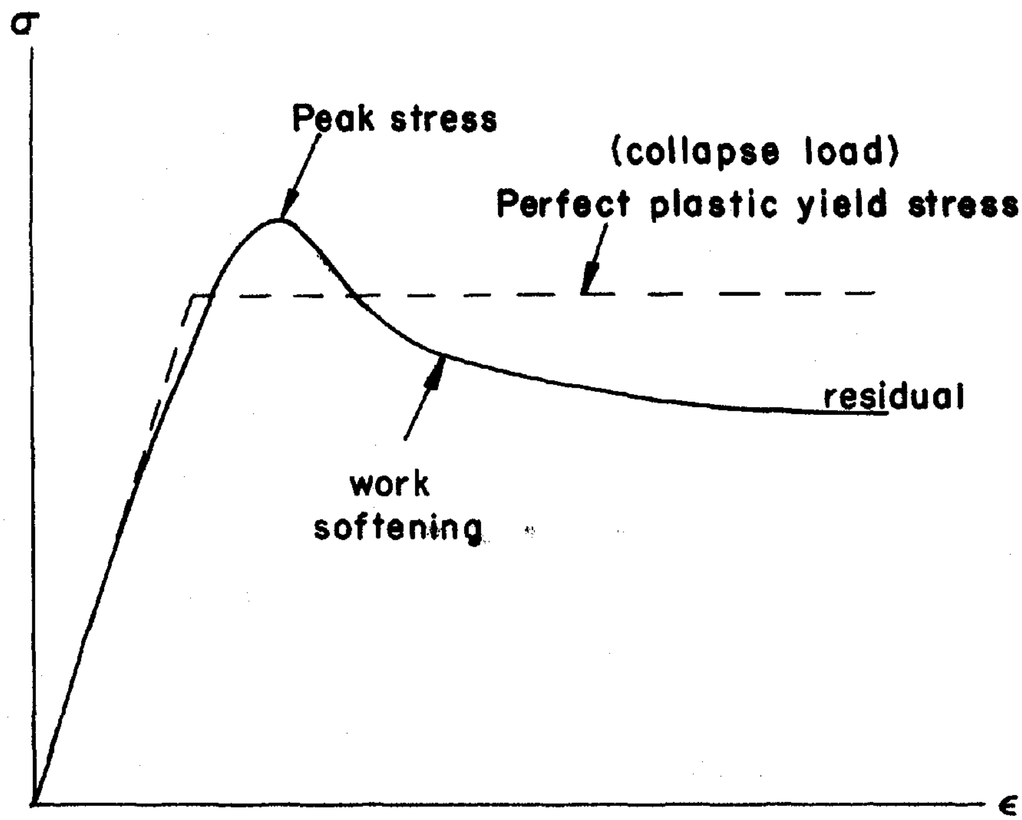

Fig. 3 Stress-Strain Relationship for Real and Idealized Soil Behavior.

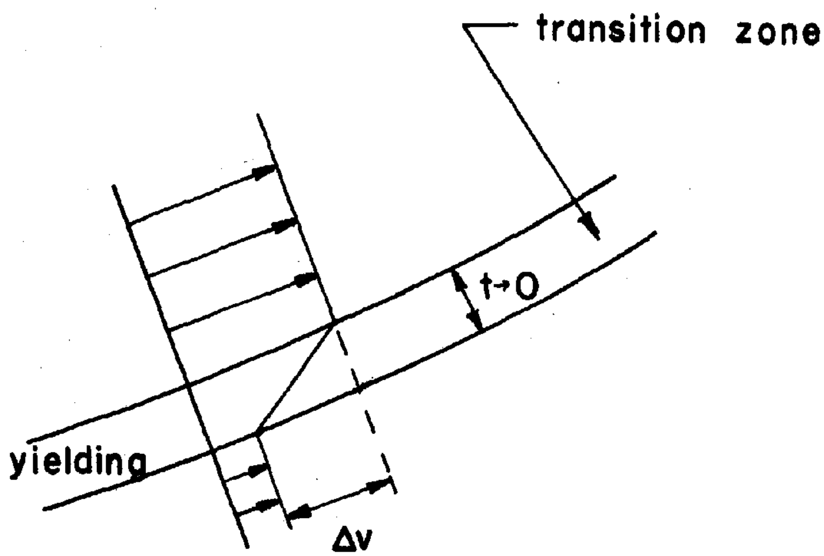

Fig. 4 Velocity Discontinuity.

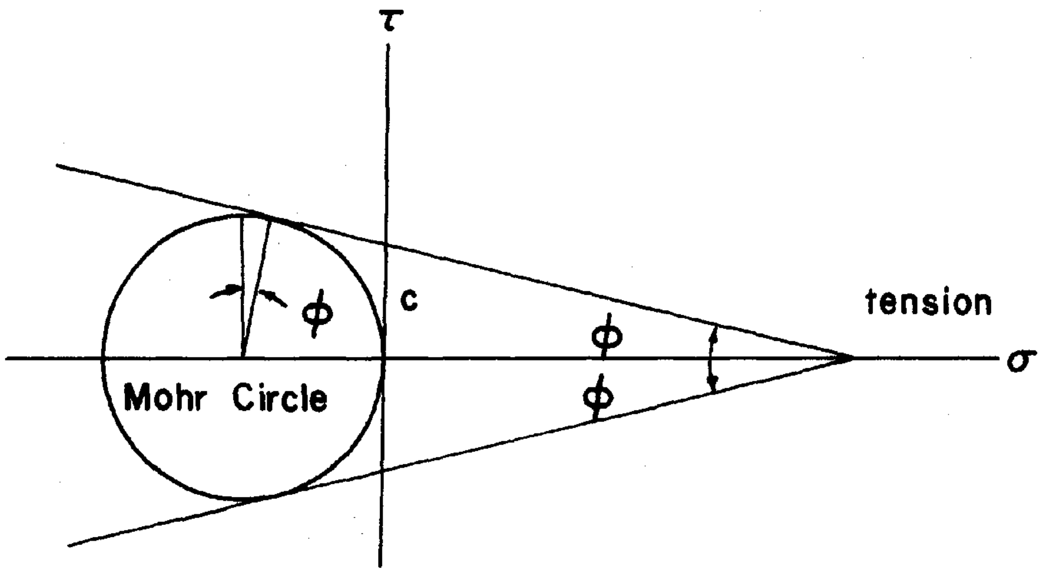

Fig. 5 Coulomb's Criterion for Soil.

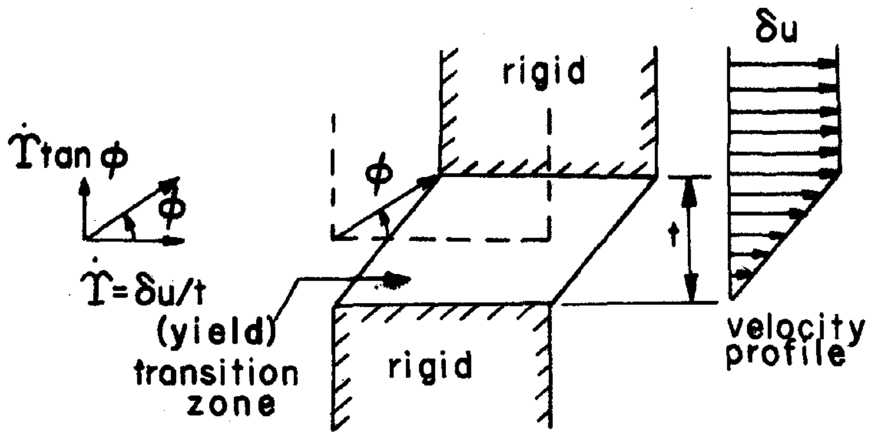

Fig. 6 Simple Slip Accompanied by Dilatancy for Soil.

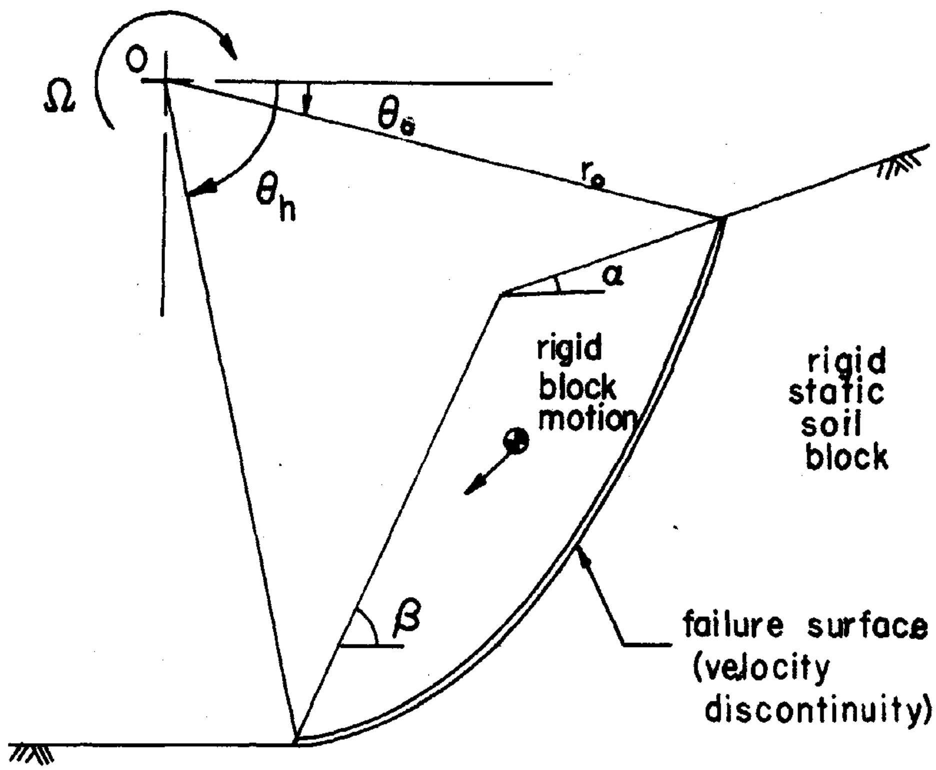

Fig. 7 The Rigid Block Motion of the Soil Mass Above the Slip Surface as the Result of Yield Flow on the Surface.

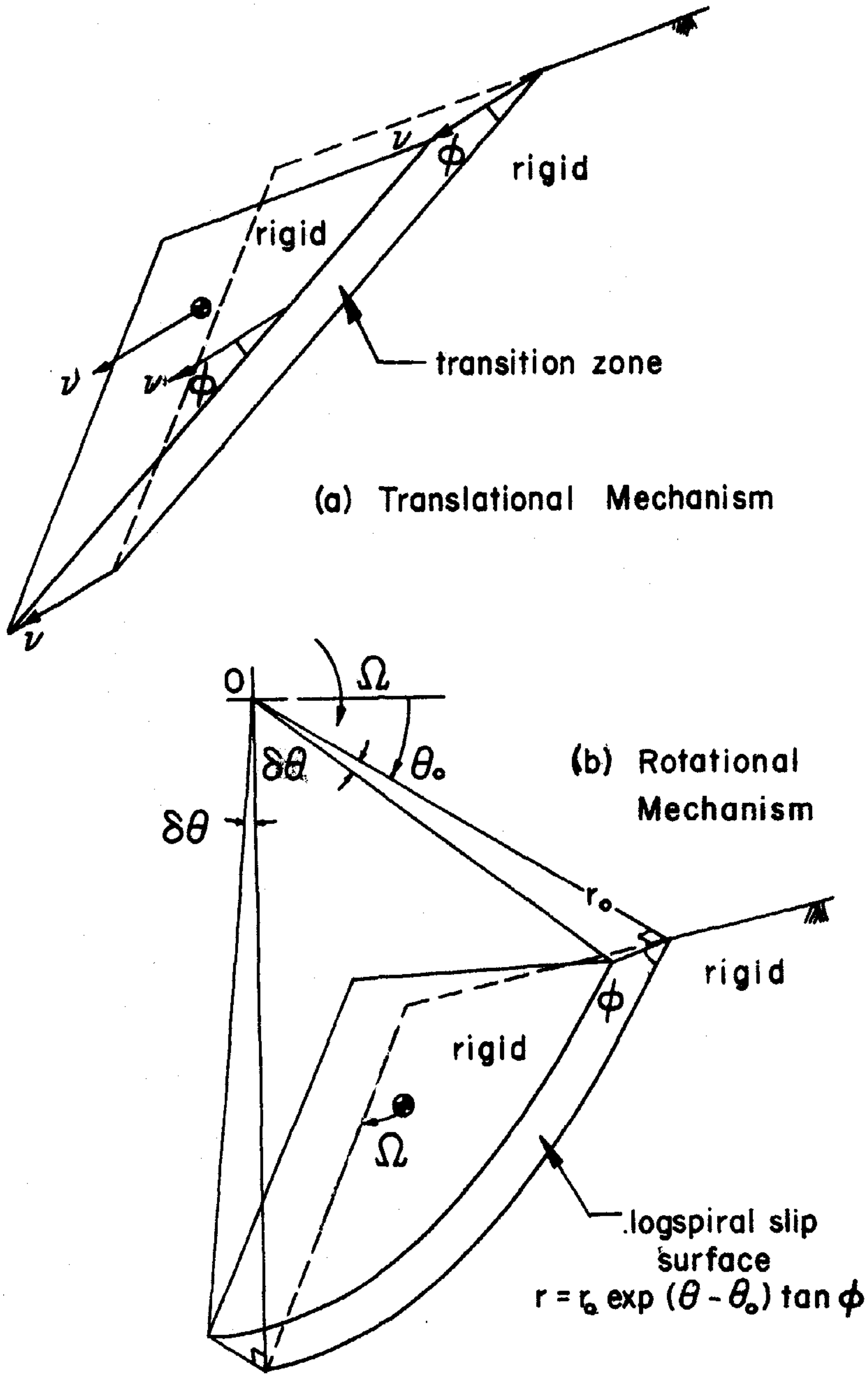

Fig. 8 The Only Two Kinematically Admissible Failure Mechanisms for Soil.

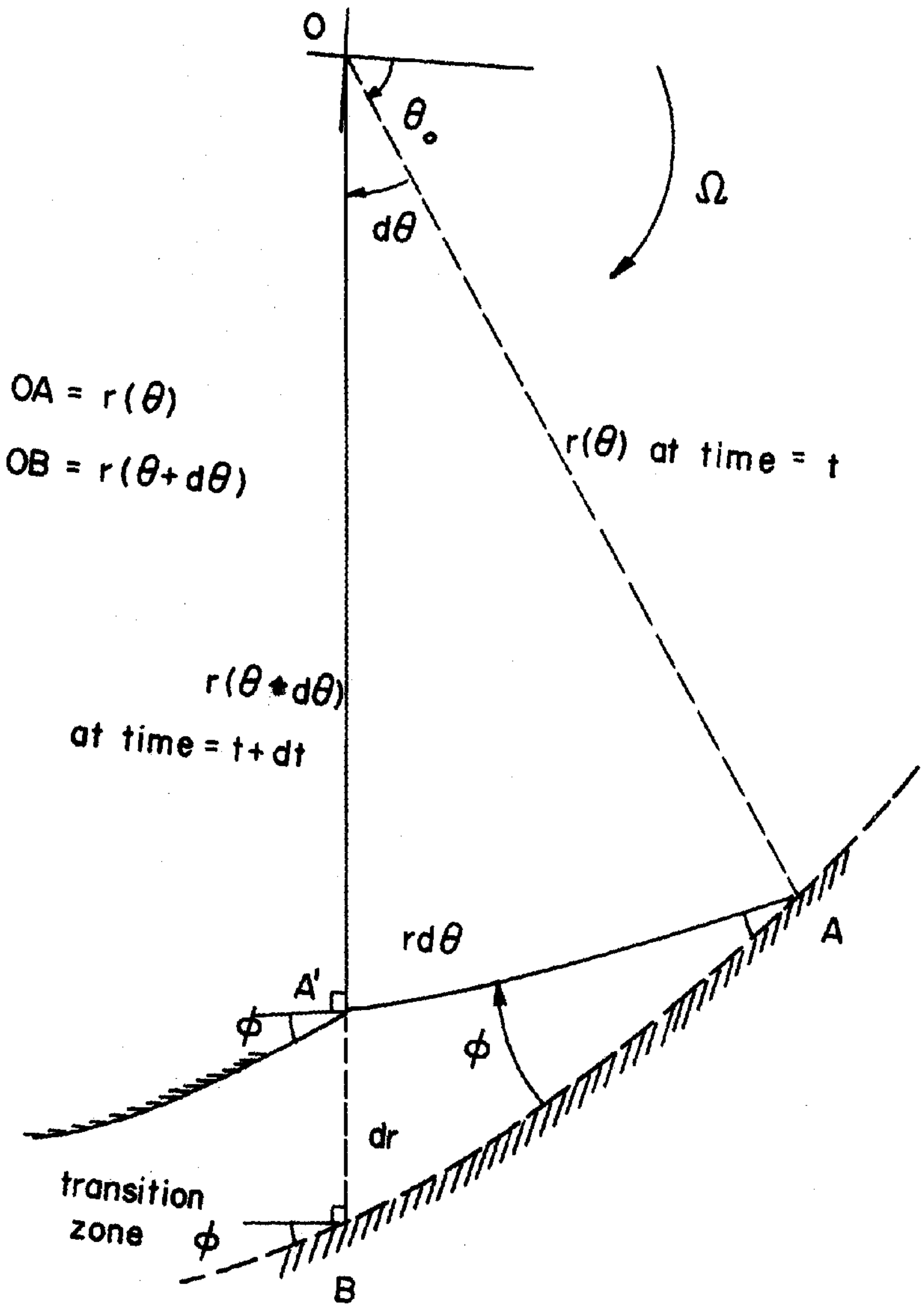

Fig. 9 The Movement of the Logspiral Mechanism.

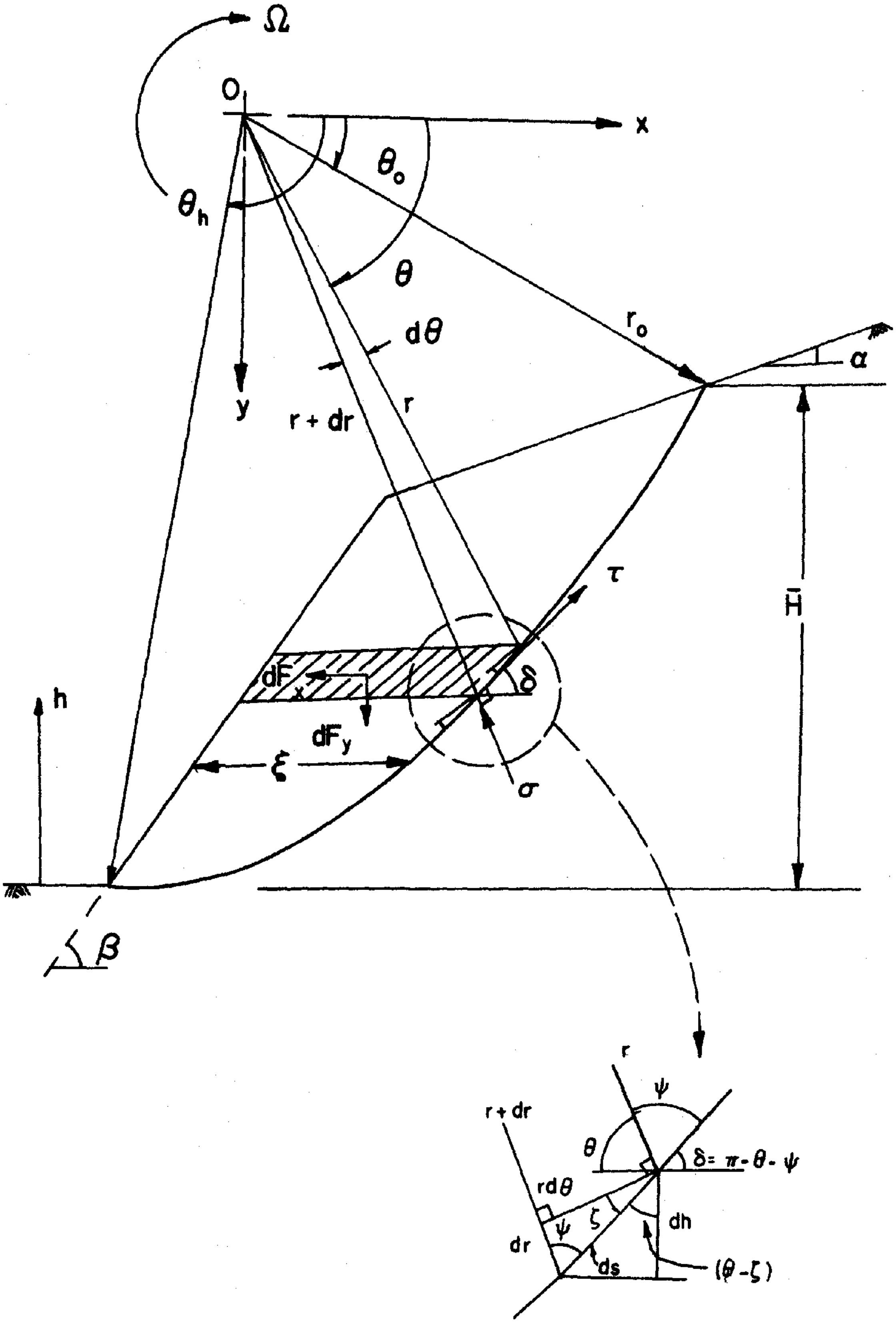

Fig. 10 Arbitrary Potential Failure Surface.

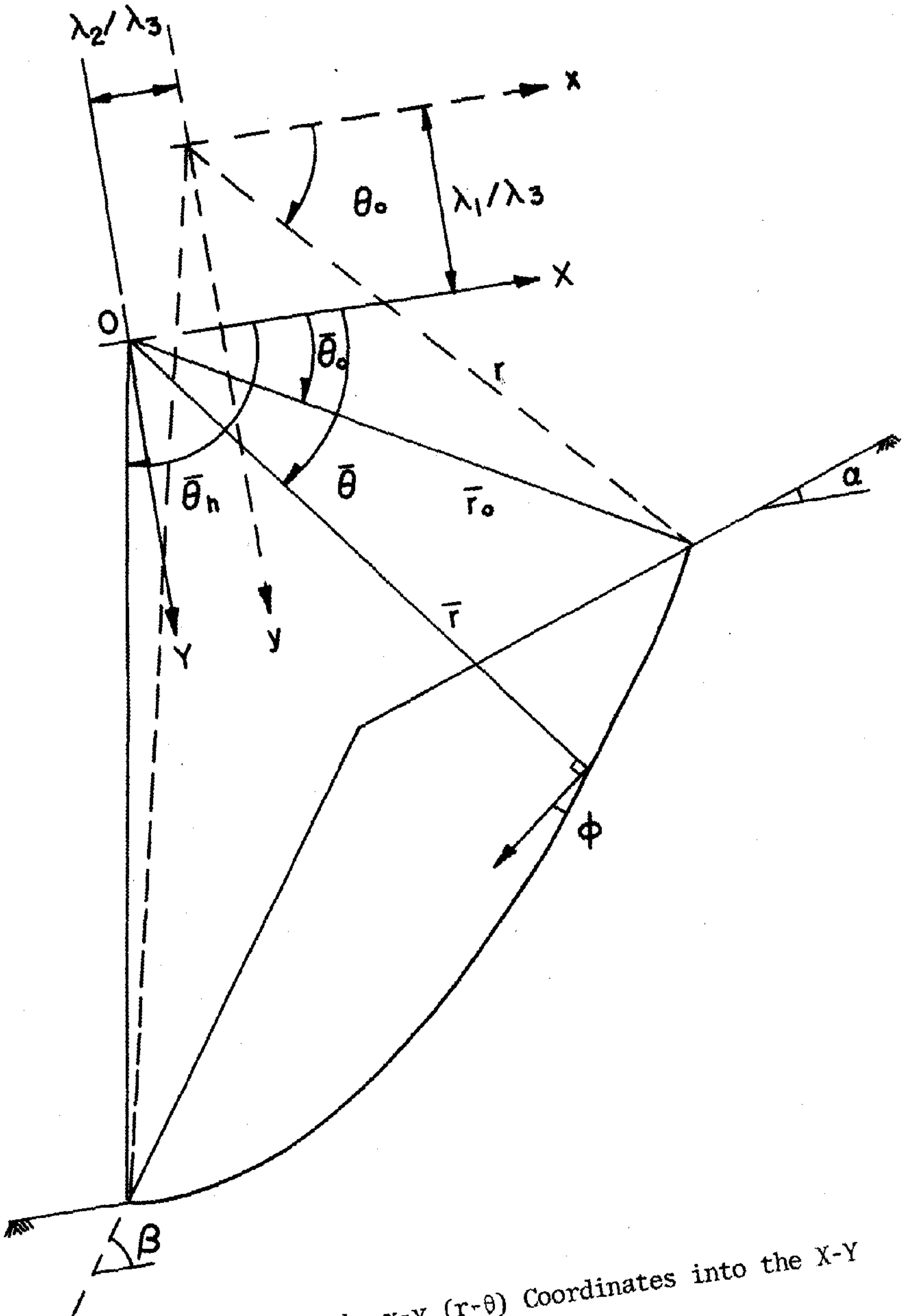

Fig. 11 Transformation of the x-y (r-θ) Coordinates into the X-Y ($\bar{r}$-$\bar{\theta}$) Coordinates.

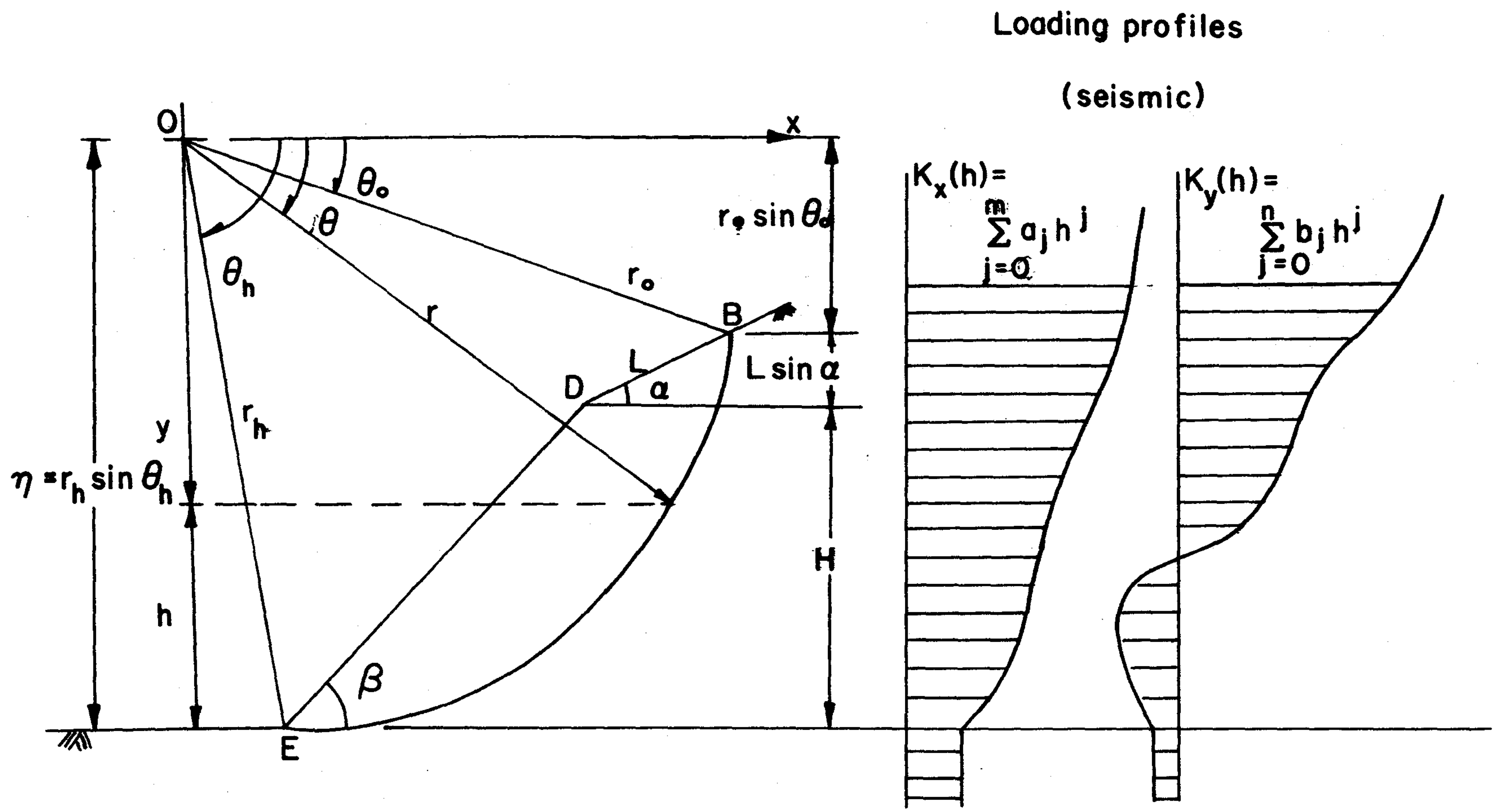

Fig. 12 Relation of the Loading Profiles to the Geometry of the Slope.

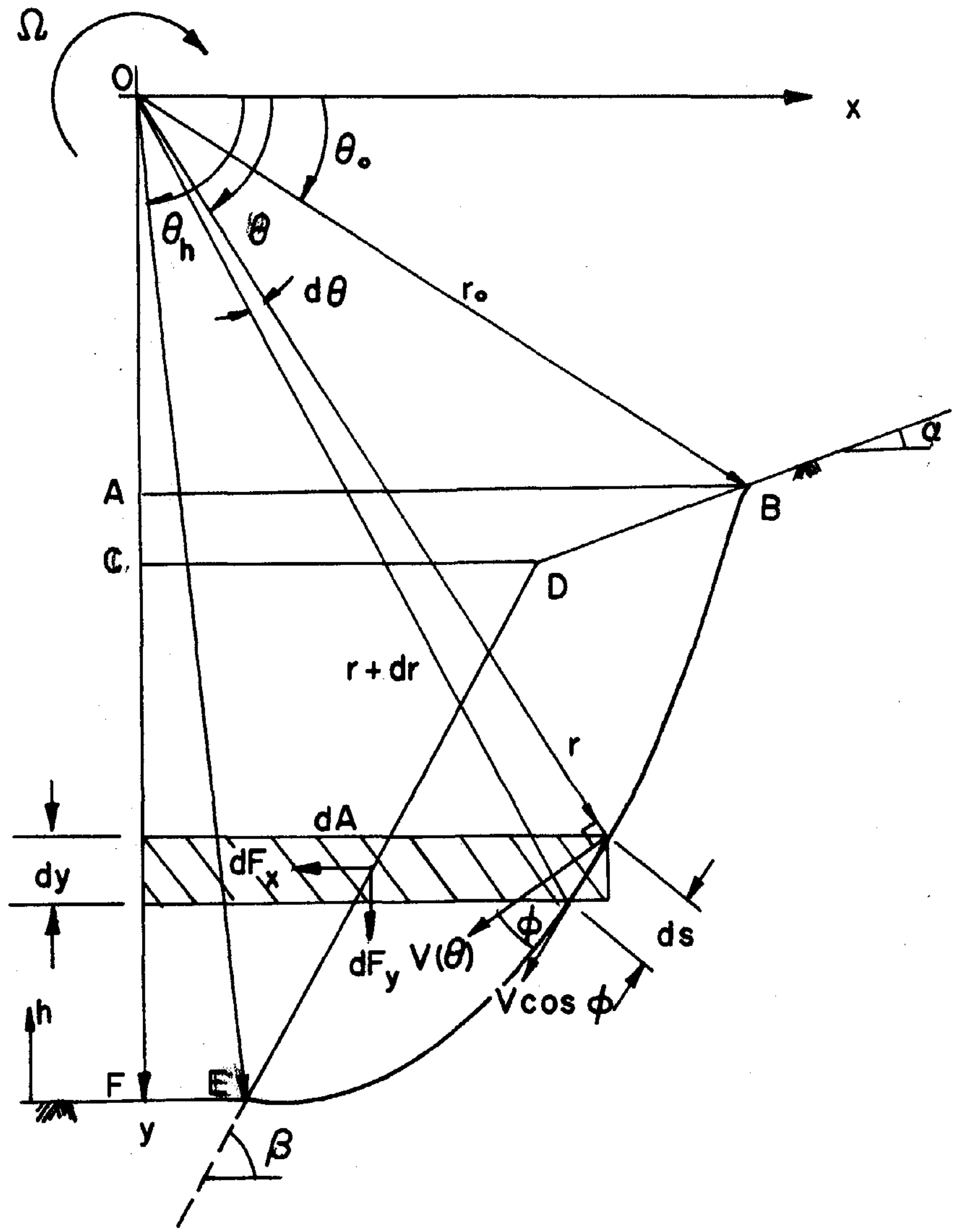

Fig. 13 Logspiral Slip Surface for Seismic Loading, Calculation of the Gross External Work Rate.

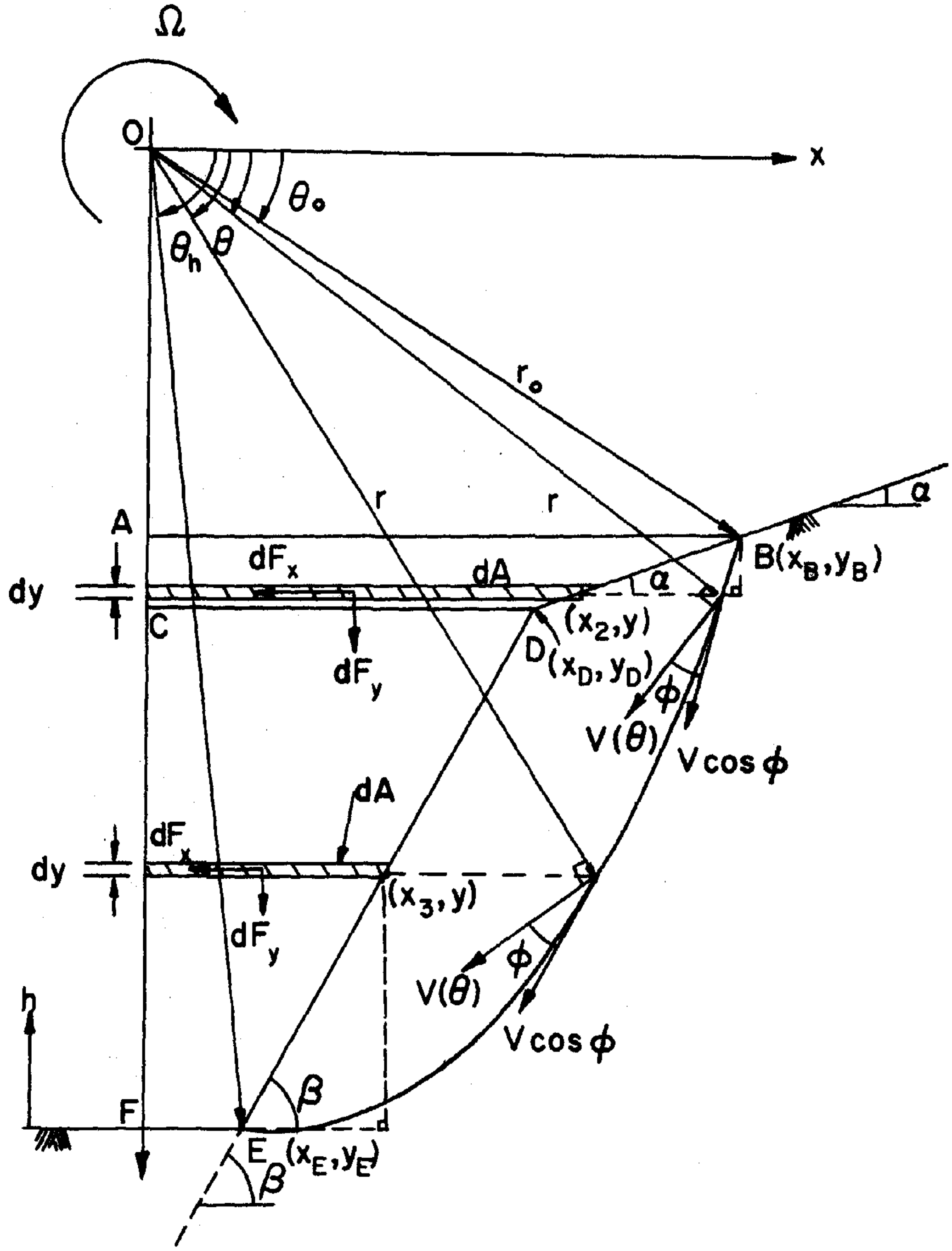

Fig. 14 Logspiral Slip Surface for Seismic Loading, Calculation for the Fictitious External Work Rate.

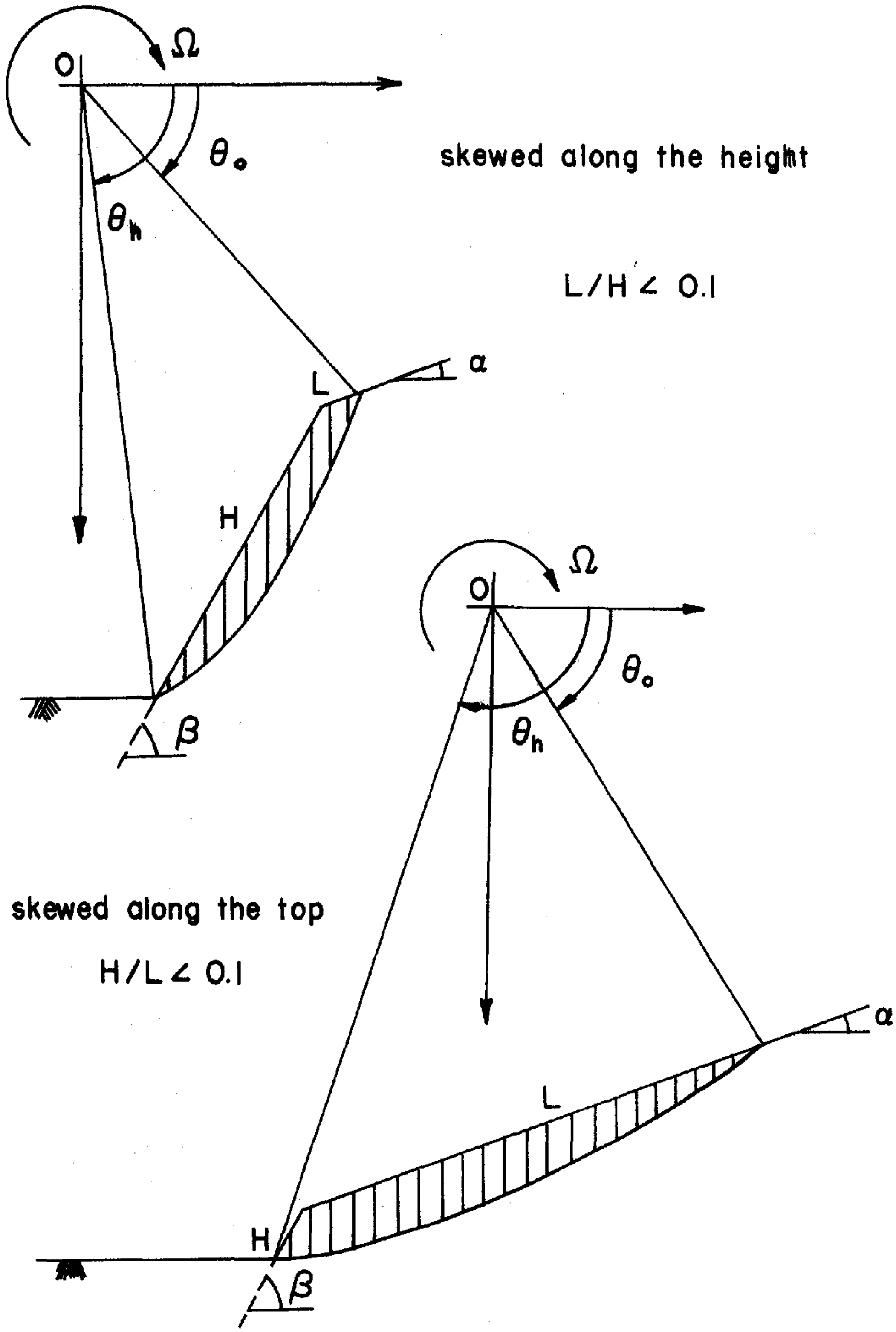

Fig. 15 Skewed Spirals.

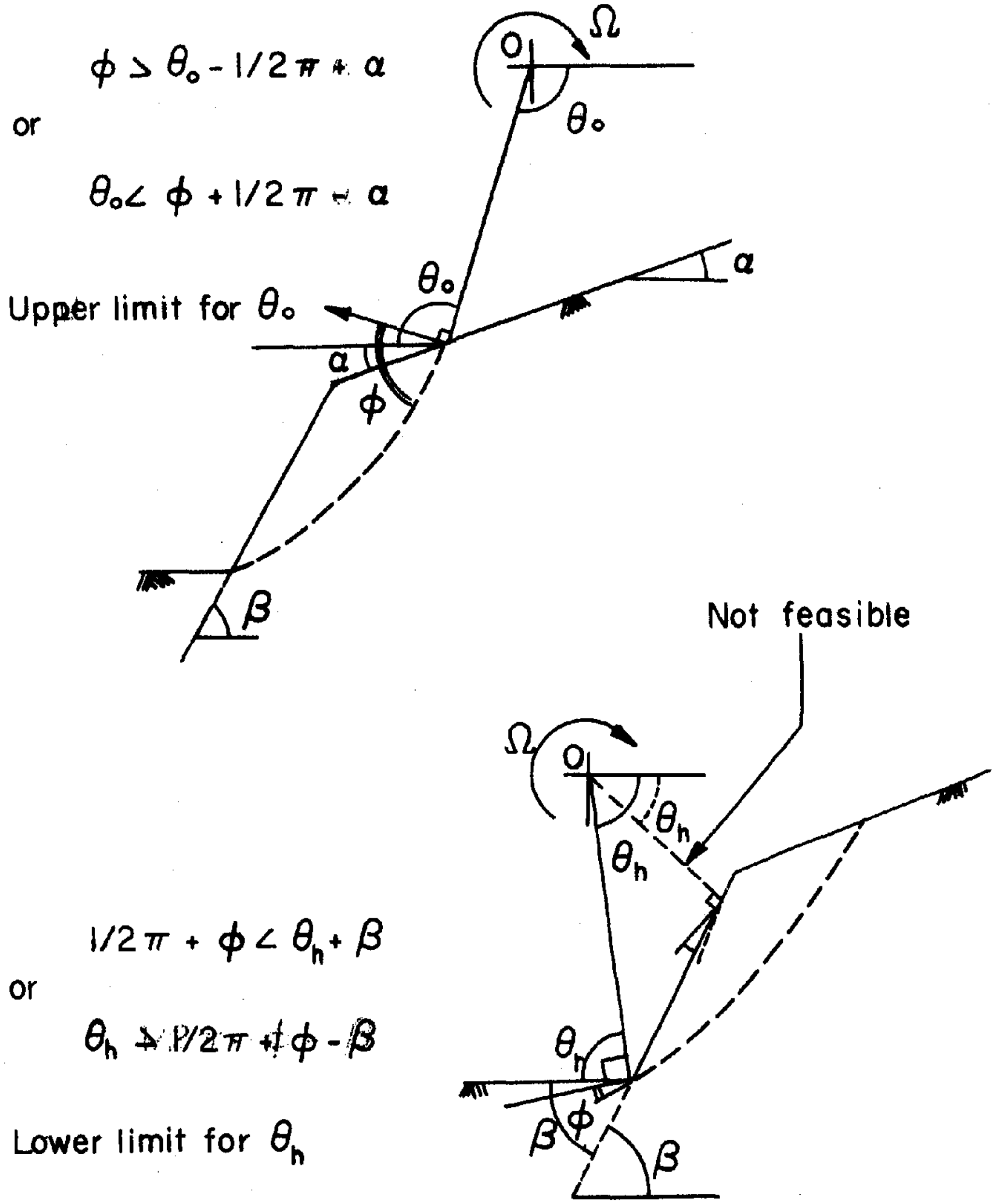

Fig. 16 Partial Limits for θ_o and θ_h.

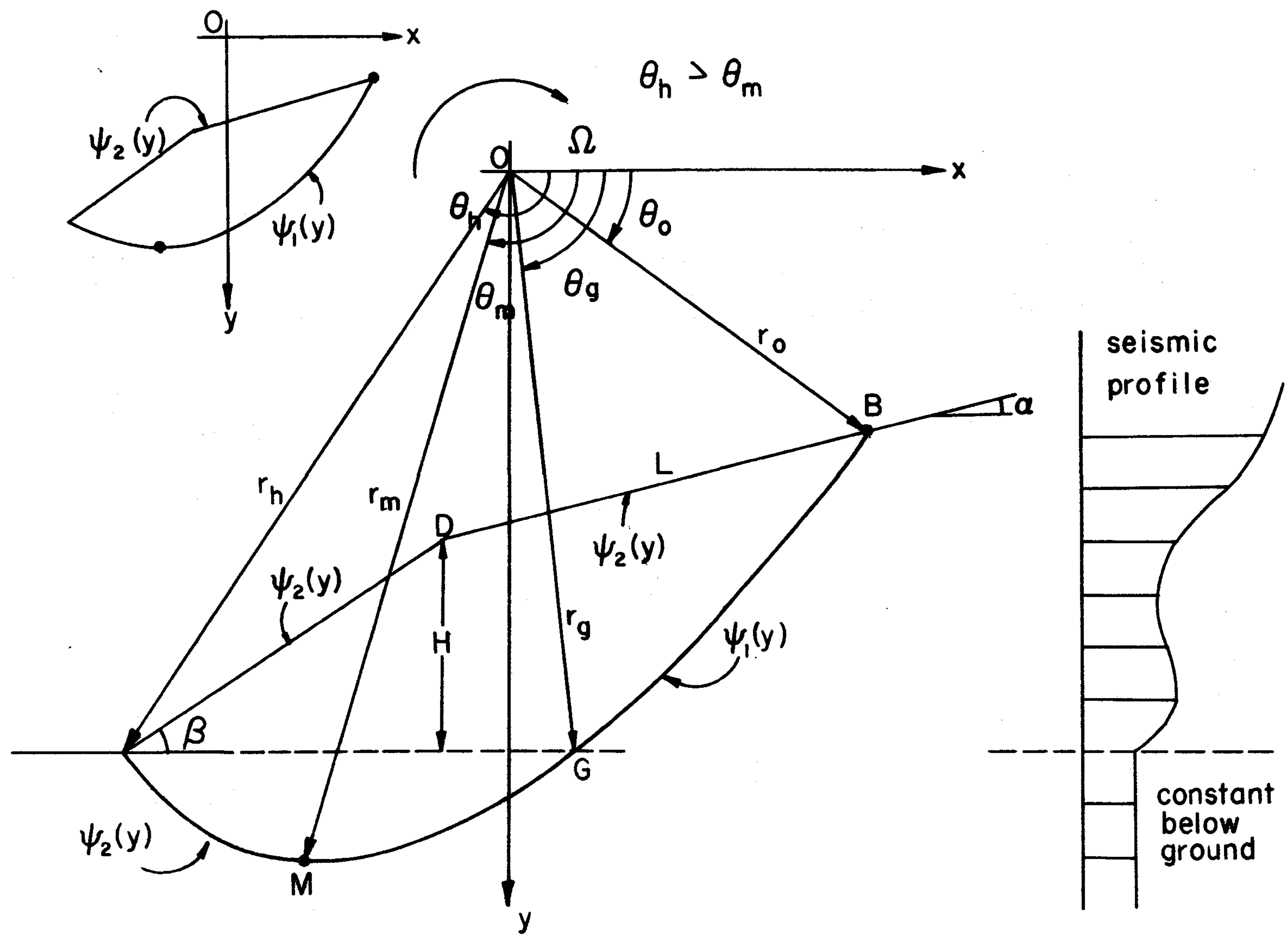

Fig. 17 Sagging Spiral.

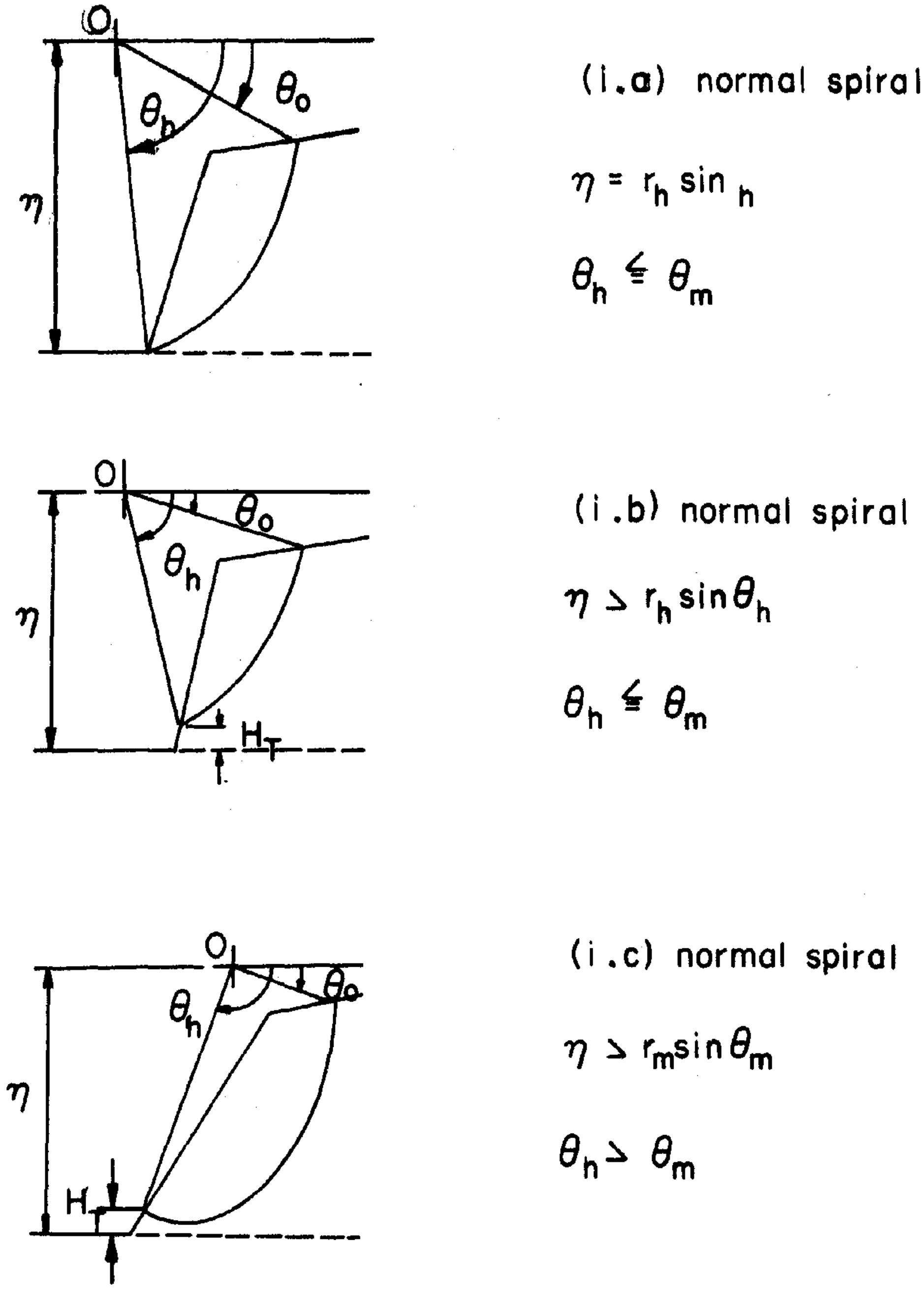

Fig. 18 Four Major Categories of Spirals.

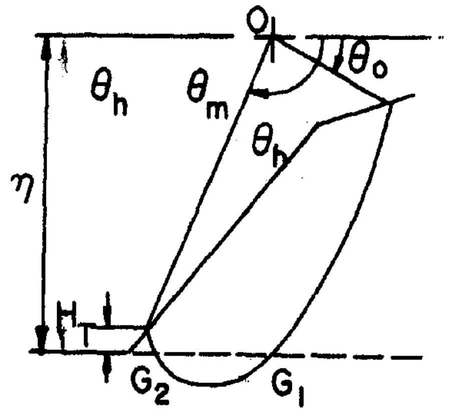

(ii) partially sunken spiral

$r_h \sin\theta_h < \eta < r_m \sin\theta_m$

$\theta_h > \theta_m$

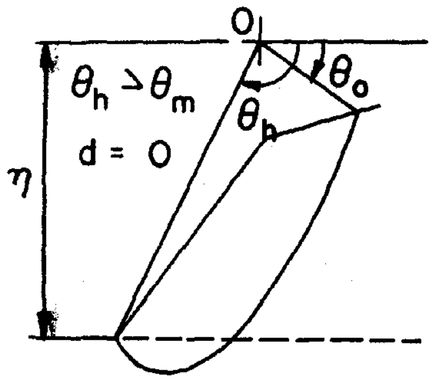

(iii) sunken spiral

$r_h \sin\theta_h = \eta < r_m \sin\theta_m$

$\theta_h > \theta_m$

d = 0

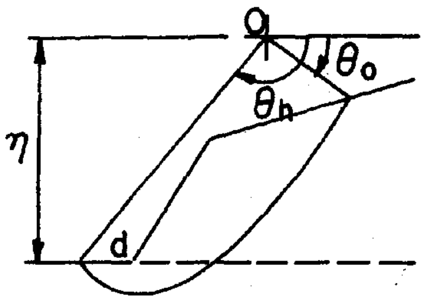

(iv) stretced spiral

$r_h \sin\theta_h = \eta \nless r_m \sin\theta_m$

$\theta_h > \theta_m$

d > 0

Fig. 18 (Cont'd)

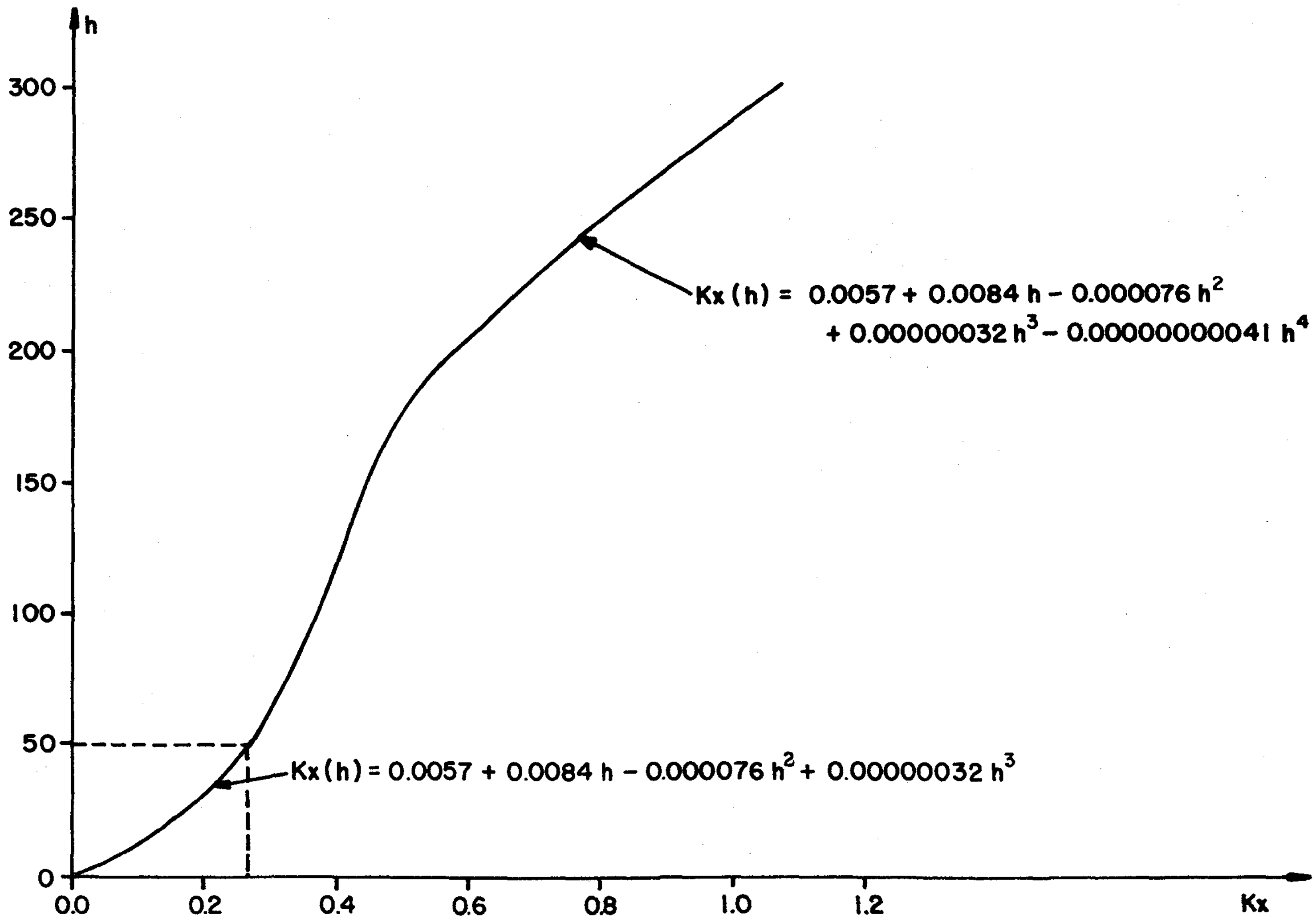

Fig. 19. The General Average Seismic Profile (Horizontal).

LIST OF REFERENCES

LIST OF REFERENCES

1. Prager, W. , "Recent Developments in the Mathematical Theory of Plasticity," J. Applied Physics, v.20,#3 (1949)

2. Drucker, D.C. , "Some implications of Work Hardening and Ideal Plasticity," Quarterly of Appl. Math., v.7,#4(1950)

3. Drucker, D.C. , W. Prager, and H.J. Greenberg, "Extended Limit Analysis Theorems for Continuous Media," Quart. of Appl. Math., v.9,#4 (1952).

4. Drucker, D.C. , and W. Prager, "Soil Mechanics and Plastic Analysis or Limit Design," Quart. of Appl. Math., v.10,#2 (1953).

5. Hodge, P.G. Jr. , "The Mathematical Theory of Plasticity," Surveys in Applied Mathematics Series I: Elasticity & Plasticity, John Wiley & Sons, Inc. (1958).

6. Prager, W. , An Introduction to Plasticity, Addison-Wesley Publishing Co., Inc. (1959).

7. Newmark, N.M. , "Effects of Earthquakes on Dams and Embankments," Geotechnique, Inst. of Civil Engineers, London, v.15 (1965).

8. Seed, H.B. , and G.R. Martin, "The Seismic Coefficient in Earth Dam Design," J. of Soil Mech. & Foundations Div., Proc. of the Am. Soc. of Civ. Eng., v.92,#SM3 (1966).

9. Ambraseys, N.N. , and S.K. Sarma, "The Response of Earth Dams to Strong Earthquakes," Geotechnique, Ins. of Civ. Eng., London, v.17 (1967).

10. Seed, H.B. , "Slope Stability During Earthquakes," J. of Soil Mech & Found. Div., Proc. of the Am. Soc. of Civ. Eng., v.93,#SM4 (1967).

11. Finn, W.D.L. , "Applications of Limit Plasticity in Soil Mechanics," J. Soil Mech. & Found. Div., Proc. Am. Soc. Civ. Eng., v.93,#SM5 (1968).

12. Chen, W.F. , "Discussion of 'the Applications of Limit Plasticity in Soil Mechanics by W.D. Liam Finn'," J. Soil Mech. & Found. Div., Proc. Am. Soc. Civ. Eng., v.94,#SM2 (1968).

13. Chen, W.F. , "Soil Mechanics and Theorems of Limit Analysis," J. Soil Mech. & Found. Div., Proc. Am. Soc. Civ. Eng., v.95,#SM2 (1969).

14. Chen, W.F. , M. . Giger, and H.Y. Fang, "On the Limit Analysis of Stability of Slopes," Soils & Found. Japan. Soc. Soil Mech. & Found. Eng., v.9,#4 (1969).

15. Chen, W.F. , Limit Analysis and Soil Plasticity, Elsevier Scientific Publishing Co., (1975).

16. Karal, K. , Energy Method for Soil Stability Analysis, Doctoral Dissertation, River & Harbour Lab., The Norwegian Institue of Technology, Trondheim, Norway (1977)

17. Chen, W.F. , C.J. Chang, and J.T.P. Yao, "Limit Analysis of Earthquake-Induced Slope Failure," Proc. 15th Annual Meeting, Soc. Eng. Sci., Inc., (1978)

18. Chen, W.F. , and S.L. Koh, "Earthquake-Induced Landslide Problems," Proc. Cen. Am. Conf. on Earthquake Eng., San Salvador, El Salvador (1978).

19. Koh, S.L. , and W.F. Chen, "The Prevention and Control of Earthquake," Proc. U.S.-S.E.Asia Sym. on Eng. for Nat'l Hazards Protection, Manila, Philippines, Sept.'77; U. of Illinois Press, (1978).

20. Prater, E.G. , "Yield Acceleration for Seismic Stability of Slopes," J. Geotech. Eng. Div., Proc. Am. Soc. Civ. Eng., v.105,#GT5 (1979).

21. Chen, W.F. , "Plasticity in Soil Mechanics & Landslides," J. Eng. Mech. Div., Proc. Am. Soc. Civ. Eng., June 1980.

22. Chan, S.W. , W.F. Chen, and S.L. Koh, "Limit Analysis of Seismic Slope Stability," Proc. 7th World Conf. Earthquake Eng., Istanbul, Turkey, Sept. 1980.

23. Root, R.R. , and K.M. Ragsdell, BIAS: A Nonlinear Programming Code in Fortran IV; User's Manual, Design Group, School of Mech. Eng., Purdue University. (1977).

APPENDICES

Appendix A

Computer Coding

For the easy application of the analysis developed here, a computer coding of the model has been implemented. Ample demonstrations are included for references: Fig.A1 shows the complete listing of the program itself; Fig.A2 is a flow chart of the subroutine-interactions; and Fig.A3 is a sample output.

```
      PROGRAM LASSIE(INPUT,OUTPUT,TAPE5=INPUT,TAPE6=OUTPUT)
C
C******************* L A S S I E ***********************************
C LIMIT ANALYSIS ON STABILITY OF SEISMIC INFIRMED EARTHSLOPE
C
C THIS IS A RESULT OF THE NATIONAL SCIENCE FOUNDATION FUNDED PROJECT
C NO. PRF-7809326.
C THIS PROGRAM IS THE CODING OF THE FORMULATIONS FOR THE SEISMIC
C CRITICAL HEIGHT OF AN EARTHSLOPE BASED ON THE UPPER BOUND LIMIT
C ANALYSIS OF PERFECT PLASTICITY.
C WRITTEN BY S.W. CHAN, AT PURDUE UNIVERSITY; LAST REVISION: 7/10/80.
C FOR ANY FURTHER INFORMATIONS, PLEASE CONTACT PROF. S.L. KOH OF
C MECHANICAL ENGINEERING DEPARTMENT, OR PROF. W.F. CHEN OF CIVIL
C ENGINEERING DEPARTMENT.
C
C TO USE THIS PROGRAM, PLEASE PROVIDE THE FOLLOWING INFORMATIONS:
C    IWRITE = +1 : TABULATED OUTPUT OF THE SLOPE HEIGHT FOR EACH
C                  COMBINATION OF RO,THETAO, ^ THETAH DURING THE
C                  PHASE OF FINDING THE STARTING POINT FOR OPTIMIZATION
C              0 : NO TABULATED OUTPUT WHEN FINDING THE STARTING POINT
C             -1 : NO TABULATED OUTPUT BECAUSE THE STARTING POINT IS
C                  TO BE INPUTTED.
C    M = THE DEGREE OF THE HORIZONTAL SEISMIC PROFILE POLYNOMIAL.
C    NN = THE DEGREE OF THE VERTICAL SEISMIC PROFILE POLYNOMIAL.
C    AIN = THE INITIAL VALUE (DEG.) FOR SLOPE ANGLE ALPHA.
C    BIN = THE INITIAL VALUE (DEG.) FOR SLOPE ANGLE BETA.
C    PIN = THE INITIAL VALUE (DEG.) FOR INTERNAL FRICTION ANGLE PSI.
C    BB = THE ARRAY CONTAINING THE (M+1) COEFFICIENTS FOR THE
C         HORIZONTAL PROFILE.
C    A = THE ARRAY CONTAINING THE (NN+1) COEFFICIENTS FOR THE VERTICAL
C        PROFILE.
C    CRATE = THE RATIO OF C/GAMMA.
C    IFLAG = 1 : FOR NON-STRETCHED SPIRAL
C            2 : FOR STRETCHED SPIRAL.
C    XO = THE INITIAL VALUES FOR THE 4 VARIABLES RO,THETAO,THETAH,
C         (RADIANS), ^ HTOE OR D; ONLY NEEDED FOR IWRITE=-1 .
C ---(THE FOLLOWING ANGLES IN DEGREES)---
C    XMIN = THE LOWER LIMITS FOR THE 4 INDEPENDENT VARIABLES.
C    XMAX = THE UPPER LIMITS FOR THE 4 INDEPENDENT VARIABLES.
C    DX = THE INCREMENTS FOR THE 4 INDEPENDENT VARIABLES IN THE
C         BRUTE FORCE SEARCH FOR THE STARTING POINT, (IWRITE=0 OR 1).
C    PSIM = THE FINAL VALUE FOR PSI (AND ALPHA).
C    BETAM = THE FINAL VALUE FOR BETA.
C    DPSI = THE INCREMENT FOR PSI.
C    DALPHA = THE INCREMENT FOR ALPHA.
C    DBETA = THE INCREMENT FOR BETA.
C*******************************************************************
C
      DIMENSION SAVE(3,3),XMIN(4),XMAX(4),CON(11),DX(3),XO(4),XM(4)
      DIMENSION A(10),BB(10),ZMU(10),ZNU(10)
      NAMELIST /INFO1/IWRITE,M,NN,AIN,BIN,PIN,BB,A,CRATE,IFLAG,HMAX
      NAMELIST /INFO2/XO,XMIN,XMAX,DX,PSIM,BETAM,DPSI,DALPHA,DBETA
      COMMON /A1/TNPSI,BETA,ALPHA,SNALFA,SNBMA,THETAM,SNTM,CRATE,HMAX
      COMMON /A2/SNBETA,TNALFA,TNBETA,TNALSQ,TNBESQ,HTOE,TG1,TG2,CSTM
      COMMON /A3/NP1,A,ZMU
      COMMON /A4/MP1,BB,ZNU,TORQTL
      COMMON /A5/BC(9,9)
      COMMON /BR1/CF,IFLAG,NB
C
C THE FOLLOWING PARAMETERS ARE FOR THE SUBROUTINE ≠BIAS≠ ONLY, FOR
```

Figure A1 Program Listing.

```
C THEIR MEANINGS, PLEASE CONSULT THE ~BIAS USER MANUAL~.
C
      COMMON/B1/B(100)
      COMMON/B2/XMAX
      COMMON/B3/XMIN
      COMMON/B4/FR,MAXM,EPSLS
      DATA IPR,IDATA,MAXM/1,1,1000/
      DATA EPSI,EPSLS,FR,R/1.E-4,1.E-4,1.E-8,10./
C
C INITIATION OF VARIABLES.
C
      DATA ZMU,ZNU/20*0./
      DATA BC/81*0./
      DATA A,BB/20*0./
      DATA XO/4*0./
      READ(5,INFO1)
      WRITE(6,INFO1)
      READ(5,INFO2)
      WRITE(6,INFO2)
      NP1=NN+1
      MP1=M+1
      NB=NP1
      IF(MP1 .GT. NP1)NB=MP1
      CALL BINOM(NB)
      DO 500 II=1,3
C
C THE VALUES OF DX,XMIN,XMAX ARE SAVED FOR LATER USES.
C
      SAVE(1,II)=DX(II)
      SAVE(2,II)=XMIN(II)
500   SAVE(3,II)=XMAX(II)
      ANGP=PIN
400   ANGA=AIN
300   ANGB=BIN
C
C CHANGE FROM DEGREES TO RADIANS.
C
200   ALPHA=ANGA*0.0174533
      BETA=ANGB*0.0174533
      THM=90.+ANGP
      THETAM=THM*0.0174533
      PSIA=ANGP*0.0174533
      TNPSI=TAN(PSIA)
      SNBETA=SIN(BETA)
      SNALFA=SIN(ALPHA)
      SNBMA=SIN(BETA-ALPHA)
      TNALFA=TAN(ALPHA)
      IF(BETA .LT. 1.570796)GOTO 25
      TNBETA=1.
      GOTO 15
25    TNBETA=TAN(BETA)
15    TNALSQ=TNALFA*TNALFA
      TNBESQ=TNBETA*TNBETA
      SNTM=SIN(THETAM)
      CSTM=COS(THETAM)
      DO 700 II=1,3
      DX(II)=SAVE(1,II)
      XMIN(II)=SAVE(2,II)
700   XMAX(II)=SAVE(3,II)
      IF(IFLAG .EQ. 1)XO(4)=0.
```

Fig.A1 (Cont'd)

```
      WRITE(6,10)ANGP,ANGA,ANGB
10    FORMAT(≠1≠,50(≠-≠)/≠ FOR  :  PSI=≠,F5.0,5X,≠ALPHA=≠,F5.0,5X,
     $≠BETA=≠,F5.0)
      IF(IWRITE .EQ. -1)GOTO 750
      CALL BRUTE(IWRITE,ANGP,ANGA,ANGB,XMIN,XMAX,DX,XO)
      DO 600 II=1,3
      XMIN(II)=SAVE(2,II)
600   XMAX(II)=SAVE(3,II)
750   CALL RANGE(ANGB,ANGA,ANGP,XMIN,XMAX,DX)
      DO 650 II=2,3
      XMIN(II)=XMIN(II)*0.0174533
650   XMAX(II)=XMAX(II)*0.0174533
      IF(XO(1) .LT. XMAX(1))GOTO 800
C
C IN CASE NO FESIBLE STARTING POINT IS FOUND, THE POINT OF MID-RANGES
C IS USED AS THE STARTING POINT.
C
      XO(1)=(XMIN(1)+XMAX(1))/2.
      XO(2)=(XMIN(2)+XMAX(2))/2.
      XO(3)=(XMIN(3)+XMAX(3))/2.
800   K=9
C
C IF HMAX IS NON-ZERO, THE SLOPE HEIGHT IS GIVEN; AND THE PROBLEM IS
C TO LOCATE THE MOST CRITICAL SURFACE.
C
      IF(HMAX .GT. 0.)K=10
C
C CALLS ≠BIAS≠ FOR OPTIMIZATION, SEE ~BIAS USER MANUAL~.
C
      CALL BIAS(4,K,1,CON,XO,R,EPSI,IPR,IDATA,XM)
      IF(HMAX .GT. 0.)WRITE(6,65)HMAX
65    FORMAT(≠0 THE HEIGHT OF THE SLOPE WAS GIVEN AS ≠,F7.2)
      IF(IFLAG .EQ. 1)GOTO 900
      WRITE(6,30)XM(4)
30    FORMAT(≠0 THE SPIRAL IS STRETCHED ≠,F10.5,≠ UNITS≠)
      WRITE(6,35)TG1,TG2
      GOTO 100
45    FORMAT(≠0 TG1=≠,F10.5,≠  TG2=≠,F10.5/
     +≠ IF TG1=TG2=X(3), SPIRAL IS NORMAL≠/
     +≠ IF TG1<TG2=X(3), SPIRAL IS SUNKEN≠/
     +≠ IF TG1<TG2<X(3), SPIRAL IS PARTIALLY SUNKEN≠)
900   WRITE(6,40)HTOE
40    FORMAT(≠0 THE SPIRAL IS RAISED ≠,F10.5,≠ UNITS≠)
      WRITE(6,45)TG1,TG2
35    FORMAT(≠0 TG1=≠,F10.5,≠  TG2=≠,F10.5)
C
C TORQUE PER UNIT AREA IS CALCULATED.
C
100   TORQTL=TORQTL*XM(1)**3
      WRITE(6,55)TORQTL
55    FORMAT(≠0 THE TOTAL EXTERNAL TORQUE INTENSITY IS ≠,F15.5)
C
C READY TO CONSIDER NEXT SLOPE GEOMETRY.
C
105   ANGB=ANGB+DBETA
      IF(ANGB .LE. ANGA)GOTO 105
      IF(ANGB .LE. BETAM)GOTO 200
      ANGA=ANGA+DALPHA
      IF(ANGA .LE. ANGP .AND. ANGA .LE. PSIM)GOTO 300
      ANGP=ANGP+DPSI
```

Fig.A1 (Cont'd)

```
      IF(ANGP .LE. PSIM)GOTO 400
      STOP
      END
C
C. . . . . . . . . . . . . . . . . . . . . . . . . . . . . . . . . . .
C
      FUNCTION F(X)
C
C TO CALCULATE THE SAFETY FACTOR FOR THE SLOPE STABILITY.
C THE FORM OF THIS SUBPROGRAM CONFORMS WITH THE REQUIREMENTS OF ≠BIAS≠
C
      DIMENSION X(4)
      COMMON /A1/TNPSI,BETA,ALPHA,SNALFA,SNBMA,THETAM,SNTM,CRATE,HMAX
C
C FOR THE USE OF ≠BIAS≠ ONLY.
C
      COMMON/1/NF,NC
      NF=NF+1
C
      ICALL=1
      CALL SPIRAL(ICALL,X,EF,FNET,EXTRA)
      F=EF*SIN(X(3)+ALPHA)-SIN(X(2)+ALPHA)
      FACTOR=X(3)-X(2)
      IF(TNPSI .GT. 1.E-4)FACTOR=(EF*EF-1.)/2./TNPSI
C
C THE STABILITY FACTOR:
C
      F=F*FACTOR*FNET+EXTRA
C
C THE ACTUAL CRITICAL HEIGHT:
C
      F=F*CRATE
      RETURN
      END
C
C. . . . . . . . . . . . . . . . . . . . . . . . . . . . . . . . . . .
C
      SUBROUTINE CONST(X,CON)
C
C TO SPECIFY THE CONSTRAINTS FOR EFFECTIVE OPTIMIZATION.
C THE SUBROUTINE FORM IS IN CONFORMATION WITH SPECIFICATION OF ≠BIAS≠.
C
      DIMENSION X(4),CON(11)
      COMMON /A1/TNPSI,BETA,ALPHA,SNALFA,SNBMA,THETAM,SNTM,CRATE,HMAX
      COMMON /BR1/CF,IFLAG,NB
      COMMON /C1/CLR,SNTH,RH,SNTO,CSTO,CSTH
C
C FOR ≠BIAS≠ ONLY.
C
      COMMON/1/NF,NC
      NC=NC+1
C
      ICALL=0
      CON(10)=X(3)-X(2)-0.01
      IF(CON(10) .GT. 1.E-4)GOTO 200
      DO 300 I=1,10
300   CON(I)=-10.
      RETURN
200   CALL SPIRAL(ICALL,X,CE,FNET,EXTRA)
C
```

Fig.A1 (Cont'd)

```
C THE VERTICAL DISTANCE OF THE SLOPE KNEE FROM THE ROTATION CENTER.
C
      CK=X(1)*SNTO+CLR*SNALFA
C
C THE VERTICAL DISTANCE OF THE SPIRAL TERMINATION POINT FROM THE CENTER.
C
      CH=RH*SNTH
      R=CRATE*(X(3)-X(2))/FNET
      IF(TNPSI .GT. 1.E-4)R=CRATE*(CE*CE-1.)/2./TNPSI/FNET
      TOL=3.1415927-2.*BETA
      TOU=7.
      IF(TNPSI .LE. 1.E-6)TOU=3.1415927-2.*ALPHA
      C8=(CE*SIN(X(3)+ALPHA)-SIN(X(2)+ALPHA))*SIN(BETA)/SNBMA
C
C THE SLOPE HEIGHT (OR THE SPIRAL HEIGHT IF HMAX>0):
C
      CF=R*C8+EXTRA
C
      IF(HMAX .GT. 0.)CON(11)=HMAX-CF
      CON(9)=TOU-X(3)-X(2)
      CON(8)=X(2)+X(3)-TOL
      CON(7)=C8
      CON(6)=CF/CLR-0.1
      CON(5)=CLR/CF-0.1
      CON(4)=FNET
      CON(3)=CLR-0.01
      CON(2)=CH-CK-0.01
      CON(1)=X(1)-R
C
C THE MEANINGS OF THE CONSTRAINTS ARE :
C   CON NO.            COMMENT
C  ---------    ------------------------------------------------------
C      1        THE RADIUS IDENTITY FOR QUALIFYING SLOPE.
C    2 ^ 3      TOGETHER ASSURE THE SPIRAL CUTS THROUGH BOTH THE
C               ALPHA AND BETA REGIONS OF THE SLOPE.
C    4 ^ 7      TOGETHER RULE OUT UNREALISTIC VALUES FOR SLOPE HEIGHTS.
C    5 ^ 6      TOGETHER GUARD AGAINST SKEWED SPIRALS.
C    8 ^ 9      THE SPIRAL ANGLES INEQUALITIES FOR ANGLE RANGES.
C     10        THE SPIRAL MUST NOT GO BACKWARD.
C     11        THE SPIRAL HEIGHT MUST NOT BE GREATER THAN THE SLOPE
C               HEIGHT, (FOR LOCATING THE MOST CRITICAL SPIRAL).
C
      RETURN
      END
C
C. . . . . . . . . . . . . . . . . . . . . . . . . . . . . . . . . . . .
C
      SUBROUTINE BRUTE(IWRITE,ANGP,ANGA,ANGB,XMIN,XMAX,DX,X)
C
C THE BRUTE FORCE APPROACH TO LOCATE A ROUGH MINIMUM (AS THE FEASIBLE
C STARTING POINT FOR ≠BIAS≠) BY SEARCHING THROUGH THE RANGE OF EACH
C VARIABLE (EXCEPT THE 4TH ONE) AT CHOSEN INCREMENTS.
C
      DIMENSION CN(11),XMIN(4),XMAX(4),DX(3),X(4),OUT(2,100),REG(3,100)
      COMMON /BR1/CF,IFLAG,NB
      DATA REG/300*0./
C
C PARAMETERS RELATED TO THE DECLARATION OF A MINIMUM.
C
      CRITE=0.005
```

Fig.A1 (Cont'd)

```
      COMPARE=1000.
      DIFMIN=100000.
C
C ITERATION NUMBER (MAXIMUM OF 5 ITERATIONS ALLOWED).
C
      KOUNT=1
1200  CHECK=COMPARE
      CALL RANGE(ANGB,ANGA,ANGP,XMIN,XMAX,DX)
      IF(IWRITE .EQ. 1)WRITE(6,70)KOUNT
70    FORMAT(≠0 ITERATION≠,I3)
      JK=0
      X(1)=XMIN(1)
400   TH=XMIN(3)
      IF(IWRITE .EQ. 0)GOTO 500
      WRITE(6,10)X(1)
10    FORMAT(≠0≠,110(≠$≠)/≠ R=≠,F5.1/)
      WRITE(6,20)
20    FORMAT(≠    TH    *≠,10(4X,≠TO≠,4X)/8X,≠*≠,10(3X,≠(F)≠,4X)/1X,110
     ^(≠-≠))
500   J=0
C
C VARYING THETAO FIRST.
C
      TO=XMIN(2)
      DO 700 K1=1,2
      DO 700 K2=1,100
700   OUT(K1,K2)=1000.
      X(3)=TH*0.0174533
      IF(IWRITE .EQ. 1)WRITE(6,40)TH
40    FORMAT(1X,F6.2,≠ *≠)
200   J=J+1
      X(2)=TO*0.0174533
C
C FIRST DECIDE IF THE VALUE IS ACCEPTABLE.
C
      CALL CONST(X,CN)
      DO 150 I=2,10
      IF(CN(I) .LE. 0.)GOTO 600
150   CONTINUE
      ACN=ABS(CN(1))
C
C THE RADIUS IDENTITY IS USUALLY HARD TO SATISFY IN HERE, SO IF THE ERROR
C IS LESS THAN THE LAST REPORTED, THE VALUE IS QUALIFY FOR FURTHER
C CONSIDERATION.
C
      IF(ACN .LE. 0.1)GOTO 2250
      IF(ACN .GT. DIFMIN)GOTO 600
2250  OUT(1,J)=TO
      OUT(2,J)=CF
C
C IF THE VALUE IS WITHIN THE TOLERABLE RANGE OF THE LAST REPORTED VALUE
C THEN THIS VALUE IS RECORDED.
C
2200  IF(OUT(2,J) .GE. COMPARE+CRITE)GOTO 600
      IF(OUT(2,J)+CRITE .GT. COMPARE)GOTO 1000
      JK=0
      COMPARE=OUT(2,J)
1000  JK=JK+1
      DIFMIN=ACN
C
```

Fig.A1 (Cont'd)

```
C REGISTER THE POINT CORRESPONDING TO THE RECORDED VALUE.
C
      REG(1,JK)=X(1)
      REG(2,JK)=TH
      REG(3,JK)=TO
C
C ADVANCE THE POINT ALONG THE THETAO AXIS.
C
600   TO=TO+DX(2)
      IF(TO .LE. XMAX(2) .AND. TO .LT. TH)GOTO 200
      IF(IWRITE .EQ. 0)GOTO 300
      WRITE(6,30)(OUT(1,I),I=1,10),(OUT(2,I),I=1,10)
      IF(J .LE. 10)GOTO 300
      WRITE(6,30)(OUT(1,I),I=11,20),(OUT(2,I),I=11,20)
      IF(J .LE. 20)GOTO 300
      WRITE(6,30)(OUT(1,I),I=21,30),(OUT(2,I),I=21,30)
      IF(J .LE. 30)GOTO 300
      WRITE(6,30)(OUT(1,I),I=31,40),(OUT(2,I),I=31,40)
30    FORMAT(8X,≠*≠,10(1X,F6.2,3X)/8X,≠*≠,10(≠(≠,F6.2,≠)  ≠))
C
C NEXT ADVANCE THE POINT ONE INCREMENT IN THE THETAH AXIS.
C
300   TH=TH+DX(3)
      IF(TH .LE. XMAX(3))GOTO 500
C
C THEN ADVANCE THE POINT ONE INCREMENT IN THE RO AXIS.
C
      X(1)=X(1)+DX(1)
      IF(X(1) .LE. XMAX(1))GOTO 400
C
C IF THE SMALLEST VALUE RECORDED IN THIS ITERATION DOESN≠T IMPROVE
C APPRECIABLY OVER THAT OF THE LAST ITERATION, CONVERGENCY OF BRUTE
C FORCE SEARCH IS DECLARED.
C
      IF(CHECK-COMPARE .LE. CRITE)GOTO 2000
C
C IF 5 ITERATIONS HAS BEEN RUN, NO NEED TO GO ON ANY FURTHER.
C
2800  IF(KOUNT .EQ. 5)GOTO 1400
C
C FOR THE NEXT ITERATION, INCREMENTS ARE HALVED.
C
      DO 1300 I=1,3
1300  DX(I)=DX(I)/2.
C
C IF NO FEASIBLE VALUES WERE RECORDED IN THE LAST ITERATION, CAN≠T GO
C ON ANY FURTHER WITH BRUTE FORCE SEARCH.
C
      IF(JK .EQ. 0)RETURN
C
C IF THE INCREMENTS HAVE BECOME TOO SMALL, THEN CONDITIONAL CONVERGENCY
C OF THE BRUTE FORCE SEARCH IS DECLARED.
C
      IF(DX(3) .LT. 0.01)GOTO 1600
C
C THE SPACE OF SEARCH IS NOW SHRUNKEN IN ACCORDANCE WITH INFORMATIONS
C FROM THE LAST ITERATION.
C
      XMIN(1)=REG(1,1)
      XMAX(1)=REG(1,JK)
```

Fig.A1 (Cont'd)

```
      XMIN(3)=REG(2,1)-DX(3)
      XMAX(3)=REG(2,JK)+DX(3)
      GREAT=-1000.
      SMALL=1000.
      DO 1100 I=1,JK
      IF(REG(3,I) .GE. GREAT)GREAT=REG(3,I)
      IF(REG(3,I) .LE. SMALL)SMALL=REG(3,I)
1100  CONTINUE
2700  XMIN(2)=SMALL-DX(2)
      XMAX(2)=GREAT+DX(2)
C
C READY TO START THE NEXT ITERATION.
C
      KOUNT=KOUNT+1
      GOTO 1200
C
C THE FOLLOWING ARE SUMMARY STATEMENTS AT THE END OF BRUTE FORCE SEARCH
C IN ACCORDANCE WITH DIFFERENT OUTCOMES.
C
1400  WRITE(6,80)
80    FORMAT(≠0 CONVERGENCY NOT YET DECLARED↓≠)
      GOTO 2000
1600  WRITE(6,90)KOUNT
90    FORMAT(≠0 CONDITIONAL CONVERGENCY AT ITERATION≠,I3)
2000  WRITE(6,50)COMPARE
50    FORMAT(≠0 THE POSSIBLE CRITICAL VALUE IS≠,F7.2//≠ AT≠,10X,≠R≠,15
     ^X,≠TH≠,15X,≠TO≠/8X,10(≠-≠),7X,10(≠-≠),7X,10(≠-≠))
      IF(JK .EQ. 0)RETURN
      DO 1500 I=1,JK
1500  WRITE(6,60)(REG(IK,I),IK=1,3)
60    FORMAT(4X,3(4X,F8.2,5X))
      X(1)=REG(1,JK)
      X(2)=REG(3,JK)*0.0174533
      X(3)=REG(2,JK)*0.0174533
      RETURN
      END
C
C. . . . . . . . . . . . . . . . . . . . . . . . . . . . . . . . . . . .
C
      SUBROUTINE RANGE(ANGB,ANGA,ANGP,XMIN,XMAX,DX)
C
C THIS SUBROUTINE DEFINES THE ACCEPTABLE RANGES OF THETAO AND THETAH.
C
      COMMON /BR1/CF,IFLAG,NB
      DIMENSION DX(3),XMIN(4),XMAX(4)
      TOMAX=90.+ANGP-ANGA
      IF(XMAX(2) .GT. TOMAX)XMAX(2)=TOMAX
      IF(XMIN(2) .LT. 0.)XMIN(2)=0.
      IF(XMIN(3) .LT. 90.-ANGB+ANGP)XMIN(3)=90.-ANGB+ANGP
      IF(IFLAG .EQ. 2)XMIN(3)=90.+ANGP
      IF(XMIN(3) .LE. XMIN(2))XMIN(3)=XMIN(2)+DX(3)
      IF(XMAX(3) .GT. 180.-ANGA)XMAX(3)=180.-ANGA
      IF(XMAX(3) .GE. 180.)XMAX(3)=XMAX-DX(3)
      RETURN
      END
C
C. . . . . . . . . . . . . . . . . . . . . . . . . . . . . . . . . . . .
C
      SUBROUTINE SPIRAL(ICALL,X,EFTH,FNET,EXTRA)
C
```

Fig.A1 (Cont'd)

```
C THIS SUBROUTINE FINDS THE TORQUE INTENSITY AS WELL AS OTHER PHYSICAL
C ^ GEOMETRICAL INFORMATIONS OF THE SPIRAL.
C
      COMMON /A1/TNPSI,BETA,ALPHA,SNALFA,SNBMA,THETAM,SNTM,CRATE,HMAX
      COMMON /A2/SNBETA,TNALFA,TNBETA,TNALSQ,TNBESQ,HTOE,TG1,TG2,CSTM
      COMMON /A3/NP1,A,ZMU
      COMMON /A4/MP1,BB,ZNU,TORQTL
      COMMON /BR1/CF,IFLAG,NB
      COMMON /C1/ZL,SNTH,RH,SNTO,CSTO,CSTH
      COMMON /S1/THETAF,THETAI
      DIMENSION X(4),A(10),BB(10),ZMU(10),ZNU(10)
      RO=X(1)
      THETAO=X(2)
      THETAH=X(3)
      SNTH=SIN(THETAH)
      CSTH=COS(THETAH)
      EFTH=EXP((THETAH-X(2))*TNPSI)
      SNTO=SIN(THETAO)
      CSTO=COS(THETAO)
      EFTO=1.
C
C A SPIRAL IS ASSUMED NORMAL UNLESS PROVEN OTHERWISE.
C
      NIT=1
      NCOUNT=1
      RH=RO*EFTH
C
C THE TOP LENGTH OF THE SPIRAL:
C
      ZL=(RO*SIN(THETAO+BETA)-RH*SIN(THETAH+BETA))/SNBMA
C
C ADJUSTMENTS FOR RAISED SPIRAL AND STRETCHED SPIRAL.
C
      IF(IFLAG .EQ. 2)GOTO 120
      HTOE=X(4)
      EXTRA=0.
      GOTO 130
120   EXTRA=X(4)*SNBETA/SNBMA
      HTOE=0.
130   ZL=ZL-EXTRA
C
C THE VERTICAL DISTANCE OF THE CENTER FROM THE GROUND:
C
      ETA=RH*SNTH+HTOE
      IF(HMAX .EQ. 0.)GOTO 140
      ETA=RO*SNTO+ZL*SNALFA+HMAX
C
C IF THE SLOPE HEIGHT IS SPECIFIED, THEN HTOE, THE HEIGHT OF THE SLOPE
C TERMINATION POINT, IS NO LONGER AN INDEPENDENT VARIABLE.
C
      HTOE=ETA-RH*SNTH
140   F1X=0.
      F1Y=0.
C
C EXPRESSING THE SEISMIC PROFILES IN THE SPIRAL COORDINATES.
C
      CALL COEFF(ETA,BB,ZNU,MP1)
      CALL COEFF(ETA,A,ZMU,NP1)
C
C THE GROUNDING ANGLE IS TAKEN TO BE THE TERMINATING ANGLE UNLESS
```

Fig.A1 (Cont'd)

```
C PROVEN OTHERWISE.
C
      TG1=THETAH
      TG2=THETAH
      SNTG1=SNTH
      CSTG1=CSTH
      EFTG1=EFTH
      IF(THETAH .LE. THETAM-0.0001)GOTO 110
C
C IF THE SPIRAL IS SAGGING, IT MIGHT NOT BE NORMAL.
C
      ETAM=RO*EXP((THETAM-THETAO)*TNPSI)*SNTM-0.0001
      IF(ETA .GE. ETAM)GOTO 110
C
C AT LEAST PART OF THE SPIRAL IS SUNKEN, GROUDING ANGLE IS NOT THETAH.
C
      NIT=NIT+1
C
C LIMITS FOR SEARCHING FOR THE GROUNDING ANGLE, TG1 :
C
      GLIM1=THETAO
      GLIM2=THETAM
C
C FIRST ESTIMATE OF TG1:
C
      TG1=2.*THETAM-THETAH
      CALL NEWTON(X(2),RO,ETA,GLIM1,GLIM2,TG1,SNTG1,CSTG1,EFTG1)
C
C THE DEGROUDING ANGLE IS TAKEN TO BE THETAH UNLESS OTHERWISE PROVEN.
C
      SNTG2=SNTH
      CSTG2=CSTH
      EFTG2=EFTH
      IF(HTOE .LE. 1.E-5)GOTO 110
C
C IF THE TERMINATION POINT OF THE SPIRAL IS ABOVE THE GROUND, THEN THE
C SPIRAL IS PARTIALLY SUNKEN, AND THETAH CANNOT BE THE DEGROUNDING ANGLE.
C
C
C LIMITS FOR SEARCHING FOR THE DEGROUNDING ANGLE, TG2 :
C
      GLIM1=THETAM
      GLIM2=THETAH
C
C FIRST ESTIMATE OF TG2:
C
      TG2=2.*THETAM-TG1
      CALL NEWTON(X(2),RO,ETA,GLIM1,GLIM2,TG2,SNTG2,CSTG2,EFTG2)
      NIT=NIT+1
C
C FIRST ROUND, INTEGRATING FROM THETAO TO TG1.
C
110   ARG1=SNTG1
      ARG2=SNTO
      ARG3=CSTG1
      ARG4=CSTO
      ARG5=EFTG1
      ARG6=EFTO
      THETAI=THETAO
      THETAF=TG1
```

Fig.A1 (Cont'd)

```
4200  NC=NP1
      MC=MP1
C
C CALCULATING F1Y:
C
150   EFTHP=ARG5*ARG5
      EFTOP=ARG6*ARG6
      YAF=0.
      YAI=0.
      ROPR=1./RO
      SNITHR=1.
      SNITOR=1.
      SNITH=1.
      SNITO=1.
      STH=ARG1
      STO=ARG2
      DO 1000 I=1,NC
      ROPR=ROPR*RO
      APSI=I+2
      APSI=APSI*TNPSI
      SQA=APSI*APSI
      EFTHP=EFTHP*ARG5
      EFTOP=EFTOP*ARG6
      IM2=I-2
      IF(IM2)1100,1200,1300
1200  IF(APSI .GT. 1.E-4)YAF=1./APSI
      IF(APSI .GT. 1.E-4)YAI=1./APSI
      GOTO 1400
1300  CALL SUMS(IM2,APSI,SQA,ARG3,ARG4,ARG1,ARG2,SNITHR,SNITOR,YAF,YAI)
      SNITHR=SNITHR*ARG1
      SNITOR=SNITOR*ARG2
1400  SNITH=SNITH*ARG1
      SNITO=SNITO*ARG2
1100  ZI=I
      COMPAF=APSI*ARG3+ZI*ARG1
      COMPAI=APSI*ARG4+ZI*ARG2
      COMPBF=COMPAF+2.*ARG1
      COMPBI=COMPAI+2.*ARG2
      DEN=SQA+ZI*ZI
      COMPAF=COMPAF*SNITH/DEN
      COMPAI=COMPAI*SNITO/DEN
      CORA=I-1
      CORA=-CORA*APSI/DEN
      CALL SUMS(I,APSI,SQA,ARG3,ARG4,ARG1,ARG2,SNITH,SNITO,YBF,YBI)
      STH=STH*ARG1
      STO=STO*ARG2
      ZI=I+2
      DEN=SQA+ZI*ZI
      COMPBF=COMPBF*STH/DEN
      COMPBI=COMPBI*STO/DEN
      CALL SUMS(I+2,APSI,SQA,ARG3,ARG4,ARG1,ARG2,STH,STO,YCF,YCI)
      CORB=I+1
      CORB=CORB*APSI/DEN+TNPSI
      YF=(YAF*CORA+COMPAF+YBF*CORB-COMPBF-YCF*TNPSI)*EFTHP
      YI=(YAI*CORA+COMPAI+YBI*CORB-COMPBI-YCI*TNPSI)*EFTOP
      COEF=ZMU(I)
      IF(NCOUNT .EQ. 2)COEF=A(I)
1000  F1Y=F1Y+COEF*ROPR*(YF-YI)
C
C CALCULATING F1X:
```

Fig.A1 (Cont'd)

```
C
      SNITHR=1.
      SNITOR=1.
      ROPR=1./RO
      EFTHP=ARG5*ARG5
      EFTOP=ARG6*ARG6
      DO 1500 I=1,MC
      EFTHP=EFTHP*ARG5
      EFTOP=EFTOP*ARG6
      ROPR=ROPR*RO
      ZIP2=I+2
      APSI=ZIP2*TNPSI
      SQA=APSI*APSI
      CALL SUMS(I,APSI,SQA,ARG3,ARG4,ARG1,ARG2,SNITHR,SNITOR,XAF,XAI)
      SNITHR=SNITHR*ARG1
      SNITOR=SNITOR*ARG2
      SNITH=SNITHR*ARG1
      SNITO=SNITOR*ARG2
      COMPAF=(APSI*ARG3+ZIP2*ARG1)*SNITH
      COMPAI=(APSI*ARG4+ZIP2*ARG2)*SNITO
      DEN=TNPSI/(SQA+ZIP2*ZIP2)
      COMPAF=COMPAF*DEN
      COMPAI=COMPAI*DEN
      CALL SUMS(I+2,APSI,SQA,ARG3,ARG4,ARG1,ARG2,SNITH,SNITO,XBF,XBI)
      CORR=I+1
      CORR=1.-CORR*APSI*DEN
      XF=(XAF*CORR+COMPAF-XBF)*EFTHP
      XI=(XAI*CORR+COMPAI-XBI)*EFTOP
      COEF=ZNU(I)
      IF(NCOUNT .EQ. 2)COEF=BB(I)
1500  F1X=F1X+COEF*ROPR*(XF-XI)
      IF(NCOUNT .GT. 1)GOTO 3300
C
C NEXT CALCULATES F2X+F3X :
C
C
C THE Y COORDINATE OF THE SPIRAL STARTING POINT:
C
      VB=RO*SNTO
C
C THE Y COORDINATE OF THE SLOPE KNEE:
C
      VD=VB+ZL*SNALFA
C
C THE Y COORDINATE OF THE SPIRAL TOE (OR TERMINATING POINT):
C
      VE=RH*SNTH
      IF(TNALFA .GT. 1.E-4)GOTO 2100
      XI2=0.
      PARTB=0.
      GOTO 2220
2100  XI2=VB/TNALFA+RO*CSTO
2220  IF(BETA .LT. 1.570796)GOTO 2200
      XI3=RH*CSTH
      GOTO 2210
2200  XI3=VE/TNBETA+RH*CSTH
2210  ROQ3=RO**3
      IF(IFLAG .EQ. 2)XI3=XI3+X(4)
      VDSV=VD
      VBSV=VB
```

Fig.A1 (Cont'd)

```
      VESV=VE
      F23X=0.
      DO 2000 I=1,MP1
      ZIP1=I+1
      ZIP2=ZIP1+1.
      VE=VE*VESV
      PARTE=XI3/ZIP1
      VB=VB*VBSV
      VD=VD*VDSV
      IF(TNALFA .GT. 1.E-4)GOTO 2300
      PARTD=-XI3/ZIP1
      GOTO 2310
2300  PARTB=VB*(XI2/ZIP1-VBSV/TNALFA/ZIP2)
      PARTD=(XI2-XI3)/ZIP1-VDSV/TNALFA/ZIP2
2310  IF(BETA .GE. 1.570796)GOTO 2400
      PARTE=PARTE-VESV/TNBETA/ZIP2
      PARTD=PARTD+VDSV/TNBETA/ZIP2
2400  PARTE=PARTE*VE
      PARTD=PARTD*VD
2000  F23X=F23X+ZNU(I)*(PARTD+PARTE-PARTB)/ROQ3
C
C NEXT CALCULATES F2Y+F3Y :
C
      IF(XI2 .GT. 1.E-4)GOTO 2700
      XI2SQ=0.
      GOTO 2800
2700  XI2SQ=XI2*XI2
2800  XI3SQ=XI3*XI3
      VE=1.
      VB=1.
      VD=1.
      F23Y=0.
      DO 2500 I=1,NP1
      ZIP0=I
      ZIP1=ZIP0+1.
      ZIP2=ZIP1+1.
      VE=VE*VESV
      PARTE=XI3SQ/ZIP0
      PARTB=0.
      VB=VB*VBSV
      VD=VD*VDSV
      IF(TNALFA .GT. 1.E-4)GOTO 2600
      PARTD=-XI3SQ/ZIP0
      GOTO 3000
2600  PARTB=VB*(XI2SQ/ZIP0-(2.*XI2/ZIP1/TNALFA-VBSV/ZIP2/TNALSQ)*VBSV)
      BLOCK2=VDSV/TNALSQ/ZIP2
      BLOCK1=2.*XI2/TNALFA/ZIP1
      PARTD=(XI2SQ-XI3SQ)/ZIP0+(BLOCK2-BLOCK1)*VDSV
3000  IF(BETA .GE. 1.570796)GOTO 2900
      PARTE=PARTE-(2.*XI3/ZIP1/TNBETA-VESV/ZIP2/TNBESQ)*VESV
      PARTD=PARTD+(XI3/TNBETA/ZIP1*2.-VDSV/TNBESQ/ZIP2)*VDSV
2900  PARTE=PARTE*VE
      PARTD=PARTD*VD
2500  F23Y=F23Y+ZMU(I)*(PARTE+PARTD-PARTB)/ROQ3
C
C IF SPIRAL IS NORMAL, THEN INTEGRATION IS COMPLETED, SO PROCEED REGULARLY.
C
3300  IF(NCOUNT .EQ. NIT)GOTO 4400
      NCOUNT=NCOUNT+1
      IF(NCOUNT .EQ. 3)GOTO 4300
```

Fig.A1 (Cont'd)

```
C
C FOR INTEGRATION OF TG1 TO TG2:
C
      ARG2=SNTG1
      ARG4=CSTG1
      ARG6=EFTG1
      ARG1=SNTG2
      ARG3=CSTG2
      ARG5=EFTG2
      THETAI=TG1
      THETAF=TG2
      NC=1
      MC=1
      GOTO 150
C
C FOR INTEGRATION OF TG2 TO THETAH IF THE SPIRAL IS PARTIALLY SUNKEN:
C
4300  ARG1=SNTH
      ARG2=SNTG2
      ARG3=CSTH
      ARG4=CSTG2
      ARG5=EFTH
      ARG6=EFTG2
      THETAI=TG2
      THETAF=THETAH
      GOTO 4200
C
C WITH ADDITIONAL ADJUSTMENTS, CALCULATIONS OF THE SPIRAL PARAMETERS
C ARE COMPLETE.
C
4400  TORQTL=F1X-F23X+(F1Y-F23Y)/2.
      FNET=TORQTL
      IF(FNET .EQ. 0.)FNET=-1.E-6
      IF(IFLAG .EQ. 2)GOTO 4700
4500  EXTRA=HTOE
      IF(HMAX .GT. 0.)EXTRA=0.
      GOTO 4600
4700  EXTRA=EXTRA*SNALFA
4600  IF(ICALL .EQ. 0)RETURN
      FNET=SNBETA/SNBMA/FNET
      RETURN
      END
C
C. . . . . . . . . . . . . . . . . . . . . . . . . . . . . . . . . . .
C
      SUBROUTINE NEWTON(TO,RO,ETA,GLIM1,GLIM2,TG,SNTG,CSTG,EFTG)
C
C TO FIND THE GROUNDING THETA VALUE BY THE NEWTON METHOD
C
      COMMON /A1/TNPSI,BETA,ALPHA,SNALFA,SNBMA,THETAM,SNTM,CRATE,HMAX
200   EFTG=EXP((TG-TO)*TNPSI)
      SNTG=SIN(TG)
      CSTG=COS(TG)
      G=ETA-RO*EFTG*SNTG
      IF(ABS(G) .LE. 0.0001)GOTO 100
      DG=-EFTG*(TNPSI*SNTG+CSTG)*RO
      TGNEW=TG-G/DG
      IF(TGNEW .LT. GLIM1)TGNEW=GLIM1+0.1
      IF(TGNEW .GT. GLIM2)TGNEW=GLIM2-0.01
      IF(TG .LT. 1.E-8)TG=1.E-8
```

Fig.A1 (Cont'd)

```
      DIFF=(TGNEW-TG)/TG
      TG=TGNEW
      IF(ABS(DIFF) .GT. 1.E-8)GOTO 200
100   RETURN
      END
C
C. . . . . . . . . . . . . . . . . . . . . . . . . . . . . . . . . .
C
      SUBROUTINE SUMS(M,A,SQA,CSF,CSI,SNF,SNI,SNMF,SNMI,SUMF,SUMI)
C
C FOR THE SUMMSTIONS OF THE SEQUENCES IN THE ITEGRATION FORMULA FOR
C F1X ^ F1Y.
C
      COMMON /S1/TF,TI
      J=0
      LL=M/2
      ASNF=A*SNF
      ASNI=A*SNI
      SN2F=SNF*SNF
      SN2I=SNI*SNI
      ZM=M
      DENOM=SQA+ZM*ZM
      PD=1/DENOM
      TERMF=SNMF/DENOM
      TERMI=SNMI/DENOM
      SUMF=TERMF*(ASNF-ZM*CSF)
      SUMI=TERMI*(ASNI-ZM*CSI)
      IF(LL .EQ. 0)GOTO 400
      DO 100 I=1,LL
      J=J+2
      Z=(M-J+1)*(M-J+2)
      ZM=ZM-2.
      DENOM=SQA+ZM*ZM
      IF(DENOM .GT. 1.E-6)GOTO 500
      SUMF=SUMF+PD*Z*TF
      SUMI=SUMI+PD*Z*TI
      RETURN
500   PD=PD*Z/DENOM
      IF(ABS(TERMF) .LE. 0.000001)GOTO 200
      TERMF=TERMF/SN2F/DENOM
      GOTO 250
200   CALL ZERO(ZM,CSF,SUMF,A,PD)
250   IF(ABS(TERMI) .LE. 0.000001)GOTO 300
      TERMI=TERMI/SN2I/DENOM
      GOTO 350
300   CALL ZERO(ZM,CSI,SUMI,A,PD)
350   TERMF=TERMF*Z
      TERMI=TERMI*Z
      SUMF=SUMF+TERMF*(ASNF-ZM*CSF)
100   SUMI=SUMI+TERMI*(ASNI-ZM*CSI)
400   RETURN
      END
C
C. . . . . . . . . . . . . . . . . . . . . . . . . . . . . . . . . .
C
      SUBROUTINE ZERO(ZM,CS,SUM,A,PD)
C
C THIS SUBROUTINE TAKES CARE OF THE SPECIAL CASE
C WHEN THE ANGLE IS ZERO
C
```

Fig.A1 (Cont'd)

```
      IF(ZM-1.)100,200,300
100   SUM=SUM+A*PD
      RETURN
200   SUM=SUM-CS*PD
300   RETURN
      END
C
C. . . . . . . . . . . . . . . . . . . . . . . . . . . . . . . . .
C
      SUBROUTINE COEFF(ETA,A,ZMU,N)
C
C CALCULATES THE COEFFICIENTS OF THE TRANSFORMED SEISMIC PROFILE.
C
      DIMENSION A(10),ZMU(10)
      COMMON /A5/BC(9,9)
      DO 100 I=1,N
100   ZMU(I)=A(I)
      IF(N .EQ. 1)RETURN
      ETAX=1.
      NM2=N-2
      IF(NM2 .EQ. 0)GOTO 400
      DO 200 I=1,NM2
      NMI=N-I
      ETAX=ETAX*ETA
      ZMU(1)=ZMU(1)+A(I+1)*ETAX
      DO 200 J=2,NMI
200   ZMU(J)=ZMU(J)+A(I+J)*BC(J-1,I)*ETAX
400   ZMU(1)=ZMU(1)+A(N)*ETAX*ETA
      SIGN=-1.
      DO 300 L=1,N
      SIGN=SIGN*(-1.)
300   ZMU(L)=ZMU(L)*SIGN
      RETURN
      END
C
C. . . . . . . . . . . . . . . . . . . . . . . . . . . . . . . . .
C
      SUBROUTINE BINOM(ND)
C
C TO CALCULATE THE BINOMIAL COEFFICIENTS FOR THE MAXIMUM EXPANSION
C OF 10TH POWER OR LESS
C
      COMMON /A5/BC(9,9)
      IF(ND .EQ. 1)RETURN
      DO 100 J=1,9
100   BC(1,J)=J+1
      DO 200 I=2,ND
      ADD=1.
      IF10=10-I
      DO 200 J=1,IF10
      BC(I,J)=BC(I-1,J)+ADD
200   ADD=BC(I,J)
      RETURN
      END
C
C. . . . . . . . . . . . . . . . . . . . . . . . . . . . . . . . .
C
C
C THE REST ARE THE INPUT DATA STORED IN THE TWO INPUT NAMELISTS.
C
```

Fig.A1 (Cont'd)

```
$INFO1 IWRITE=-1,M=3,NN=3,AIN=0.,BIN=30.,PIN=0.,A(1)=1.00057,
         A(2)=0.00084,A(3)=-0.0000076,A(4)=0.000000032,
        BB(1)=0.0057,BB(2)=0.0084,BB(3)=-0.000076,
        BB(4)=0.00000032,BB(5)=0.,CRATE=1.,IFLAG=2,HMAX=0. $
$INFO2 XMIN(1)=1.,XMIN(2)=0.,XMIN(3)=10.,XMIN(4)=0.,
       XMAX(1)=400.,XMAX(2)=90.,XMAX(3)=170.,XMAX(4)=100.,
       XO(1)=12.023,XO(2)=0.35,XO(3)=2.12,
       DX(1)=5.,DX(2)=20.,DX(3)=20.,
       PSIM=0.,DPSI=10.,DALPHA=10.,BETAM=90.,DBETA=90. $
```

Fig.A1 (Cont'd)

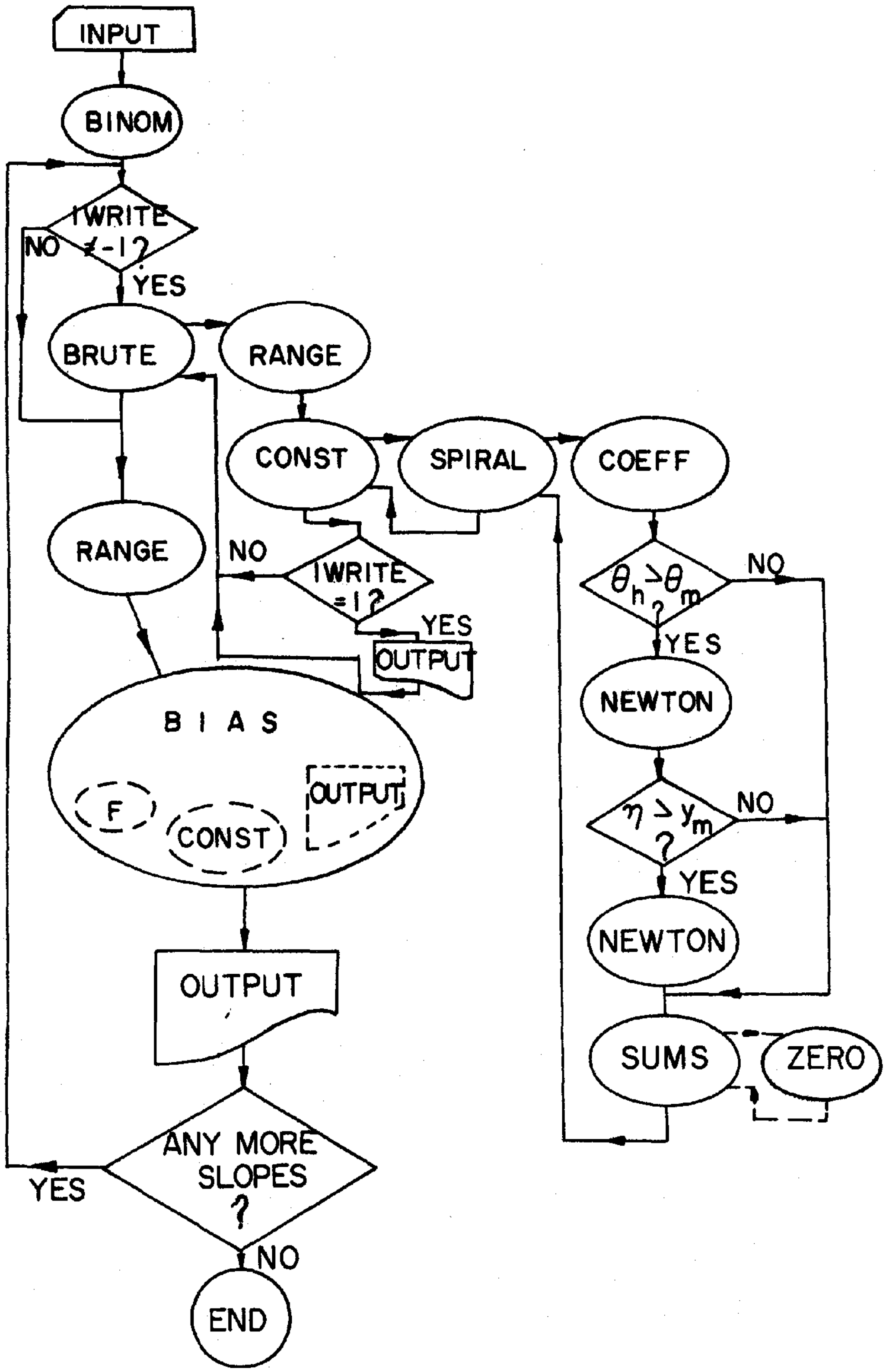

Fig. A2 Flow Chart of Subroutines.

```
$INFO1
IWRITE  =  1,
M       =  3,
NN      =  0,
AIN     =  0.0,
BIN     =  0.3E+02,
PIN     =  0.1E+02,
BB      =  0.57E-02,  0.84E-02, -0.76E-04,  0.32E-06,  0.0,  0.0,  0.0,  0.0,  0.0,  0.0,
A       =  0.1E+01,  0.0,  0.0,  0.0,  0.0,  0.0,  0.0,  0.0,  0.0,  0.0,
CRATE   =  0.1E+01,
IFLAG   =  1,
HMAX    =  0.5E+02,
$END
$INFO2
XO      =  0.12023E+02,  0.35E+00,  0.212E+01,  0.0,
XMIN    =  0.1E+01,  0.0,  0.1E+02,  0.0,
XMAX    =  0.5E+02,  0.9E+02,  0.17E+03,  0.1E+03,
DX      =  0.25E+02,  0.2E+02,  0.2E+02,
PSIM    =  0.0,
BETAM   =  0.9E+02,
DPSI    =  0.1E+02,
DALPHA  =  0.1E+02,
DBETA   =  0.9E+02,
$END
-------------------------------------------------
FOR  :  PSI=   10     ALPHA=    0     BETA=   30
 ITERATION  1
$$$$$$$$$$$$$$$$$$$$$$$$$$$$$$$$$$$$$$$$$$$$$$$$$$$$$$$$$$$$$$$$$$$$$$$$$$$$$$$$$$$$$$$$$$$$$$$$$$$$$$$$$$$
R=  1.0

  TH    *    TO        TO        TO        TO        TO        TO        TO        TO        TO        TO
        *   (F)       (F)       (F)       (F)       (F)       (F)       (F)       (F)       (F)       (F)
----------------------------------------------------------------------------------------------------------
 70.00  *
        * *00.00    *00.00    *00.00    *00.00    *00.00    *00.00    *00.00    *00.00    *00.00    *00.00
        *(*00.00)  (*00.00)  (*00.00)  (*00.00)  (*00.00)  (*00.00)  (*00.00)  (*00.00)  (*00.00)  (*00.00)
 90.00  *
        * *00.00    *00.00    *00.00    *00.00    *00.00    *00.00    *00.00    *00.00    *00.00    *00.00
        *(*00.00)  (*00.00)  (*00.00)  (*00.00)  (*00.00)  (*00.00)  (*00.00)  (*00.00)  (*00.00)  (*00.00)
110.00  *
        * *00.00    *00.00    *00.00    *00.00    *00.00    *00.00    *00.00    *00.00    *00.00    *00.00
        *(*00.00)  (*00.00)  (*00.00)  (*00.00)  (*00.00)  (*00.00)  (*00.00)  (*00.00)  (*00.00)  (*00.00)
130.00  *
        * *00.00    *00.00     40.00    *00.00    *00.00    *00.00    *00.00    *00.00    *00.00    *00.00
        *(*00.00)  (*00.00)  (  6.29)  (*00.00)  (*00.00)  (*00.00)  (*00.00)  (*00.00)  (*00.00)  (*00.00)
150.00  *
        * *00.00    *00.00    *00.00    *00.00    *00.00    *00.00    *00.00    *00.00    *00.00    *00.00
        *(*00.00)  (*00.00)  (*00.00)  (*00.00)  (*00.00)  (*00.00)  (*00.00)  (*00.00)  (*00.00)  (*00.00)
170.00  *
        * *00.00    *00.00    *00.00    *00.00    *00.00    *00.00    *00.00    *00.00    *00.00    *00.00
        *(*00.00)  (*00.00)  (*00.00)  (*00.00)  (*00.00)  (*00.00)  (*00.00)  (*00.00)  (*00.00)  (*00.00)
```

Figure A3 Sample Output.

```
$$$$$$$$$$$$$$$$$$$$$$$$$$$$$$$$$$$$$$$$$$$$$$$$$$$$$$$$$$$$$$$$$$$$$$$$$$$$$$$$$$$$$$$$$$$$$$$$$$$$$$$$$$$$$$$
R= 26.0

 TH    *    TO         TO         TO         TO         TO         TO         TO         TO         TO         TO
       *   (F)        (F)        (F)        (F)        (F)        (F)        (F)        (F)        (F)        (F)
---------------------------------------------------------------------------------------------------------------------
 70.00 *
       * *00.00     *00.00     *00.00     *00.00     *00.00     *00.00     *00.00     *00.00     *00.00     *00.00
       *(*00.00)  (*00.00)   (*00.00)   (*00.00)   (*00.00)   (*00.00)   (*00.00)   (*00.00)   (*00.00)   (*00.00)
 90.00 *
       * *00.00     *00.00     *00.00     *00.00     *00.00     *00.00     *00.00     *00.00     *00.00     *00.00
       *(*00.00)  (*00.00)   (*00.00)   (*00.00)   (*00.00)   (*00.00)   (*00.00)   (*00.00)   (*00.00)   (*00.00)
110.00 *
       * *00.00     *00.00      40.00      60.00     *00.00     *00.00     *00.00     *00.00     *00.00     *00.00
       *(*00.00)  (*00.00)   (  6.83)   (  6.23)   (*00.00)   (*00.00)   (*00.00)   (*00.00)   (*00.00)   (*00.00)
130.00 *
       * *00.00     *00.00     *00.00     *00.00     *00.00     *00.00     *00.00     *00.00     *00.00     *00.00
       *(*00.00)  (*00.00)   (*00.00)   (*00.00)   (*00.00)   (*00.00)   (*00.00)   (*00.00)   (*00.00)   (*00.00)
150.00 *
       * *00.00     *00.00     *00.00     *00.00     *00.00     *00.00     *00.00     *00.00     *00.00     *00.00
       *(*00.00)  (*00.00)   (*00.00)   (*00.00)   (*00.00)   (*00.00)   (*00.00)   (*00.00)   (*00.00)   (*00.00)
170.00 *
       * *00.00     *00.00     *00.00     *00.00     *00.00     *00.00     *00.00     *00.00     *00.00     *00.00
       *(*00.00)  (*00.00)   (*00.00)   (*00.00)   (*00.00)   (*00.00)   (*00.00)   (*00.00)   (*00.00)   (*00.00)
 ITERATION  2
$$$$$$$$$$$$$$$$$$$$$$$$$$$$$$$$$$$$$$$$$$$$$$$$$$$$$$$$$$$$$$$$$$$$$$$$$$$$$$$$$$$$$$$$$$$$$$$$$$$$$$$$$$$$$$$
R= 26.0

 TH    *    TO         TO         TO         TO         TO         TO         TO         TO         TO         TO
       *   (F)        (F)        (F)        (F)        (F)        (F)        (F)        (F)        (F)        (F)
---------------------------------------------------------------------------------------------------------------------
100.00 *
       * *00.00     *00.00     *00.00     *00.00     *00.00     *00.00     *00.00     *00.00     *00.00     *00.00
       *(*00.00)  (*00.00)   (*00.00)   (*00.00)   (*00.00)   (*00.00)   (*00.00)   (*00.00)   (*00.00)   (*00.00)
110.00 *
       * *00.00      60.00     *00.00     *00.00     *00.00     *00.00     *00.00     *00.00     *00.00     *00.00
       *(*00.00)  (  6.23)   (*00.00)   (*00.00)   (*00.00)   (*00.00)   (*00.00)   (*00.00)   (*00.00)   (*00.00)
120.00 *
       * *00.00     *00.00     *00.00     *00.00     *00.00     *00.00     *00.00     *00.00     *00.00     *00.00
       *(*00.00)  (*00.00)   (*00.00)   (*00.00)   (*00.00)   (*00.00)   (*00.00)   (*00.00)   (*00.00)   (*00.00)
 THE POSSIBLE CRITICAL VALUE IS   6.23

AT          R                TH                TO
        ----------       ----------       ----------
          26.00            110.00           60.00
```

Fig.A3 (Cont'd)

```
                BIAS

COPYRIGHT PURDUE RESEARCH FOUNDATION
LAST REVISION-SEPT. 1977



   INFORMATION FROM START
X(  1) =  2.60000000E+01
X(  2) =  1.04719800E+00
X(  3) =  1.91986300E+00
X(  4) =   .0

     F =  6.22689014E+00

CON(  1) = -1.07587078E+00
CON(  2) =  5.96946212E+00
CON(  3) =  1.30050322E+01
CON(  4) =  3.77402197E-02
CON(  5) =  1.99013358E+00
CON(  6) =  3.78438321E-01
CON(  7) =  2.29979312E-01
CON(  8) =  8.72666300E-01
CON(  9) =  4.03293900E+00
CON( 10) =  8.62665000E-01
CON( 11) =  4.37731099E+01
```

```
DBETA    =  0.9E+02,
$END
----------------------------------------------------------
FOR  :  PSI=    0      ALPHA=    0      BETA=   30



                          BIAS

             COPYRIGHT PURDUE RESEARCH FOUNDATION
             LAST REVISION-SEPT. 1977
```

No search for the starting point will be undertaken if IWRITE=-1 (starting point inputted).

```
             -INPUT DATA-

NUMBER OF INDEPENDENT VARIABLES.........N =    4
NUMBER OF INEQUALITY CONSTRAINTS........K =   10
NUMBER OF EQUALITY CONSTRAINTS..........L =    1
PENALTY FUNCTION PARAMETER..............R =   1.000000E+01
PARTIAL DERIVATIVE PARAMETER...........FR =   1.000000E-08
CONVERGENCE CRITERIA.................EPSI = 1.00000000E-04
LINE SEARCH CONVERGENCE CRITERIA....EPSLS = 1.00000000E-04
OUTPUT CONTROL PARAMETER..............IPR =    1
MAXIMUM NUMBER OF CYCLES.............MAXM = 1000

XMAX(  1) =  5.00000000E+01     XMIN(  1) =  1.00000000E+00
XMAX(  2) =  1.57079700E+00     XMIN(  2) =   .0
XMAX(  3) =  2.96706100E+00     XMIN(  3) =  1.22173100E+00
XMAX(  4) =  1.00000000E+02     XMIN(  4) =   .0
```

Fig.A3 (Cont'd)

```
OPTIMIZATION BY THE BIAS PENALTY/DFP TECHNIQUE

        CYCLE          F                        PF                       X(I)


     THE SCALING FACTORS ARE:

THE CONSTRAINTS:
 1.476767E-01   2.625130E-01   9.236075E-02   3.049794E+00
 9.236075E-01   9.236075E-01   1.155958E+00   7.749724E-01
 7.749724E-01   7.749724E-01   2.875212E-01

THE VARIABLES:

 8.292133E-02   1.000000E+00   1.000000E+00   5.005809E-06
****
      RESULTS AT END OF    1 STAGES
           15       5.92202198E+00       5.92227562E+00       1.43673175E+01     7.71015957E-01
                                                              2.05970982E+00     6.30506290E-03
****

****
      RESULTS AT END OF    2 STAGES
           20       5.92252961E+00       5.92252948E+00       1.44051126E+01     7.71123927E-01
                                                              2.05963720E+00     6.30640929E-03
****

 BIAS CONVERGENCE ACHIEVED

                 2 TOTAL STAGES

                20 TOTAL CYCLES

  277 TOTAL FUNCTION EVALUATIONS
  278 TOTAL CONSTRAINT EVALUATIONS
```

Fig.A3 (Cont'd)

```
OPTIMUM FOUND TO BE,

X(  1)= 1.44051126E+01
X(  2)= 7.71123927E-01
X(  3)= 2.05963720E+00
X(  4)= 6.30640929E-03

     F =  5.92252961E+00
```

These statements will appear instead if IFLAG=2.

```
THE SPIRAL IS STRETCHED   32.72462 UNITS
TG1=     .49541  TG2=   2.64618
THE TOTAL EXTERNAL TORQUE INTENSITY IS      4094.49305
```

```
CON(  1)= 8.67206171E-06
CON(  2)= 5.91253318E+00
CON(  3)= 8.55240416E+00
CON(  4)= 1.13233271E-01
CON(  5)= 1.34573429E+00
CON(  6)= 5.91690033E-01
CON(  7)= 4.11141055E-01
CON(  8)= 7.36366422E-01
CON(  9)= 4.16923888E+00
CON( 10)= 1.27851327E+00
CON( 11)= 4.40774704E+01
THE HEIGHT OF THE SLOPE WAS GIVEN AS    50.00
THE SPIRAL IS RAISED    44.07747 UNITS
TG1=    2.05964  TG2=    2.05964
IF TG1=TG2=X(3), SPIRAL IS NORMAL
IF TG1<TG2=X(3), SPIRAL IS SUNKEN
IF TG1<TG2<X(3), SPIRAL IS PARTIALLY SUNKEN
THE TOTAL EXTERNAL TORQUE INTENSITY IS      338.47299
```

These 2 statements will not appear if HMAX=0.

Fig.A3 (Cont'd)

Appendix B

Derivation of Equation 14

In section III.C, the function ξ, Eq.(14), was defined as

$$\xi = \xi(\alpha,\beta,r,\theta). \tag{B1}$$

Its value depends on the slip surface Ψ_1 and the perimeter function Ψ_2 of the slope (Fig. B1). Recoursing to the rectangular coordinates for the time being, we have

$$\xi = \Psi_1(y)-\Psi_2(\alpha,\beta,y) = \xi(\alpha,\beta,y). \tag{B2}$$

Note that the actual form of Ψ_2 is immaterial here. It can be any complicated function or even a Fourier series to account for the kink at the knee. Also notice that Eq.B2 is so general that it is true for any other slope-surface combinations. (See Fig.B2 and B3.)

By transformation back to polar coordinates, ξ becomes

$$\xi = \xi(\alpha,\beta,r,\theta), \tag{B3}$$

which is in the same form as Eq.14.

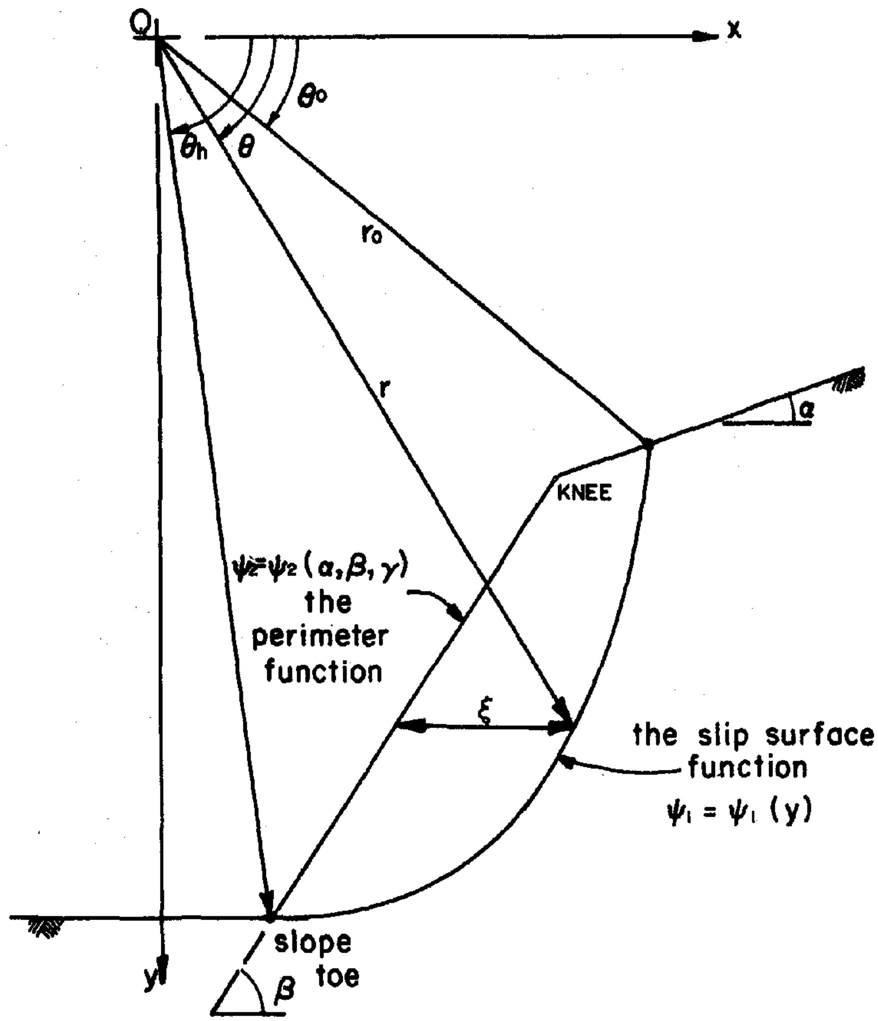

Fig. B1 The Equivalency of ξ, the Horizontal Slice Length, for a Toe-Surface of Failure.

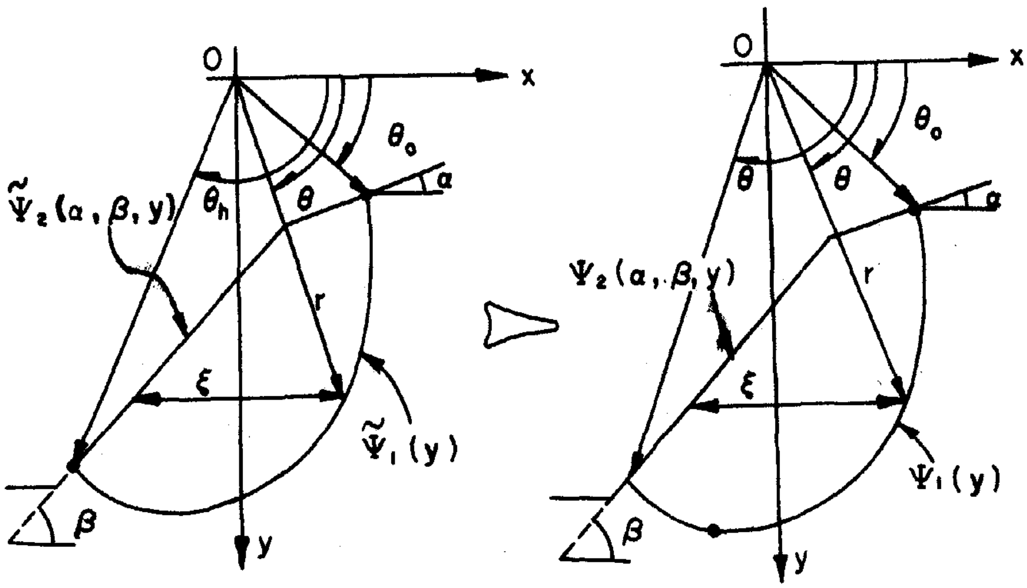

Fig. B2 The Equivalency of ξ for a Raised Sagging Slip Surface.

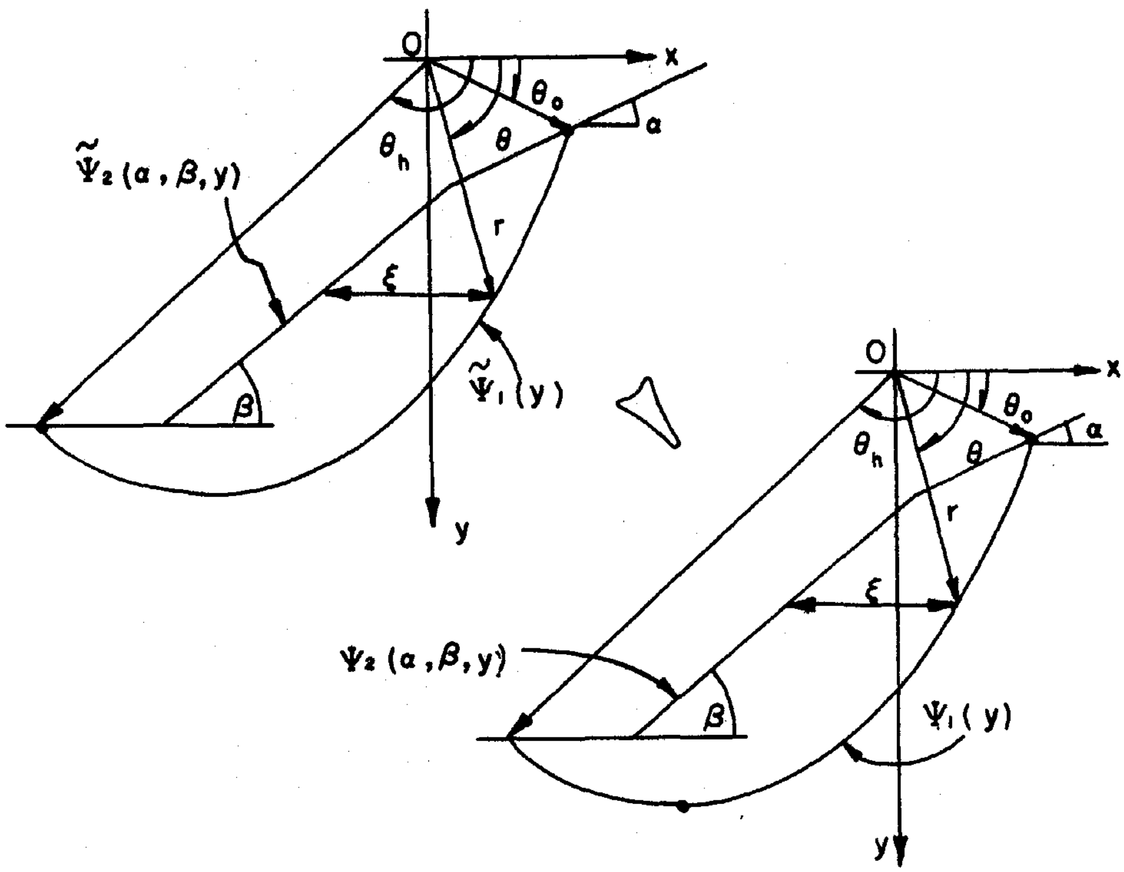

Fig. B3 The Equivalency of ξ for a Stretched Slip Surface.

Appendix C

Derivation of Equation 111

Equation (111) of section IV.B is derived as follows. We expand Eq.(110) iteratively as

$$\int e^{A\theta}\sin^B\theta d\theta = \frac{1}{A^2+B^2}\{e^{A\theta}\sin^{B-1}\theta(A\sin\theta-B\cos\theta)+B(B-1)\cdot$$

$$\{\frac{1}{A^2+(B-2)^2}[e^{A\theta}\sin^{B-3}\theta\{A\sin\theta-(B-2)\cos\theta\}+$$

$$(B-2)(B-3)\int e^{A\theta}\sin^{B-4}\theta d\theta]\}\}$$

$$= e^{A\theta}\{\frac{\sin^{B-1}\theta(A\sin\theta-B\cos\theta)}{A^2+B^2}+\frac{B(B-1)\sin^{B-3}\theta}{A^2+B^2}\cdot$$

$$\frac{A\sin\theta-(B-2)\cos\theta}{A^2+(B-2)^2}+\frac{B(B-1)(B-2)(B-3)\sin^{B-5}\theta}{(A^2+B^2)[A^2+(B-2)^2]}\cdot$$

$$\frac{A\sin\theta-(B-4)\cos\theta}{A^2+(B-4)^2}+\ldots\}+\ell \quad , \tag{C1}$$

where ℓ is the last term of the series. The expression for ℓ depends on whether B is even or odd. If B is even, then

$$\ell_e = k_e\int e^{A\theta}d\theta = \begin{cases} k_e\frac{e^{A\theta}}{A} & , \text{ if } A \neq 0 \\ k_e\theta & , \text{ if } A = 0 \end{cases} \tag{C2}$$

with

$$k_e = \frac{B(B-1)(B-2)(B-3)\ldots[B-(B-1)]}{(A^2+B^2)[A^2+(B-2)^2]\ldots\{A^2+[B-(B-2)]^2\}} \quad (C3)$$

or

$$\ell_e = \begin{cases} e^{A\theta}\{\dfrac{(B)(B-1)\ldots.(1)(A)}{(A^2+B^2)[A^2+(B-2)^2]\ldots(A^2+2^2)(A^2)}\} , & \text{if } A \neq 0 \\ \dfrac{(B)(B-1)\ldots(1)}{(B^2)(B-2)^2\ldots(2)^2} , & \text{if } A = 0 \end{cases} \quad (C4)$$

If B is odd, then

$$\ell_o = k_o \int e^{A\theta}\sin\theta d\theta = k_o[\frac{A\sin\theta-\cos\theta}{A^2+1}e^{A\theta}] , \quad (C5)$$

with

$$k_o = \frac{B(B-1)\ldots[B-(B-2)]}{(A^2+B^2)\ldots\{A^2+[B-(B-3)]^2\}} \quad (C6)$$

or

$$\ell_o = e^{A\theta}[\frac{(B)(B-1)\ldots(1)(A\sin\theta-\cos\theta)}{(A^2+B^2)\ldots(A^2+3^2)(A^2+1^2)}] . \quad (C7)$$

Now, since $\qquad [{B \atop 2s}] = \dfrac{(B)(B-1)\ldots(B-2s+1)}{(2s)!}$,

and $\qquad [{B \atop 0}] = 1$;

then, Eq.(C1) can be expressed as

$$\int e^{A\theta}\sin^B\theta d\theta = e^{A\theta} \sum_{s=0}^{\text{int}(\frac{B}{2})} \{[{B \atop 2s}](2s)!\frac{[A\sin\theta-(B-2s)\cos\theta]\sin^{B-2s-1}\theta}{\prod_{t=0}^{s}[A^2+(B-2t)^2]}\},$$

(C8)

where $\quad \mathrm{int}(\frac{B}{2})$ = the integer part of $(\frac{B}{2})$

Note that the last term, ℓ_e or ℓ_o, is included. For, if B is even, then

$$\mathrm{int}(\tfrac{B}{2}) = B/2 \;,$$

and the last term in the sum of Eq.(C8) is

$$\frac{B(B-1)\ldots[B-2(B/2)+1](\sin\theta)^{-1}(A\sin\theta)}{(A^2+B^2)\ldots\{A^2+[B-(B-2)]^2\}[A^2]}e^{A\theta} = \ell_e \;;$$

if B is odd, then

$$\mathrm{int}(\tfrac{B}{2}) = (B-1)/2$$

and the last term in the sum of Eq.(C8) is

$$\frac{B(B-1)\ldots[B-2(b-1)/2+1](\sin\theta)^{0}(A\sin\theta-\cos\theta)}{(A^2+B^2)\ldots(A^2+3^2)(A^2+1^2)}e^{A\theta} = \ell_o \;.$$